

©2017

Wei Liu

ALL RIGHTS RESERVED

**DEVELOPING FUNCTIONAL INORGANIC-ORGANIC HYBRID
MATERIALS BASED ON I-VII SEMICONDUCTORS FOR
ENERGY-RELATED APPLICATIONS**

by

WEI LIU

A dissertation submitted to the

School of Graduate Studies

Rutgers, The State University of New Jersey

In partial fulfillment of the requirements

For the degree of

Doctor of Philosophy

Graduate Program in Chemistry

Written under the direction of

Jing Li

And approved by

New Brunswick, New Jersey

OCTOBER 2017

ABSTRACT OF THE DISSERTATION

Developing functional inorganic-organic hybrid materials based on I-VII semiconductors for
energy related applications

By WEI LIU

Dissertation Director:

Prof. Jing Li

Crystalline inorganic–organic hybrid materials have been explored for decades. They are both fundamentally and technologically important due to the fact that they integrate the functionality of inorganic compounds (e.g., electronic, magnetic, optical, thermal, and mechanical properties) and the advantages of organic species (e.g., structural flexibility, ease processability, light weight, and low cost) into a single-crystal lattice. A number of structure types have been reported to date, all of which show great promise for energy-related applications.

Inorganic-organic hybrid materials based on I-VII binary semiconductors have been studied intensively because of their unique photo-physical and photochemical properties, as well as their applications for light emitting devices, sensing devices, solar cells, and artificial photosynthesis. Therefore, my research has been focused on hybrid materials based on I-VII semiconductors, particularly for the purpose of developing better-performing rare-earth-elements (REEs) free lighting phosphors. The parent I-VII binary compounds are well-known for their optical properties. One of the well-studied members, copper iodide (CuI), exists in γ phase at room temperature, with a weak violet emission ($\lambda_{\text{em}} = 420 \text{ nm}$). Though

the luminescence of the parent structure is relatively poor, its hybrid materials, generally constructed through Cu-N/P/S covalent bond by reacting copper iodide with either aromatic or aliphatic organic ligands, generally exhibit interesting optical properties and enhanced photoluminescence.

To meet the requirements as highly efficient phosphors for solid-state-lighting (SSL) technology, the materials should have a number of characteristics, such as high internal quantum yields (IQYs), high photo-/thermal stability and optical tunability, etc. The main strategy applied to develop CuI-based phosphors has been centered on fulfilling these requirements. In this thesis I describe the design, synthesis, structure characterization and modification, as well as comprehensive optical property study of various structure types with an emphasis on improving their photoluminescence performances, including the recently developed AIO type of structures as the most promising and best-performing CuI-based phosphors to date. Such new designing strategies and developing approaches may not only be applicable to the copper halide based inorganic-organic hybrid structures, but also be innovative and useful for the construction of many other material classes.

ACKNOWLEDGEMENT

First of all, I would like to express my deepest gratitude to my advisor, Prof. Jing Li. In my heart, she is not only a great advisor, but also a role model of life. Under her guidance, I changed a lot of bad habits of life, and am becoming better and better day by day. With her guidance and support, I determined to be a scientist as my career. I will try my best to be a good scientist as she is. I am proud that I am her student, and I hope one day in the future she will be proud me.

I also have deep love for our group. I have been here for almost 7 years and I always consider the group as my family. I wish all our group members a wonderful future.

I would also like to thank my advisory committee members, Profs. Teddy Asefa, KiBum Lee and Dr. Long Pan, for their kind support and help. Dr. Pan is our “Big Brother”, who always helps us and encourages us. He is one of the nicest person I have ever met in the US.

I want to specially thank the “hybrid team”: Woosok, Ki, Mojgan Roushan, Xiao Zhang, Yang Fang, Kun Zhu, George Wei, Tim Lee, Charlie Jang and all the other undergraduates who have ever worked with me. In the past four years, we have been working very closely and doing great. A very systematic and in-depth work has been done by us, with three JACS and one Adv. Funct. Mater. paper published. Thanks all for your efforts and contributions and I have confidence that our team will be more productive in the future.

I want to particularly thank Hao Wang, who is my colleague in our group and my best friend, who has stayed with me every day for five years. We have so many memories together. I wish he will have a great future and a very happy family.

I want to thanks my parents and my grandparents for their encouragement and support. Nothing is more important than family.

Last but not least, I want to thanks Nancy for her years of companionship. With her support and understanding, I can focus on my graduate study and research, and have hope and passion for my future. She makes me stronger and gives me courage to fight against my weakness.

Table of Contents

ABSTRACT OF THE DISSERTATION	ii
ACKNOWLEDGEMENT.....	iv
1. Introduction.....	1
2. 1D copper bromide staircase chain based structures for white light emissions	11
2.1. Background.....	11
2.2 Diffusion synthesis for single crystal growth and ligand doping approach	12
2.3 Optical tunability and white light.....	16
2.4 Single phase white light emitters	19
2.5 DFT calculations and luminescence mechanism.....	23
2.6 Performance as lighting phosphors and thermochromic behavior.....	31
2.7 Summary	38
3. Precursor approach for the synthesis of Cu ₂ I ₂ dimer based structures and their applications	39
3.1 Background.....	39
3.2 Precursor synthesis of dimer based structures and single crystal data.....	40
3.3 “Bottom-up” approach.....	46
3.4 Enhanced thermal stability by formation of extended structures.....	50
3.5 Optical properties and luminescence mechanism	51
3.6 Performance as lighting phosphors	60
3.7 Summary	62
4. Mechanochemical synthesis of high-performance hybrid materials.....	64
4.1 Background.....	64

4.2 Solvent-free synthesis	67
4.3 New structures and phase purity analysis	70
4.4 Reaction process analysis	75
4.5 Optical properties and application as lighting phosphors	80
4.6 Summary	88
5. Copper halide monomer based structures with exceptionally high quantum efficiencies	89
5.1 Background.....	89
5.2 Ligand preparation and precursor approach for the synthesis.....	90
5.3 Structure and optical characteristics	93
6. Development of AIO type of structures and their unique properties	100
6.1 Background.....	100
6.2 Synthetic design, ligand synthesis and compound preparations	102
6.4 Optical Properties and luminescence mechanism.....	110
6.5 Significantly improve thermal-/photostability.....	120
6.6 Solution dispersability and lighting device design	123
7. References.....	129

List of Illustrations

Figure 1. The design of inorganic-organic hybrid materials based for general lighting applications.....	5
Figure 2. Illustration and introduction of the three types of copper halide based structures...	6
Figure 3. Typical structures of a monomer 0D-CuI(<i>py</i>) ₃ , a rhomboid dimer 0D-Cu ₂ I ₂ (<i>py</i>) ₄ , a cubane tetramer 0D-Cu ₄ I ₄ (<i>py</i>) ₄ , a staircase chain 1D-CuI(<i>py</i>).....	7
Figure 4. The emission spectra of 1D-CuI(<i>L</i>) staircase chain with different ligands coordinated (left) and their CIE coordinates (right).	9
Figure 5. Layerd approach for growing single crystal of both parent and doped structure (left). Crystals fromed in the middle layer as shown in the photo (right).	13
Figure 6. Illustration of the design strategy of the parent and doped structures.....	14
Figure 7. Structural plot of 1D-CuBr(3,5- <i>dm-py</i>) (Top) and 1D-CuBr(3- <i>Cl-py</i>) (bottom).	14
Figure 8. Structure plot of 0D-Cu ₂ Br ₂ (3,5- <i>dm-py</i>) ₄ (top) and 0D-Cu ₂ Br ₂ (3,5- <i>dm-py</i>) ₄ (bottom).	16
Figure 9. Optical absorption of 1D-CuBr(3,5- <i>dm-py</i>) (black), 1D-CuBr(<i>py</i>) (red), 1D-CuBr(3- <i>Cl-py</i>) (blue) and 1D-CuBr(3- <i>Br-py</i>) (green).	17
Figure 10. PXRD patterns of parent and doped structures compared with simulated pattern. From bottom to top: simulated 1D-CuBr(<i>py</i>) , as made 1D-CuBr(<i>py</i>) with different doping level: from 0% to 0.32%.....	18
Figure 11. Photoluminescence spectra of 0.05% doped (solid), 0.07% doped (dash), 0.12% doped (dash dot dot) and 0.32% dioed (short dash dot). Inset: Photos of the doped samples under UV light. Samples from left to right: parent 1D-CuBr(<i>py</i>), 0.004%, 0.008%, 0.02%, 0.05%, 0.07%, 0.12%, 0.32% <i>p</i> _z doped 1D-CuBr(<i>py</i>). $\lambda_{\text{ex}} = 365\text{nm}$	19

Figure 12. Single crystals of 1D-CuBr(<i>py</i>) (a), 0.05% doped (c), 0.12% doped (e), 0.32% doped (g) under nature light and under UV light (365nm).....	20
Figure 13. The absorption spectra for doped structures 1D-CuBr(<i>py</i>) (black), 0.05% doped (red), 0.12% doped (blue), 0.32% doped (green).....	22
Figure 14. Optical absorption of 1% doped 1D-CuBr(<i>py</i>). Inset: optical absorption of 2D-CuBr(<i>pz</i>) _{0.5}	22
Figure 15. Calculated density of states (DOS) of 1D-CuI(<i>py</i>) by DFT method: total DOS (black); Cu 3d orbitals (light blue); Br 4p orbitals (pink); C 2p orbitals (grey); N 2p orbitals (blue).	24
Figure 16. Relative intensity of the HE band at 494 nm (blue) and LE band at 545 nm (green) with various excitation wavelengths of 0.12% doped sample. The intensity of the HE band at 360 nm is set to 1. Inset: PL spectra of 2c with various excitation wavelengths.....	27
Figure 17. Luminescence decay spectra of 0.12% doped sample at 494nm (blue) and 545nm (green). $\lambda_{ex}=360\text{nm}$	28
Figure 18. TG profiles of 1D-CuBr(<i>py</i>) (black), 1D-CuBr(3-Br- <i>py</i>) (red) and 0.12 doped 1D-CuBr(<i>py</i>) (blue).....	29
Figure 19. QY scaled PL spectra of 1D-CuBr(3,5-dm- <i>py</i>) (black), 1D-CuBr(<i>py</i>) (red), 1D-CuBr(3-Cl- <i>py</i>) (blue) and 1D-CuBr(3-Br- <i>py</i>) (green).	32
Figure 20. PL spectra of 0.12% doped sample at room temperature (red) and at 77K (black). Inset: Images of the sample taken out immediately from liquid nitrogen (left) and at room temperature (right).	35
Figure 21. PL spectra of <i>pm</i> (black) and <i>pz</i> (red) doped 1D-CuBr(<i>py</i>). $\lambda_{ex}=360\text{nm}$	36
Figure 22. CIE coordinates of all white-light-emitting structures. Inset: photos of the LED bulbs under working condition. 2a-2h are labeled as increasing <i>pz</i> doping level.....	37

Figure 23. Schematic illustrating the design and construction of CuI(L) hybrid structures with a Cu ₂ I ₂ molecular dimer precursor: (a) 0D cluster, (b) 1D single chain, (c) 1D double chain, and (d) 2D layered network. Color scheme of the balls: purple, I; cyan, Cu; dark blue, N; grey, C; light green, Cl; small green, P; big green, <i>tpp</i> molecule.....	45
Figure 24. Optical absorption spectra of the precursor at solid state (red) and dissolved in acetone solution (black).....	48
Figure 25. TG profiles of selected 0D (black), 1D (blue) and 2D structures (red).	51
Figure 26. Luminescence decay profile (log scale) of 1D-Cu ₂ I ₂ (<i>tpp</i>) ₂ (<i>bpp</i>).....	53
Figure 27. PXRD patterns of 2D-Cu ₂ I ₂ (4,4'- <i>dps</i>) ₂ after various treatments. From bottom to top: simulated, freshly made, in air for six month, under blue light for a week, heated at 80 °C for a week.	56
Figure 28. PXRD patterns of compounds from bottom to top: 0D-Cu ₂ I ₂ (3- <i>pc</i>) ₄ , 0D-Cu ₂ I ₂ (3,5-dm-py) ₄ , 0D-Cu ₂ I ₂ (3- <i>Cl</i> -py) ₄ , 0D-Cu ₂ I ₂ (<i>tpp</i>) ₂ (3- <i>pc</i>) ₂ , 0D-Cu ₂ I ₂ (<i>tpp</i>) ₂ (4,6-dm-pm) ₂ , 1D-Cu ₂ I ₂ (<i>tpp</i>) ₂ (<i>bpp</i>).....	57
Figure 29. PXRD patterns of compounds 1D-Cu ₂ I ₂ (<i>tpp</i>) ₂ (4,4'- <i>dps</i>), 1D-Cu ₂ I ₂ (<i>tpp</i>) ₂ (4,4'- <i>bpy</i>), 1D-Cu ₂ I ₂ (<i>tpp</i>) ₂ (<i>pz</i>), 1D-Cu ₂ I ₂ (5-me-pm) ₂ , 2D-Cu ₂ I ₂ (<i>bpe</i>) ₂ , 2D-Cu ₂ I ₂ (3,3'- <i>bpy</i>) ₂ , 2D-Cu ₂ I ₂ (4,4'- <i>dps</i>) ₂	58
Figure 30. Emission spectrum of 2D-Cu ₂ I ₂ (4,4'- <i>dps</i>) ₂ after various treatments. From bottom to top: freshly made (black), in the air for six month (red), under blue light for a week (blue), at 80 °C for a week (cyan). λ_{ex} is 455 nm.	59
Figure 31. Photoluminescence spectra (λ_{ex} = 360 nm) of selected compounds.	60
Figure 32. Luminescence spectra of the two-component phosphors with the following weight percentage of 1D-Cu ₂ I ₂ (<i>tpp</i>) ₂ (<i>dps</i>): 0 wt% (black), 5 wt% (red), 15 wt% (blue), 25 wt% (green), 100 wt% (pink).....	61

Figure 33. LED bulbs design and displayed at working condition.....	62
Figure 34. Illustration of the grinding synthesis.	67
Figure 35. Images taken of grinding $1\text{D-Cu}_2\text{I}_2(\text{tpp})_2(2\text{-pr-pz})$ under UV light.	69
Figure 36. PXRD patterns of selected structures compared with the starting materials. From bottom to top: commercial CuI, commercial <i>tpp</i> , as made $0\text{D-Cu}_2\text{I}_2(\text{tpp})_3$, simulated $0\text{D-Cu}_2\text{I}_2(\text{tpp})_2(3\text{-pc})_2$, as made $0\text{D-Cu}_2\text{I}_2(\text{tpp})_2(3\text{-pc})_2$, simulated $1\text{D-Cu}_2\text{I}_2(\text{tpp})_2(2\text{-me-pz})$, as made $1\text{D-Cu}_2\text{I}_2(\text{tpp})_2(2\text{-me-pz})$	71
Figure 37. PXRD patterns. From bottom to top: $0\text{D-Cu}_2\text{I}_2(\text{tpp})_2(4\text{-pc})_2$, $0\text{D-Cu}_2\text{I}_2(\text{tpp})_2(3\text{-pc})_2$, $0\text{D-Cu}_2\text{I}_2(\text{tpp})_2(\text{py})_2$, $0\text{D-Cu}_2\text{I}_2(\text{tpp})_2(4,6\text{-dm-pm})_2$, $0\text{D-Cu}_2\text{I}_2(\text{tpp})_2(4\text{-me-pm})_2$, $0\text{D-Cu}_2\text{I}_2(\text{tpp})_2(3\text{-Br-py})_2$	72
Figure 38. PXRD patterns. From bottom to top: $1\text{D-Cu}_2\text{I}_2(\text{tpp})_2(\text{pm})$, $1\text{D-Cu}_2\text{I}_2(\text{tpp})_2(2,5\text{-dm-pz})$, $1\text{D-Cu}_2\text{I}_2(\text{tpp})_2(2\text{-pr-pz})$, $1\text{D-Cu}_2\text{I}_2(\text{tpp})_2(2\text{-me-pz})$, $0\text{D-Cu}_2\text{I}_2(\text{tpp})_2(1\text{-me-bzim})_2$	73
Figure 39. Mixture of CuI, <i>tpp</i> and <i>4,6-dm-pm</i> without applying mechanochemical force. Image was taken under UV bar (365nm) after the liquid N-ligand was completely dried.....	75
Figure 40. PXRD patterns of various phases. From bottom to top: simulated $0\text{D-Cu}_2\text{I}_2(3\text{-pc})_4$, as made $0\text{D-Cu}_2\text{I}_2(3\text{-pc})_4$, simulated $0\text{D-Cu}_4\text{I}_4(3\text{-pc})_4$, as made $0\text{D-Cu}_4\text{I}_4(3\text{-pc})_4$, simulated $1\text{D-CuI}(3\text{-pc})$, as made $1\text{D-CuI}(3\text{-pc})$, simulated $0\text{D-Cu}_2\text{I}_2(\text{tpp})_2(3\text{-pc})_2$, and final product $0\text{D-Cu}_2\text{I}_2(\text{tpp})_2(3\text{-pc})_2$, after grinding of the three-phase mixture.	76
Figure 41. Two possible reaction pathways for the formation.	77
Figure 42. Top: Product of $0\text{D-Cu}_2\text{I}_2(\text{tpp})_2(3\text{-pc})_2$, prepared by ball-milling under UV radiation. Bottom: PXRD patterns of $0\text{D-Cu}_2\text{I}_2(\text{tpp})_2(3\text{-pc})_2$, from bottom to top: simulated pattern, sample prepared by manual grinding, and sample prepared by ball milling.....	79

Figure 43. Optical absorption spectra of 0D-Cu ₂ I ₂ (<i>tpp</i>) ₂ (<i>3-pc</i>) ₂ , (blue), 0D-Cu ₂ I ₂ (<i>tpp</i>) ₂ (<i>4-me-pm</i>) ₂ (cyan), 1D-Cu ₂ I ₂ (<i>tpp</i>) ₂ (2,5-dm-pz) (yellow), 1D-Cu ₂ I ₂ (<i>tpp</i>) ₂ (2-me-pz) (orange) at room temperature.....	81
Figure 44. PL spectra of 0D-Cu ₂ I ₂ (<i>tpp</i>) ₂ (<i>3-pc</i>) ₂ , (blue), 0D-Cu ₂ I ₂ (<i>tpp</i>) ₂ (<i>4-me-pm</i>) ₂ (cyan), 1D-Cu ₂ I ₂ (<i>tpp</i>) ₂ (2,5-dm-pz) (yellow), 1D-Cu ₂ I ₂ (<i>tpp</i>) ₂ (2-me-pz) (orange) at room temperature; $\lambda_{\text{ex}} = 360$ nm.	82
Figure 45. Emission spectrum of the white phosphor composite obtained by one-step synthesis. Inset: CIE coordinates of the composite.....	86
Figure 46. Green chemistry logo prepared by spray coating of the samples on black plastic substrate. (left) and prototype LED lamps at “off” (top) and “on” (bottom) conditions (right).....	87
Figure 47. Illustration of precursor approach for the syntheses of monomer based structures.	93
Figure 48. (a) TG profile of 0D-CuI(<i>3-pc</i>) ₃ (black), 0D-CuI(<i>tpp</i>) ₂ (<i>1-et-im</i>) (red), 1D-CuI(<i>tpp</i>)(<i>bbipe</i>) _{0.5} (blue). Inset: selected samples in water under UV irradiation (365nm). (b) PXRD patterns. From bottom to top: simulated 1D-CuBr(<i>tpp</i>)(<i>bbipe</i>) _{0.5} , as made 1D-CuBr(<i>tpp</i>)(<i>bbipe</i>) _{0.5} , 1D-CuBr(<i>tpp</i>)(<i>bbipe</i>) _{0.5} soaked in water for 7 days. 1D-CuBr(<i>tpp</i>)(<i>bbipe</i>) _{0.5} heated at 100 °C for 7 days. (c) PL spectra of selected compounds. From bottom to top: excitation and emission spectra of 0D-CuI(<i>tpp</i>) ₂ (<i>1-et-im</i>), 0D-CuI(<i>tpp</i>) ₂ (<i>2-etox-pz</i>), 0D-CuI(<i>tpp</i>) ₂ (<i>2-pr-pz</i>). $\lambda_{\text{ex}} = 360$ nm λ_{em} = peak wavelengths of their emission spectra. (d) 3D plot of the optical data of 0D-CuI(<i>tpp</i>) ₂ (<i>1-et-im</i>) (blue), 0D-CuI(<i>tpp</i>) ₂ (<i>2-etox-pz</i>) (cyan), 0D-CuI(<i>tpp</i>) ₂ (<i>2-pr-pz</i>) (pink), 0D-CuI(<i>tpp</i>) ₂ (<i>dipe</i>) _{0.5} (dark blue), 0D-CuBr(<i>tpp</i>) ₂ (<i>dipe</i>) _{0.5} (purple), 1D-CuI(<i>tpp</i>)(<i>bbipe</i>) _{0.5} (yellow), 1D-CuBr(<i>tpp</i>)(<i>bbipe</i>) _{0.5} (dark yellow).	97

Figure 49. Synthetic approach I, II and III used to prepare cationic ligands with free binding sites marked in red.	102
Figure 50. Examples of inorganic anionic cluster motifs obtained for AIO type of compounds.....	108
Figure 51. QY scaled emission spectra of $\text{Cu}_4\text{I}_6(\text{pr-ted})_2$ (red) and $\text{Cu}_4\text{I}_8(\text{di-et-ted})_2$	111
Figure 52. Emission spectra of $\text{Cu}_4\text{I}_6(\text{pr-ted})_2$ (top) and $\text{Cu}_4\text{I}_6(\text{tpp})_2(\text{btmm})_2$ (bottom) at various temperatures ($\lambda_{\text{ex}} = 360 \text{ nm}$).	113
Figure 53. Optical absorption spectra of compounds in sub group (I).	114
Figure 54. Optical absorption spectra of compounds in sub group (II).....	115
Figure 55. Excitation and emission spectra of all compounds.	116
Figure 56. Energy diagrams of (a) compound $\text{Cu}_4\text{I}_6(\text{pr-ted})_2$ indicating phosphorescence and (b) compound $\text{Cu}_4\text{I}_6(\text{tpp})_2(\text{btmm})_2$ indicating TADF and phosphorescence emission processes. The approximate time constants for internal conversion (IC) and intersystem crossing (ISC) are indicated along with the approximate time constants for TADF and phosphorescence which are extracted from the measured PL lifetime decay times.....	118
Figure 57. Density of states (DOS) plots for compounds $\text{Cu}_5\text{I}_7(\text{i-pr-ted})_2$ and $\text{Cu}_2\text{I}_4(\text{mtp})_2$. Line color scheme: dashed black: total; cyan: Cu (3d); pink Cu (4s); red: I (5p); purple I (5d); blue: N (2p); black: C (2p).	120
Figure 58. TG plots of structures in sub group (I). $\text{Cu}_3\text{I}_5(\text{bz-ted})_2$ (black), $\text{Cu}_4\text{I}_6(\text{3-Cl-pr-ted})_2$ (red), $\text{Cu}_4\text{I}_6(\text{pr-ted})_2$ (blue), $\text{Cu}_4\text{I}_6(\text{2-Br-et-ted})_2$ (green), $\text{Cu}_5\text{I}_7(\text{i-pr-ted})_2$ (pink), $\text{Cu}_6\text{I}_8(\text{bu-ted})_2$ (gold).	121
Figure 59. TG plots of structures in sub group (II). $\text{Cu}_2\text{I}_4(\text{mtp})_2$ (black), $\text{Cu}_4\text{I}_6(\text{tpp})_2(\text{btmm})_2$ (red), $\text{Cu}_4\text{I}_6(\text{tpp})_2(\text{btmdme})_2$ (blue), and $\text{Cu}_6\text{I}_8(\text{btmdb})_2$ (green).	122

Figure 60. Plots of IQY ratios (Q_0 and Q are IQY values measured before and after heating the sample at 100 °C in air as a function of time). Inset is the plot of ratios of the IQY values after and before exposing to UV light as a function of time. Blue: 0D- $\text{Cu}_2\text{I}_2(\text{py})_4$, green: 0D- $\text{Cu}_4\text{I}_6(\text{py})_4$, red: $\text{Cu}_4\text{I}_6(\text{pr-}ted)_2$, black: $\text{Cu}_4\text{I}_6(\text{tp})_2(\text{btmm})_2$ 123

Figure 61. (a) Image of compound $\text{Cu}_4\text{I}_6(\text{pr-}ted)_2$ completely dissolved in DMF solution. (b) Thin film prepared using compound $\text{Cu}_4\text{I}_6(\text{pr-}ted)_2$ emitting green color under UV illumination. (c) Bright-field micrograph image of the spin-coated film of $\text{Cu}_4\text{I}_6(\text{pr-}ted)_2$. (d) AFM image of the thin film collected in tapping mode. (e) Illuminating LED light bulbs (110 V, 2 W) coated by selective AIO phosphors..... 124

1. Introduction

Solid-state lighting (“SSL”) technology in the form of light-emitting diodes (“LEDs”) generates high-efficient light sources, converts electricity into light up to 25% more effectively than conventional lighting sources.¹ The U.S. Department of Energy has estimated that switching to LED lighting over the next two decades could save the country \$250 billion in energy costs over that period; this reduces the electricity consumption for lighting by nearly one half, and avoid 1,800 million metric tons of carbon emission.² The essential elements of LEDs are an electron-carrying n-layer and a hole-carrying p-layer. When a forward voltage is applied to the structure (negative to the n-layer and positive to the p-layer), electrons are injected from the n-layer and holes from the p-layer.³ Electrons and holes can radiatively recombine, emitting a photon. The wavelength and color of the photon is determined by the difference in the energy levels of the electrons and holes.

The idea of LED was first demonstrated by Nick Holonyak Jr, working at General Electric in 1962 and the physics behind was able to be explained by the end of 1970s. In the following 20 years, LED technology had experienced fast development and during the 1990s, and three primary color (red, green and blue) LEDs with high brightness had been successfully produced.^{4,5} In the following decade, LED devices were viable choices for a variety of applications ranging from monochrome signaling (e.g. traffic lights) to computer display and began to be considered as a potential source of white light to replace incandescent lamps for general lighting purposes. Common approaches to produce WLEDs include blending of three primary colored LEDs, namely red, green, and blue (“RGB”)

diode.⁶⁻¹⁴ This process requires complicated doping/mixing and delicate control of multiple materials and colors, which proves both challenging and costly.

At present, commercially available WLEDs are predominantly phosphor based (e.g. a yellow-emitting phosphor, yttrium aluminum garnet or YAG: Ce³⁺, coupled with a blue-emitting InGaN/GaN diode).¹⁵⁻¹⁷ While less expensive than the RGB diodes, the YAG: Ce³⁺ type phosphors and WLEDs are still more costly than that of their conventional counterparts due to the dependence on the rare earth elements (REEs) that are in potential supply shortage, and the lack of their recyclability which is destructive to the environment. Nowadays, about 20 percent of global REEs are used in clean energy technologies. Among them lanthanum, cerium, europium, terbium and yttrium are the important components used in the phosphors for energy-efficient lighting. Since the demand for REEs as an input for different technologies is increasing, their prices have been rising constantly and make the cost issue even more crucial.¹⁸ In addition to the cost issue, the YAG:Ce³⁺ type WLEDs also suffers from unsuitability for solution process, poor color rendering index (CRI) and high correlated color temperature (CCT) which limit their widespread commercialization in general lighting market.¹⁷ These issues make developing cost effective yellow light phosphor that can replace YAG:Ce³⁺ that are solution-processable and, REEs free, a great interest worldwide. Also people started pursuing the direct white-light-emitting phosphors under UV excitation which are not only solution-processable and REEs free but with better light quality such as higher CRI and low CCT.

Crystalline inorganic–organic hybrid materials are both fundamentally and technologically important due to the fact that they integrate the functionality of inorganic compounds and the advantages of organic species into a single-crystal lattice.^{19,20} A number of structure systems have been reported to date and are of great use for energy-related applications. One

of the most famous examples is inorganic-organic perovskites, due to the recent intensive development of their photovoltaic (PV) properties.¹⁹⁻²³ Structurally, the interactions between inorganic and organic species in perovskite hybrids are primarily ionic, accompanied with relatively weak hydrogen-bonds or van der Waals forces in some cases. The most well-studied example in this system, three dimensional (3D) $\text{CH}_3\text{NH}_3\text{PbI}_3$, exhibits significant promise for high performance and low-cost solar cells due to its unique properties such as extremely high optical absorption, small effective masses for electrons and holes, etc.²⁴ The organic component of the hybrid, methyl ammonium cation, may also play a role in the special suitability of the hybrid materials for photovoltaic (PV) application, through a low barrier to reorientation within the structure and contributions to the dielectric/ferroelectric properties. Other lower dimensional (0D, 1D or 2D) perovskite hybrid structures have also been reported and studied, and interesting optical, electrical and magnetic properties have been discovered and investigated in these materials.²³

Since 2000, a unique and unprecedented family of nanostructured inorganic-organic hybrid semiconductors based on II-VI binary compounds has been developed by our group.²⁵⁻²⁷ These materials are crystalline compounds and possess strong covalent-bonding interactions between inorganic and organic components. The inorganic components in these hybrid structures are subnanometer-sized building units of II-VI semiconductors, while the mono-/diamine molecules serve as organic linkers or spacers that act as structure-directing agents.²⁷ By varying the composition and dimensionality of inorganic component and by using different organic amine molecules, over 100 members of this family have been synthesized and structurally characterized in a variety of 1D, 2D, and 3D network structures. Their optical properties have been studied, and most of them exhibit strong structure-

induced quantum confinement effect (QCE) brought about as a result of modular nature of perfectly ordered and alternating inorganic and organic motifs at nanometer or subnanometer scale. The insulating organic amine molecules serve as passivating agents (as in the cases of colloidal quantum dots synthesis) and thus, prevent interactions between the neighboring inorganic motifs.²⁵ Since the organic passivating molecules bond to the inorganic nanostructural motifs in a periodically ordered fashion, the QCE takes place within a macroscopic crystalline particle (polycrystal or single crystal), giving rise to a very large increase in their band gaps.²⁵ These attractive features make them promising candidates for various optoelectronic applications.

In the past decade, our efforts have been focused on developing REEs free lighting phosphors for SSL applications, which is environmentally friendly and being considered as a future-generation lighting technology. Very interestingly, some members from II-VI family exhibit direct broadband white light emission under UV light excitation at room temperature. In 2008, we reported the first semiconductor bulk material, namely the double layered 2D- $[\text{Cd}_2\text{S}_2(\text{ba})]$ (ba = butyl-amine) structure that generates direct white light with a IQY of around 4-5%.²⁸ Since these materials can be processed in bulk form, there is no issue related to the particle size that must be addressed in the cases of nanocrystals. After that, much efforts have been devoted to enhancing the IQYs of these structures, and later in 2012, we reported double layered $\text{Zn}_{1.7}\text{Cd}_{0.3}\text{S}_2(\text{oa})$ with 0.08 mol% Mn doping that yielded a IQY of 31-37%, exhibits a 8 fold increase compared to the previous work.²⁹ Other luminescent inorganic-organic hybrid materials based lead-halide perovskites have also been reported by Karunadasa and Bi, exhibiting potentials as lighting phosphors.^{30,31} However, the performances of these materials are still far away for practical applications when compared

to commercial phosphors, which encouraged us to explore new materials with better emitting properties.

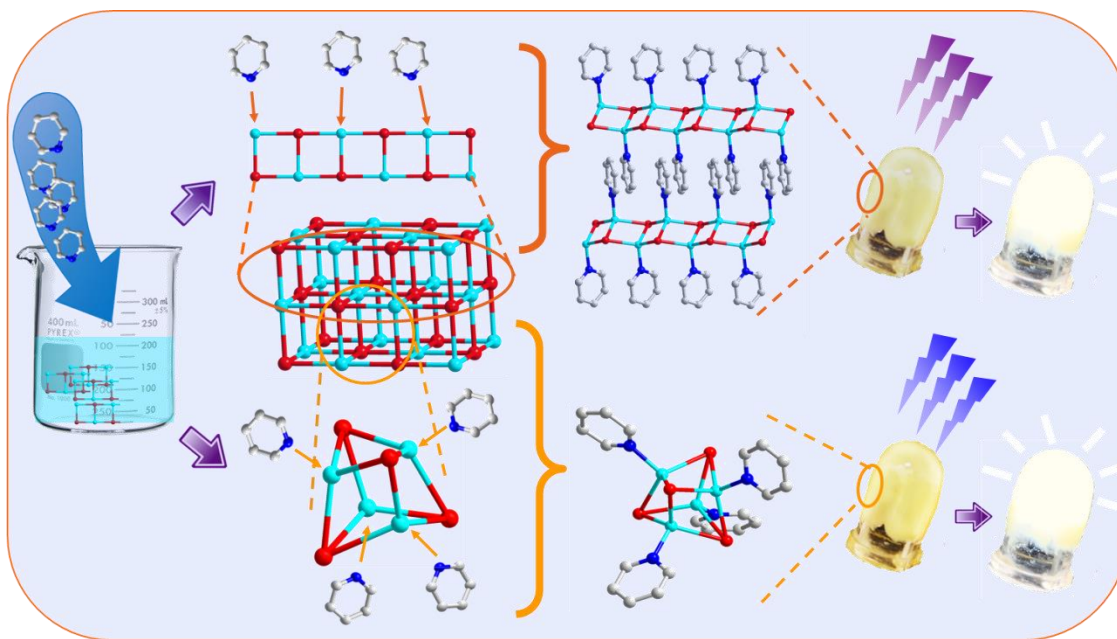


Figure 1. The design of inorganic-organic hybrid materials based for general lighting applications.

Copper halide (I-VII) based inorganic-organic hybrid materials are particular interesting due to their structure diversity, optical tunability and facile synthesis, and was considered as promising materials for LED phosphors.^{10,32,33} These hybrid materials are generally constructed though Cu-N/P/S covalent bond by reacting copper iodide with either aromatic or aliphatic organic ligands. Based on the coordination mode between the inorganic and the organic component, and the charge of the two components, we classify these materials into three types (Fig. 2): (i) when both the inorganic and organic components are neutral and they

are connected by coordination bonds, and they are called neutral or Type I structure; (ii) when both the two components are charged and they are no coordination bonds between them, we called them ionic or Type II structures; (iii) when both the two components are charged and they are connected by coordination bonds, they are classified as all-in-one (AIO) or Type III structures, which are new and developed by us.

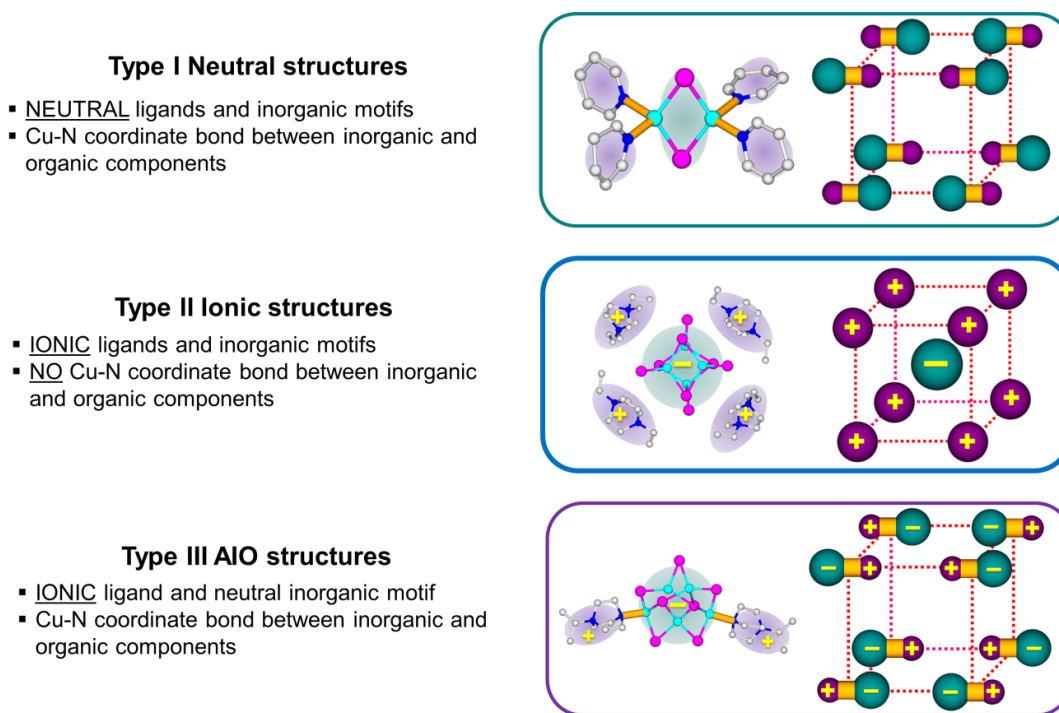


Figure 2. Illustration and introduction of the three types of copper halide based structures.

To meet the requirements as phosphors for SSL, the materials should have a number of characteristics, such as high internal quantum yields (IQYs), high photo-/thermal stability and optical tunability, etc., and our strategy to develop CuI based phosphors have been focusing on addressing these requirements. There have been quite a few research papers since 1970s reporting novel copper iodide based neutral inorganic-organic hybrid structures,

and their structural types are diverse. However, most of them could be classified into four sub-groups based on the difference of their inorganic modules with a variety of coordinating organic ligands (Fig. 3).

- (1) CuI monomer based structures
- (2) Cu_2I_2 rhomboid dimer based structures
- (3) Cu_4I_4 cubane tetramer based structures
- (4) CuI staircase chain based structures

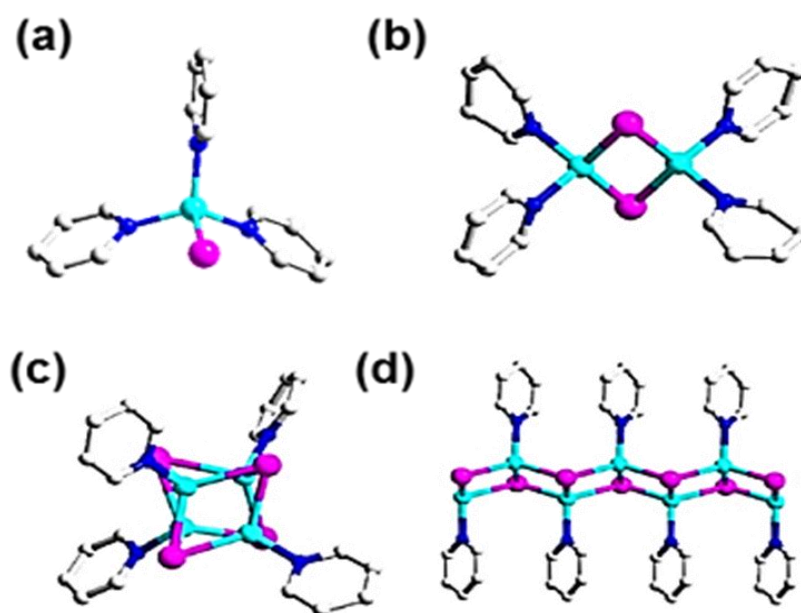


Figure 3. Typical structures of a monomer 0D-CuI(py)₃, a rhomboid dimer 0D-Cu₂I₂(py)₄, a cubane tetramer 0D-Cu₄I₄(py)₄, a staircase chain 1D-CuI(py).

Such structural diversity and types could be simply illustrated by reaction of CuI with a simple N-ligand pyridine (*py*), which may lead to a number structures depending on the reaction condition and stoichiometry (Fig. 3). When the ligand *py* is in excess, compounds of stoichiometry 1:1:3 or 1:1:2 Cu(I):I:L ratio will be formed, and they are 0D-CuI(*py*)₃ monomer and 0D-Cu₂I₂(*py*)₄ dimer. CuI mononuclear module is the simplest module and reported structures of this type are generally molecular clusters which each copper atom coordinates to three ligand molecules and one iodine atom. Cu₂I₂ rhomboid dimer is another well-known inorganic module, which each copper atom coordinates to two iodide atoms and two ligand molecules. Under ligand deficient condition, on the other hand, the 1:1:1 Cu(I):I:L ratio compounds will be formed and they are also two types. One is 0D-Cu₄I₄(*3-pc*)₄ cubane cluster with the most common inorganic module Cu₄I₄ distorted cubic tetramers, which can also be considered as two Cu₂I₂ dimer fragments oriented perpendicular to each other. In the inorganic motif, each copper atom coordinates to three iodine atoms and one ligand. Both Cu₂I₂ rhomboid dimer and Cu₄I₄ cubane tetramer may be built in 0D molecular clusters with monodentate ligands or 1D to 3D extended networks with multidentate ligands. Except those with cluster-based inorganic motif, the other structure with 1:1:1 Cu(I):I:L ratio is 1D-CuI(*py*) with the inorganic module as infinite staircase chain that can be viewed as an electronically neutral infinite ribbon cut from the parent CuI rock salt type structure. Such staircase chains could also be connected to form 2D networks by bidentate ligands. Besides those, when heating CuI, *py* and methanol as the solvent at 150 °C for three days, the *py* would go through in-situ alkylation and formed ionic structures with CuI. Ionic structures can be considered as “ligand-free” structures as the inorganic and organic components are separated and there is no covalent bonding between them. Therefore, there are lots of factors including the starting materials, solvents used, temperature etc., would influence the

formation of final products. These structures can also be classified by their dimensions, from 0D clusters to 1D chains, and from 2D sheets to three dimensional 3D frameworks.

These materials generally exhibit interesting luminescence properties based on their inorganic motifs and the organic ligands coordinated (Fig. 4). The luminescence mechanisms of these structures vary based on the structural types of the inorganic modules as well as the characteristics and the organic ligands. It has been accepted that the luminescence mechanism of these compounds are generally from metal-to-ligand charge transfer (MCLT), halide-to-ligand charge transfer (XLCT) or cluster centered (CC), or a combination of them. Typically, the luminescence of CuI monomer, dimer, trimer and chain based structures are from a combination of MCLT and XLCT, while the emission of Cu_4I_4 cubane tetramers is from a combination of XLCT and CC.³⁴

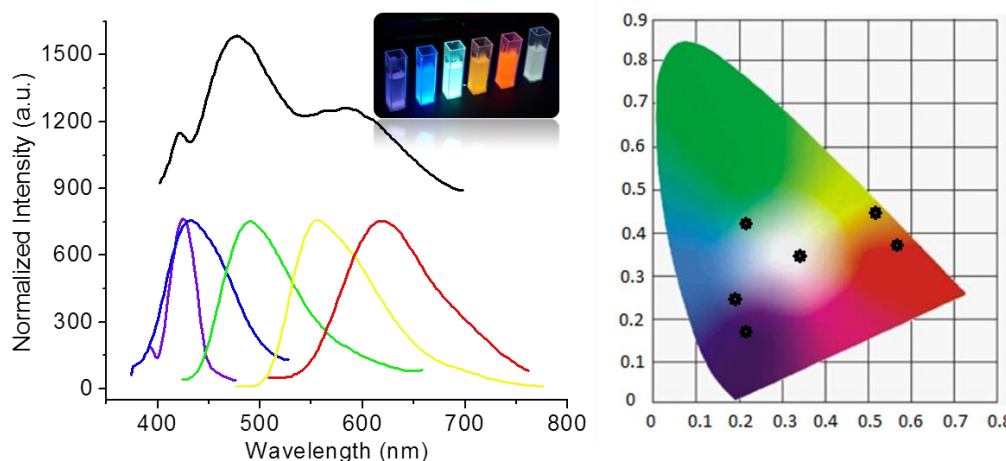


Figure 4. The emission spectra of 1D-CuI(L) staircase chain with different ligands coordinated (left) and their CIE coordinates (right).

The thermal stability of these materials is generally determined by thermal gravimetric analysis (TGA). The decomposition starts from the breaking down of the Cu-ligand bonds. Their stability is determined by their structural types and the ligands coordinated. Molecular clusters have very poor stability though they are very luminescent. Extended structures have much better stability compared to molecular species with the same inorganic module. Ionic structures have better stability compared to neutral structures; however, they are poor emitters. The AIO type of structures combines the advantages of neutral clusters and the ionic structures, with strong luminescence and high stability and is considered as the most promising and best-performing phosphors to date.

My work overall could be divided into five parts. The first work discussed in Chapter 2 is the study of the copper bromide staircase chain based structures and white-light-emission achieved by ligand doping. I found out that the broadband emission is from single crystals, which prove that the emission is from the bulk phase of the materials. Then I have done a systematic study on Cu_2I_2 dimer based structures and have developed a “bottom-up” synthetic strategy. This strategy could achieve rational design and prevent the formation of by-products. Relevant work will be covered in Chapter 3. In Chapter 4, I developed mechanochemical preparation of these materials for the purpose of large-scale and green synthesis. In Chapter 5, a family of copper halide monomer based structures has been synthesized and their performance has been studied. Chapter 6 discusses the development of AIO type of structures and their performance as lighting phosphors.

2. 1D copper bromide staircase chain based structures for white light emissions

2.1. Background

Recently, single-source, non-rare-earth, direct white-light-emitting phosphors have been developed and are attracting attention due their potential usages for lighting-related applications.^{28,35-38} These types of phosphors aim to overcome the issues for current white light LEDs fabricated by YAG: Ce, generating white light of higher quality with lower CCT values. Several types of materials have been reported till date and exhibit intriguing promises. It is reported that nanocrystal quantum dots emit white light in their bulk phases.³⁹⁻⁴¹ However, their quantum yields are low and their emissions are highly dependent on their particle sizes, which require complicated synthetic procedures for particle size control. Moreover the aggregation of the nanoparticles over time would lead to emission change, limiting their practical use. In this regard, inorganic-organic hybrid semiconductors are a unique family of semiconductor bulk materials that exhibit enhanced properties with respect to their parent structures.^{20,21,25,26,42,43} Unique properties, especially luminescence, would emerge as a result of combining both the inorganic and organic component together in a single crystal lattice.^{28,44,45}

Our recent study on I-VII binary metal halides (Cu, Ag and I, Br, Cl) based inorganic-organic hybrid semiconductors demonstrates their potentials as phosphors for modern lighting devices.⁴⁵⁻⁴⁸ They have a number of advantages compared to commercial phosphors and other reported ones, such as strong luminescence, earth abundancy, rare-earth free, and their facile one-step syntheses. The emission profiles of nearly all of these structures are single-band type, with full width at half maximum (FWHM) of around 50-100nm.,^{34,49} A

broadened emission spectra could be achieved by doping of a secondary ligand based our earlier study.⁴⁵ Herein, I expanded our understanding on a new series of doped copper (I) bromide based inorganic-organic hybrid materials with the general formula $1D-CuBr(py)_{1-x}(pz\text{ derivatives})_x$ ($x < 0.01$). These materials tunable white light emissions as well as significantly enhanced internal quantum yields (IQYs), a 6-fold improvement compared to our previous work.⁴⁵ A comprehensive study has been done by varying doping level and altering dopants with different functional groups and it is demonstrated that the overall light quality is adjustable. Blueish (“cold”) to yellowish (“warm”) white light from single crystals of these structures were achieved, indicating the white light is intrinsically from single phase bulk materials. Moreover, reversible thermochromic behavior was observed for all white-light-emitting compounds and this is the first time that such behavior is reported in copper halide staircase chain based structures. The advantages of high quantum efficiencies, facile synthesis and emission tunability make this type of phosphors promising candidates as lighting phosphors, and the thermochromic property may leads to new applications of these materials.

2.2 Diffusion synthesis for single crystal growth and ligand doping approach

Single crystals of $1D-CuBr(3,5-dm-py)$, $1D-CuBr(py)$, $1D-CuBr(3-Cl-py)$ and $1D-CuBr(3-Br-py)$ were acquired by a layering method. The reactions were conducted in glass vials or tubes. The bottom, middle and top layers were $CuBr/KBr$ saturated aqueous solution, acetonitrile, and ligand in ethanol, respectively. The crystals formed in the middle layer over 3-5 days at room temperature. Pure phase powder samples were obtained by direct mixing of $CuBr$ (0.1mmol) in saturated KI solution with ligand (0.1mmol) in ethanol. The pure phase

powder generally formed immediately after stirring. 0D- $\text{Cu}_2\text{Br}_2(3,5\text{-dm-py})_4$ and 1D- $\text{Cu}_2\text{Br}_2(5\text{-Br-py})_2$ were obtained under the same reaction conditions, except the ligands added were in excess.



Figure 5. Layerd approach for growing single crystal of both parent and doped structure (left). Crystals fromed in the middle layer as shown in the photo (right).

Various approaches have been developed for the syntheses of copper halide based structures and as far as we know, layering methods was the most ideal for staircase chain based structures. Various *py* derivatives with different functional groups were used in the syntheses. Slow mixing of CuBr in saturated KBr solution with the ligands in ethanol at room temperature would quickly form the powder products. To slow down the reaction process for fine crystal growth, a third solvent, namely acetonitrile was used between the above two solutions. It is worth mentioning that the amount of ligands added has notable influence on the final product. Chain based structures would be formed preferably in ligand deficient conditions, so ligands must be added slowly into the CuBr solution in order to avoid the formation of other types of structures. Adding the ligand quickly or in excess amount might lead to the formation of Cu_2Br_2 dimer based structures.

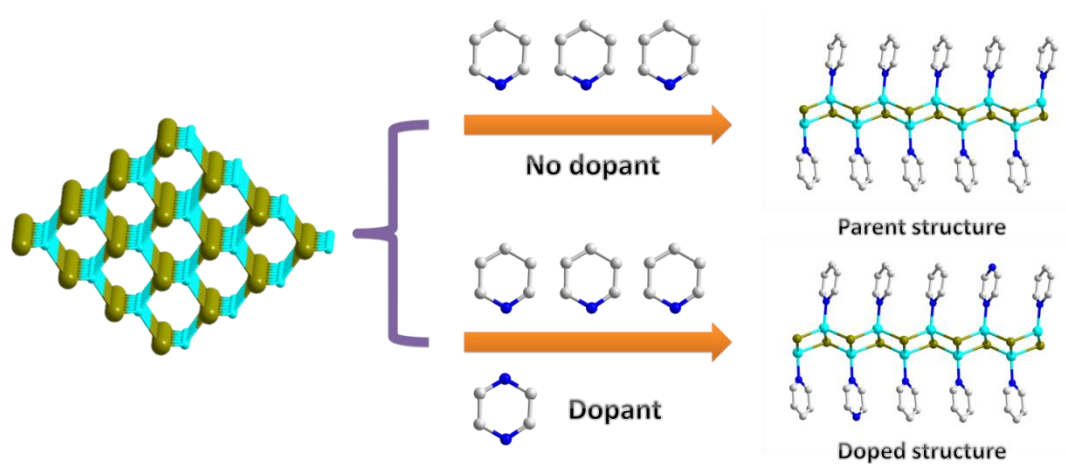


Figure 6. Illustration of the design strategy of the parent and doped structures.

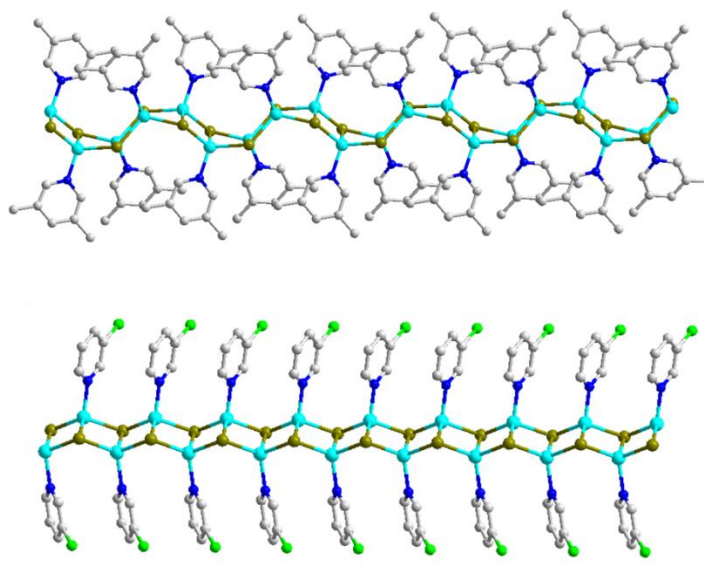


Figure 7. Structural plot of 1D-CuBr(3,5-dm-py) (Top) and 1D-CuBr(3-Cl-py) (bottom).

Table 1. Summary of crystal data of CuBr based new structures.

Compound	1D- CuBr(3,5- <i>dm-py</i>)	1D-CuBr(3- <i>Cl-py</i>)	1D-CuBr(3- <i>Br-py</i>)	0D-Cu ₂ Br ₂ (3,5- <i>dm-py</i>) ₄	1D-Cu ₂ Br ₂ (5- <i>Br-pm</i>) ₂
Empirical Formula	C ₇ H ₉ BrCuN	C ₅ H ₄ BrClCuN	C ₅ H ₄ Br ₂ CuN	C ₂₈ H ₃₆ Br ₂ Cu ₂ N ₄	C ₈ H ₆ Br ₄ Cu ₂ N ₄
FW	250.60	256.99	301.44	715.51	604.87
Space Group	C2/c	P2 ₁ /n	P2 ₁ /n	C2/c	Pbcn
a (Å)	13.910(17)	8.7438(19)	8.720(9)	17.823(11)	16.1765(16)
b (Å)	15.111(18)	3.9296(9)	3.933(4)	9.271(6)	8.3154(8)
c (Å)	8.107(10)	21.002(5)	21.11(2)	20.329(13)	21.382(2)
A(°)	90.00	90.00	90.00	90.00	90.00
B(°)	99.455(17)	100.837(3)	100.603(13)	114.054(10)	90.00
γ(°)	90.00	90.00	90.00	90.00	90.00
V (Å ³)	1681(4)	708.7(3)	711.6(12)	3068(3)	2876.2(5)
Z	8	4	4	4	8
T (K)	298(2)	298(2)	298(2)	298(2)	298(2)
λ(Å)	0.71073	0.71073	0.71073	0.71073	0.71073
R ₁	0.0396	0.0306	0.0479	0.0423	0.0351
wR ₂	0.0973	0.0817	0.1207	0.0868	0.0809
CCDC #	1506745	1506742	1506741	1506743	1506744

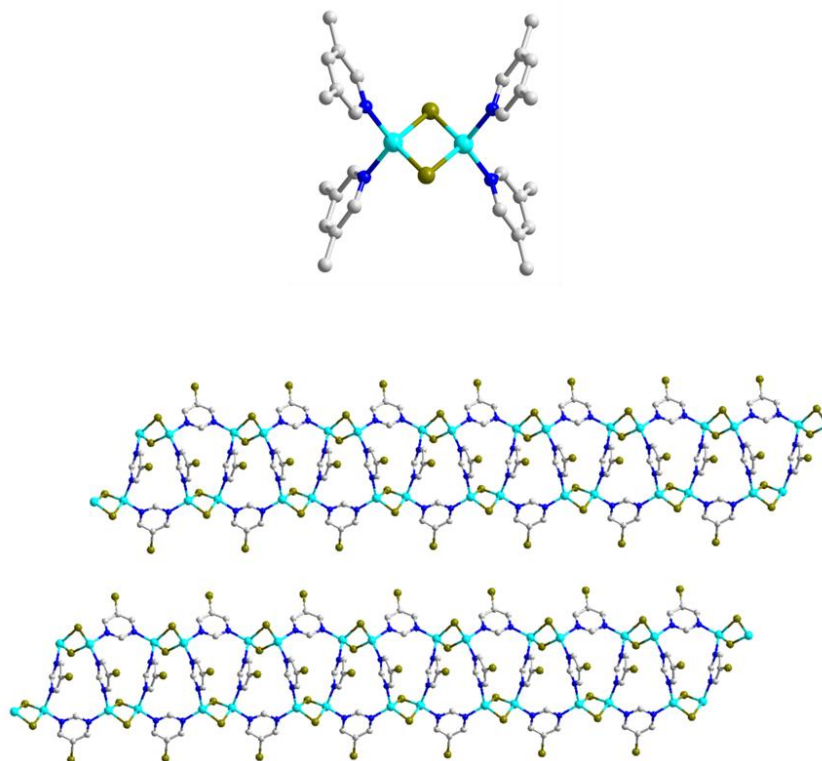


Figure 8. Structure plot of 0D-Cu₂Br₂(3,5-*dm-py*)₄ (top) and 0D-Cu₂Br₂(3,5-*dm-py*)₄ (bottom).

2.3 Optical tunability and white light

Attempts to synthesize copper bromide based hybrid semiconductors lead to the formation of six compounds with four of them staircase chain based structures (Fig 7), and two of them dimer based structures (Fig. 8). Their crystallographic data of new structures are listed in Table 1. Optical measurements based on these structures indicate that they all monochromatic emitters, with emissions ranging from blue to red (Fig 9). Based on our previous trials, one dimensional (1D) staircase chain type of structures are more likely to be doped, possibly due to the parent ligands coordinated to the infinite chains are easier to be replaced by the dopant ligands. Therefore, 1D-CuBr(*py*) was chosen as the parent structure for doping study, since it exhibit intense blue-green emission ($\lambda_{em} = 495$ nm) under near-UV

excitation ($\lambda_{\text{ex}} = 360 \text{ nm}$) with IQY as high as 48%. Adding trace amount of pyrazine (pz) together with the parent ligand py in the synthesis afforded doped structures $1\text{D-CuBr}(py)_{1-x}(pz)_x$ ($x < 0.01$). The PXRD analyses confirm that those doped structures remain iso-structural to their parents structure $1\text{D-CuBr}(py)$ (Fig. 10).

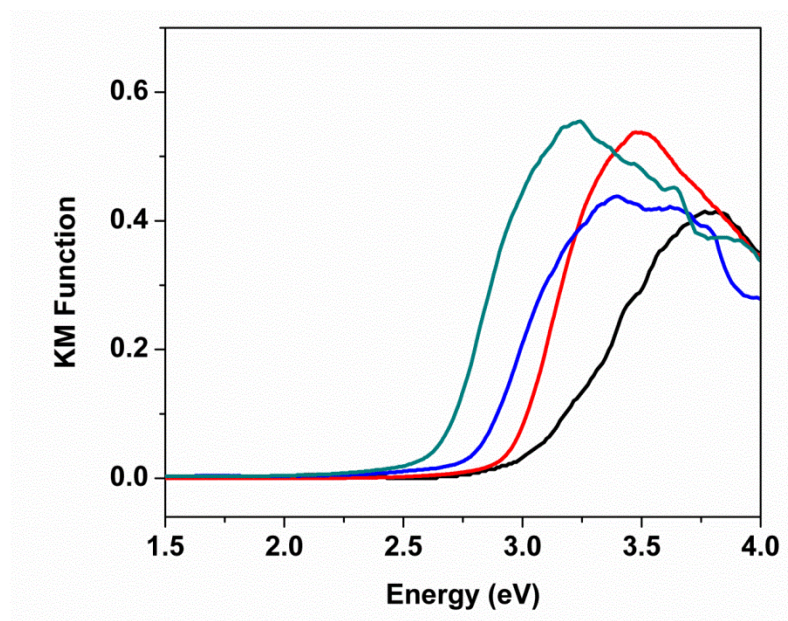


Figure 9. Optical absorption of $1\text{D-CuBr}(3,5\text{-dm-py})$ (black), $1\text{D-CuBr}(py)$ (red), $1\text{D-CuBr}(3\text{-Cl-py})$ (blue) and $1\text{D-CuBr}(3\text{-Br-py})$ (green).

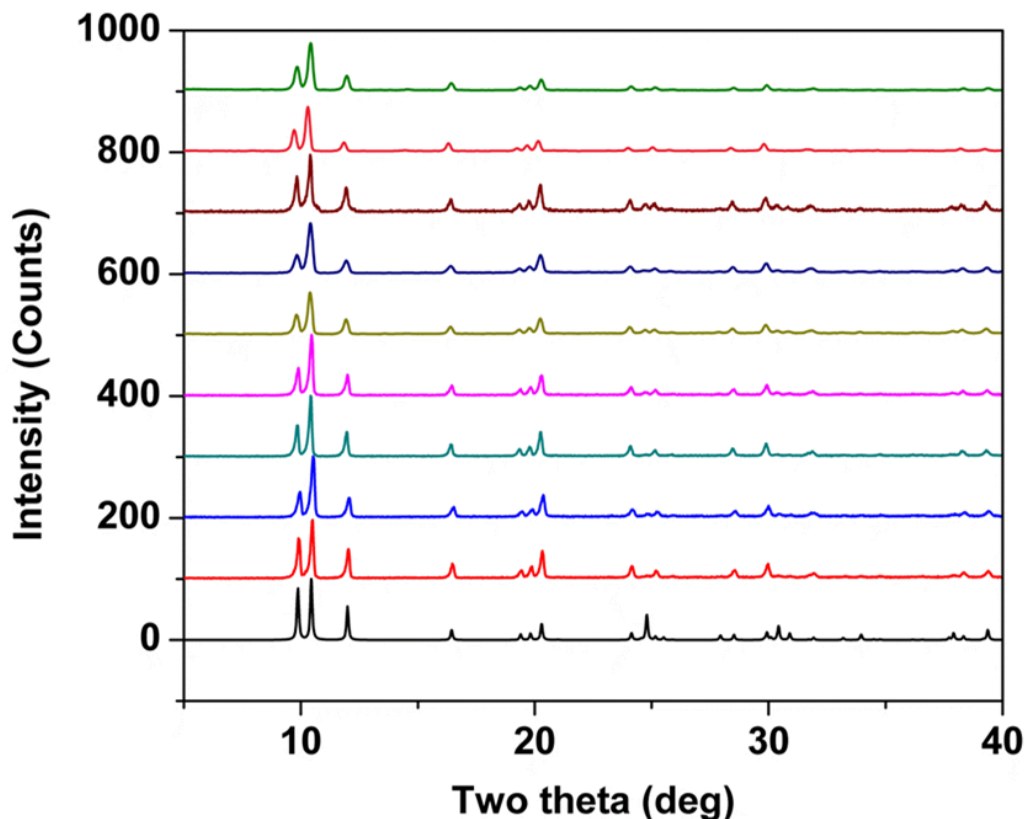


Figure 10. PXRD patterns of parent and doped structures compared with simulated pattern. From bottom to top: simulated 1D-CuBr(py) , as made 1D-CuBr(py) with different doping level: from 0% to 0.32%.

Photoluminescence (PL) measurements of the doped structures show that their emissions change significantly compared to that of their parent structure (Fig. 11). The blue-green emission band from their parent structure still remain in the higher energy (HE) region, while a second band emerges in PL spectra located at lower energy (LE) region as the effect of doping and combines with the HE band to form a broader band covering of the entire visible light region (400-700nm).

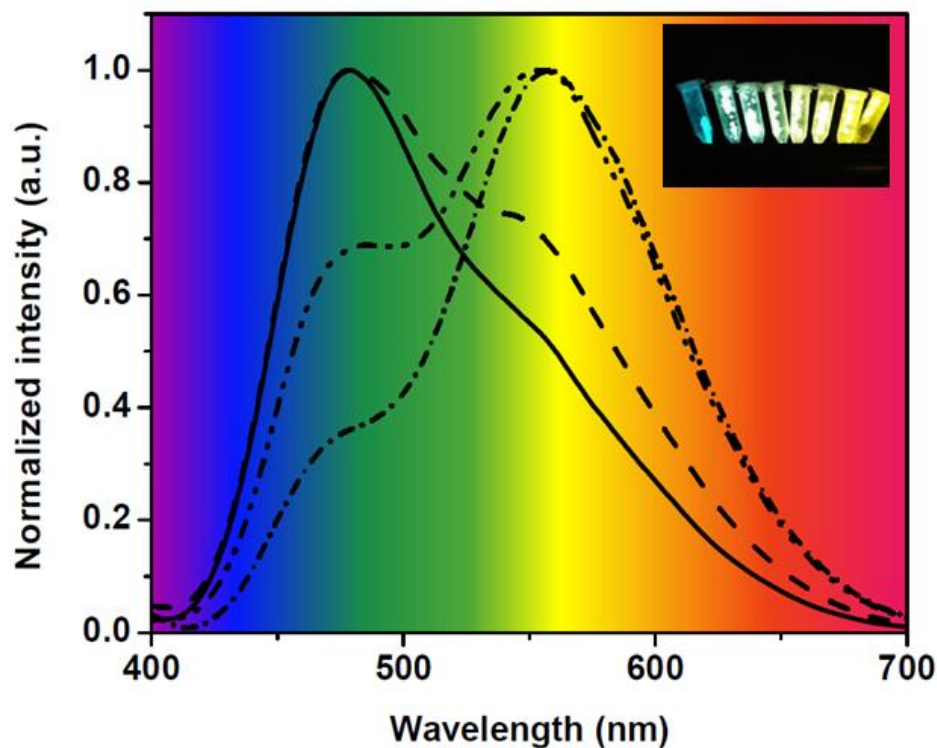


Figure 11. Photoluminescence spectra of 0.05% doped (solid), 0.07% doped (dash), 0.12% doped (dash dot dot) and 0.32% doped (short dash dot). Inset: Photos of the doped samples under UV light. Samples from left to right: parent 1D-CuBr(*pz*), 0.004%, 0.008%, 0.02%, 0.05%, 0.07%, 0.12%, 0.32% *pz* doped 1D-CuBr(*pz*). $\lambda_{\text{ex}} = 365\text{nm}$.

2.4 Single phase white light emitters

In order to prevent the measurements on powdery mixtures that may result in broaden of the emission spectra, rod-shaped cm-scaled single crystals of doped samples were obtained by layering approach and all optical measurements of the doped samples were conducted on

fine single crystals (Fig. 12). It is observed that the white light is directly coming out from the whole crystals, which also indicates that the origin of the white light is intrinsic from the bulk materials. To confirm the role of surface defects on these samples, we ground the single crystals of $1\text{D-CuBr}(py)_{1-x}(pz)_x$ ($x = 0.0012$) into fine powders, and observed no emission change before and after grinding, confirming that the luminescence is not dependent on surface defects.

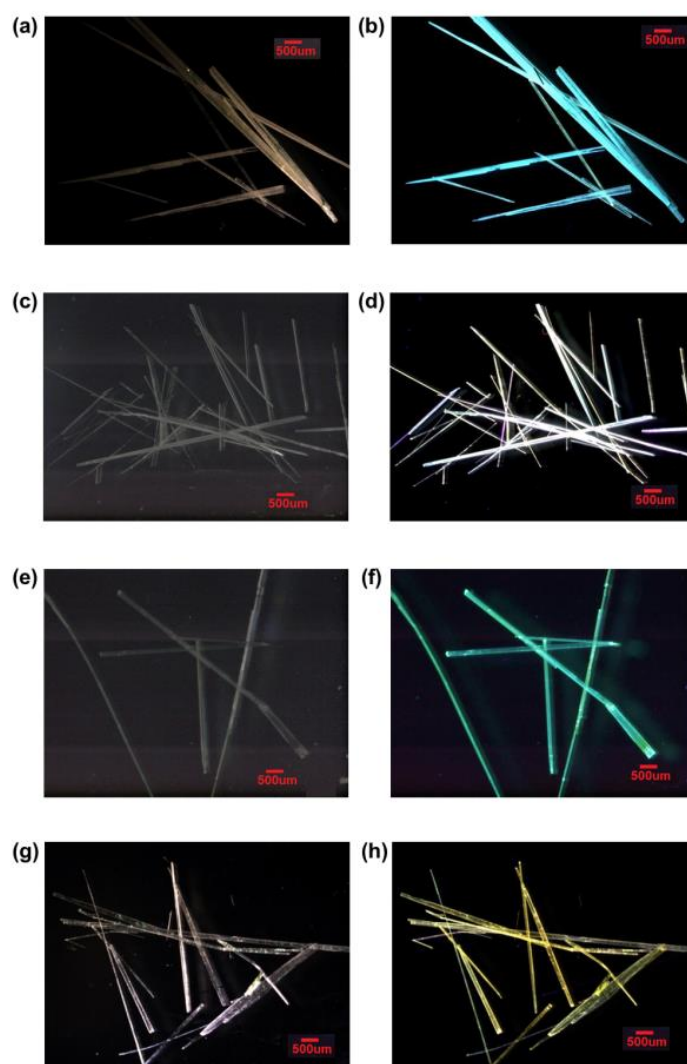


Figure 12. Single crystals of $1\text{D-CuBr}(py)$ (a), 0.05% doped (c), 0.12% doped (e), 0.32% doped (g) under nature light and under UV light (365nm).

Their phase purities were further confirmed by UV-vis absorption spectra (Fig. 13) other than PXRD since the amount of impurity phase would too low to be detected by PXRD. The most probable impurity from the introduction of $p\text{Zr}$ at such synthetic condition is the two dimensional (2D) $\text{CuBr}(p\text{Zr})_{0.5}$ staircase chain structure, and its strong absorption band is at much lower energy compared to that of 1D- $\text{CuBr}(p\text{Zr})$.⁵⁰ The spectra of the doped structures with the selected doping level exhibit a single strong absorption edge, at the same position as that of their parent structure without any absorption at lower energy region. This indicates that no other phases were formed from $p\text{Zr}$ and the $p\text{Zr}$ has been doped into the parent structure. Further increasing the doping level to $x = 0.01$ lead to the formation of a second phase, as identified by the UV-vis absorption spectra as the appearance of a second absorption band corresponding to that of 2D- $\text{CuBr}(p\text{Zr})_{0.5}$ (Fig. 14). Therefore, we keep the doping amount lower than 1 % to ensure their single phase purity.

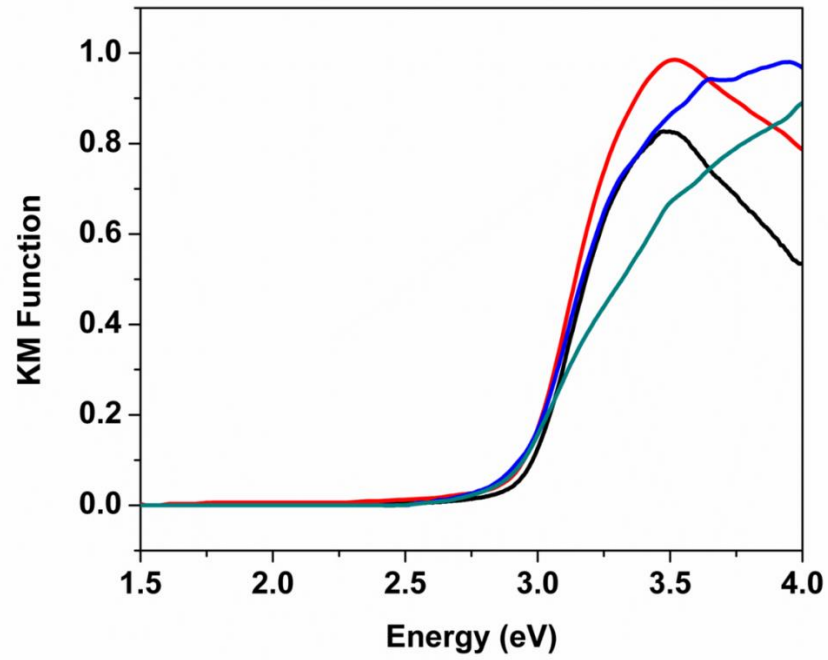


Figure 13. The absorption spectra for doped structures 1D-CuBr($p\gamma$) (black), 0.05% doped (red), 0.12% doped (blue), 0.32% doped (green).

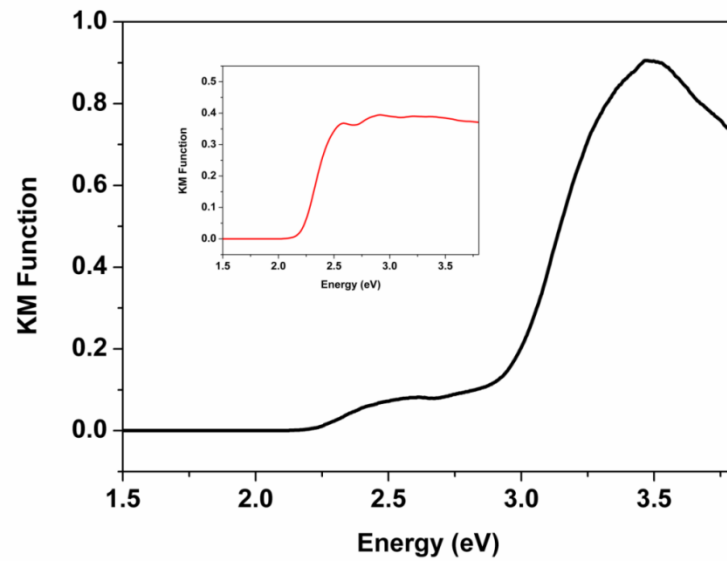


Figure 14. Optical absorption of 1% doped 1D-CuBr($p\gamma$). Inset: optical absorption of 2D-CuBr($p\gamma$)_{0.5}.

By varying the doping level of $p\mathbf{x}$, from 0.05 % to 0.32 % molar ratio to that of py , the energies of the HE and LE bands remain constant while the intensities of them vary based on the doping level. With increased doping amount, we observe a gradual decrease in intensity with the HE band along with a gradual increase with the LE band. When the doping level is as high as 0.32%, the HE is almost quenched, exhibiting an intense “yellowish” white light.

2.5 DFT calculations and luminescence mechanism

The intense blue-green emission of the parent structure 1D-CuBr(py) is primarily attributed to metal-to-ligand charge-transfer (MLCT) luminescence mechanism as confirmed by Density Functional Theory (DFT) calculations (Fig. 15). DGDZVP^{51,52} and 6-311++G(3df,3pd)⁵³⁻⁶⁰ were used for the calculation of the HUMO/LUMO energy of the ligands and the results are listed in Table 2. There is a correlation between electronic affinity of the functional groups and the energy level, as shown in the table. The band gaps and emission energies of this type of structures are correlated to the LUMO energies of the ligands. Further calculation of LUMO energies shows that $p\mathbf{x}$ has distinctly lower energy (-1.857 eV) compared to that of py (-1.120eV), indicating the parent ligand and the dopant might be responsible for the dual emissions. To understand this, we kept the parent ligand py , and changed the dopant $p\mathbf{x}$ to $p\mathbf{x}$ derivatives (2-*et*- $p\mathbf{x}$, 2-*me*- $p\mathbf{x}$, 2-*Cl*- $p\mathbf{x}$, 2-*Br*- $p\mathbf{x}$) with different LUMO energies. Single crystals were obtained with those dopants, and PXRD along with UV-vis absorption were conducted on them to confirm their phase correctness and purity. Based on their PL measurements, they all exhibit a two-band type spectrum (Fig. S20). The

energies of HE band remain constant for all of them, proving that the HE band is from the parent ligand *py*. The energies of LE band however, changes accordingly based on the LUMO energies of the dopants, providing strong evidence that the LE band is originated from the dopants.

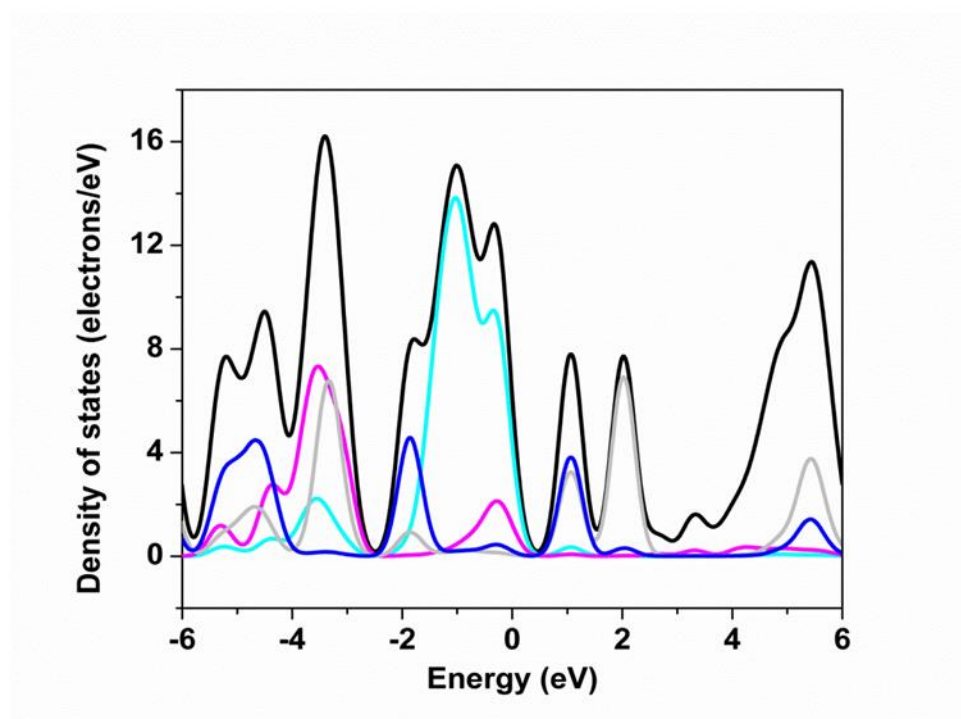
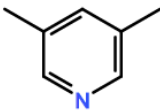
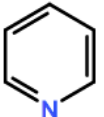
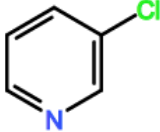
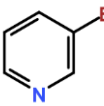
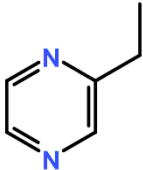
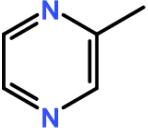
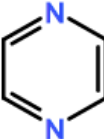
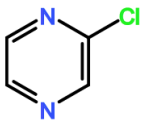
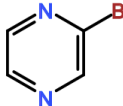
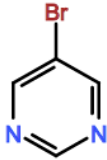
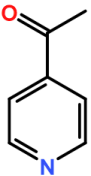
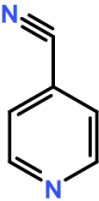


Figure 15. Calculated density of states (DOS) of 1D-CuI(*py*) by DFT method: total DOS (black); Cu 3d orbitals (light blue); Br 4p orbitals (pink); C 2p orbitals (grey); N 2p orbitals (blue).

Table 2. Calculated HOMO-LUMO energy levels of ligands.

Basis Set		DGDZVP		6-311++G(3df,3pd)	
Name	Structure	HOMO (eV)	LUMO (eV)	HOMO (eV)	LUMO (eV)
3,5-dimethylpyridine (<i>3,5-dm-py</i>)		-6.869	-0.933	-6.924	-1.039
pyridine (<i>py</i>)		-7.175	-1.041	-7.213	-1.120
3-chloro-pyridine (<i>3-Cl-py</i>)		-7.340	-1.428	-7.361	-1.473
3-bromo-pyridine (<i>3-Br-py</i>)		-7.228	-1.441	-7.264	-1.492
2-ethyl-pyrazine (<i>2-et-pz</i>)		-6.912	-1.632	-6.876	-1.690
2-methyl-pyrazine (<i>2-me-pz</i>)		-6.971	-1.668	-6.988	-1.726
Pyrazine (<i>pz</i>)		-7.146	-1.857	-7.125	-1.795

2-chloro-pyrazine (2-Cl-pz)		-7.529	-2.097	-7.467	-2.056
2-bromo-pyrazine (2-Br-pz)		-7.558	-2.146	-7.575	-2.171
5-bromopyrimidine (5-Br-pm)		-7.550	-1.943	-7.538	-1.970
4-acetyl-pyridine (4-ac-py)		-7.362	-2.406	-7.378	-2.425
4-cyano-pyridine (4-cy-py)		-7.908	-2.437	-7.922	-2.453

Furthermore, the relative intensities of the HE and LE band under various excitation wavelength have been studies (Fig. 16). The observation of their excitation-wavelength dependent emission suggests that the HE band and the LE band are from isolated luminous centers. The time-resolved PL measurements were conducted on the doped sample with the excitation wavelength of 360nm at the emission maximum of the two bands. The lifetime values at 495nm and 550nm are 17.5 μ s and 26.3 μ s, respectively (Fig. 17). The difference of the lifetime values illustrates their different excited states.

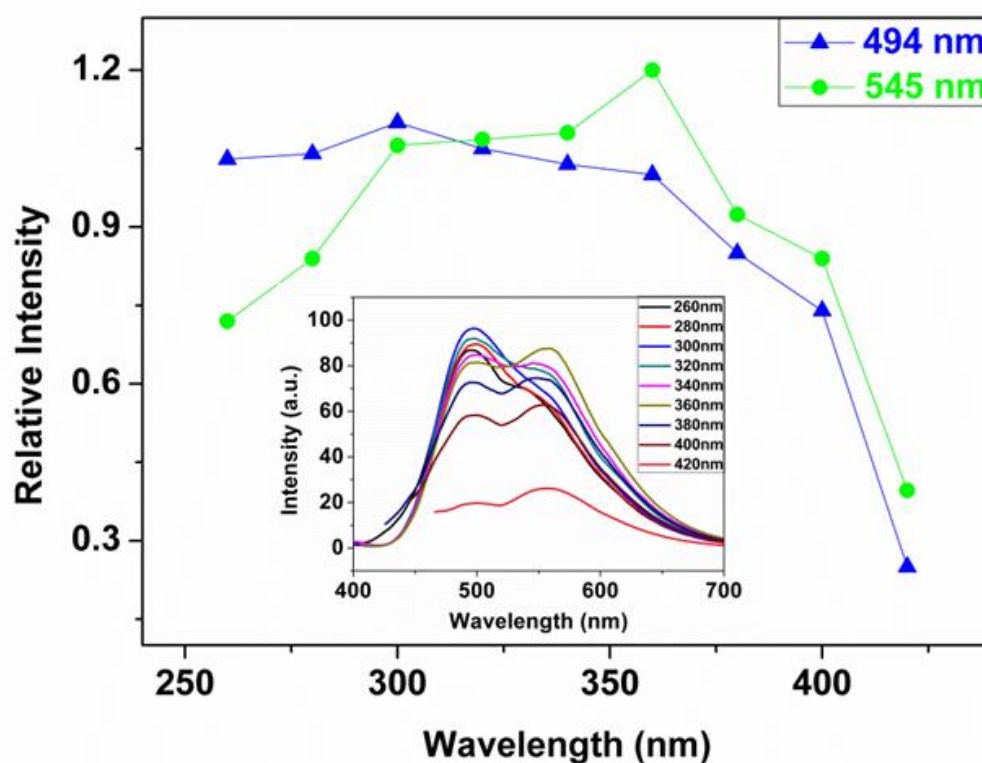


Figure 16. Relative intensity of the HE band at 494 nm (blue) and LE band at 545 nm (green) with various excitation wavelengths of 0.12% doped sample. The intensity of the HE band at 360 nm is set to 1. Inset: PL spectra of 2c with various excitation wavelengths.

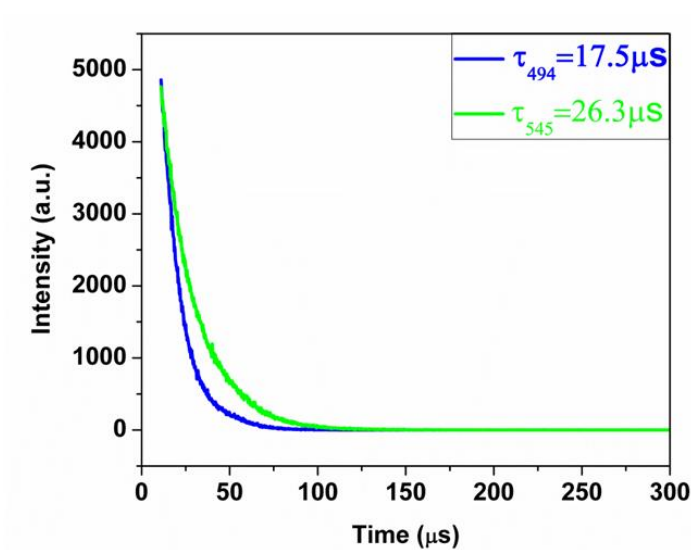


Figure 17. Luminescence decay spectra of 0.12% doped sample at 494nm (blue) and 545nm (green). $\lambda_{\text{ex}}=360\text{nm}$.

The thermogravimetric (TG) analyses were performed on selected structures. A single-step weight loss profile is found for all these samples. Based on their TG profiles, these structures, including the doped samples, have similar thermal stability and are thermally stable up to approximately 100 °C. The samples' weight loss is due to the loss of the ligand molecules, and the experimental weight loss is in agreement with the calculated results. The residues were analyzed to be CuBr.

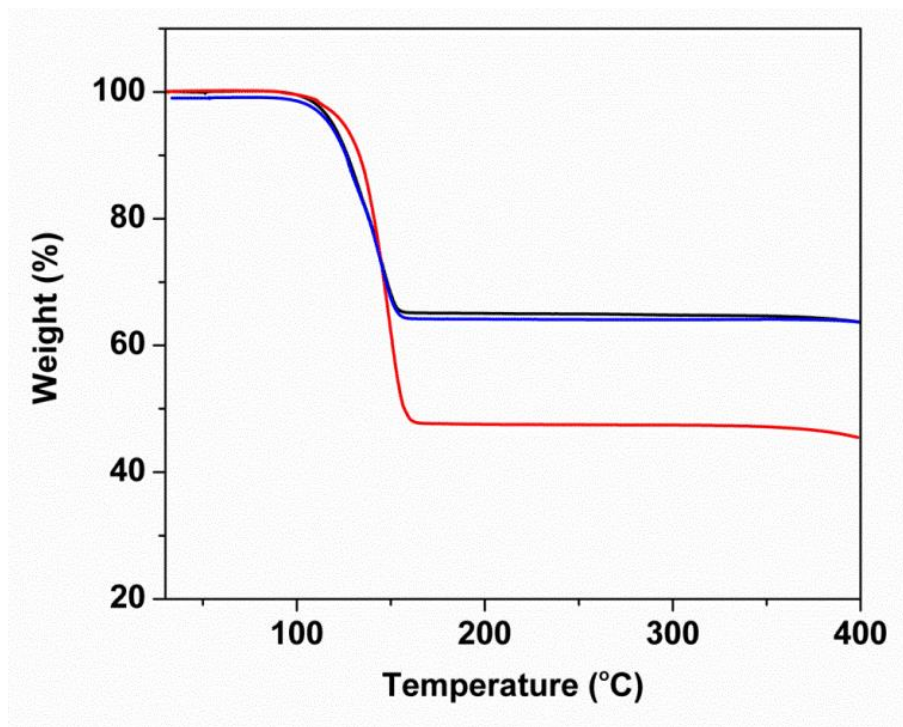


Figure 18. TG profiles of 1D-CuBr(py) (black), 1D-CuBr(3-Br-py) (red) and 0.12 doped 1D-Cur(py) (blue).

Table 3. Summary of the composition and optical properties of white-light-emitting structures.

Dopant	Dopant g amount t	Band gap (eV)	λ_{em} (nm) (298K)	λ_{em} (nm) (77K)	IQYs (%) 360nm	CIE	CRI	CCT (K)
<i>pz</i>	0.05	3.0	494 (HE) 545 (LE)	494	60	0.34, 0.41	68.4	5792
<i>pz</i>	0.07	3.0	494 (HE) 545 (LE)	494	64	0.35, 0.42	67.0	5024
<i>pz</i>	0.12	3.0	484 (HE) 545 (LE)	494	61	0.39, 0.43	67.2	3888
<i>pz</i>	0.32	3.0	494 (HE) 545 (LE)	494	54	0.42, 0.46	58.0	3658
<i>2-et-pz</i>	0.12	3.0	494 (HE) 520 (LE)	494	68	0.26, 0.36	65.4	4259
<i>2-me-pz</i>	0.12	3.0	494 (HE) 525 (LE)	494	66	0.28, 0.37	65.5	3940
<i>2-Cl-pz</i>	0.12	3.0	494 (HE) 556 (LE)	494	35	0.43, 0.42	77.2	3697
<i>2-Br-pz</i>	0.12	3.0	494 (HE) 575 (LE)	494	24	0.44, 0.40	75.6	3360

2.6 Performance as lighting phosphors and thermochromic behavior

As shown in Fig 19 and Table 4, these structures emit strongly in the visible light region and their emission colors range from blue to green. Their emission spectra are all single-band type, with an average of full width at half maximum (FWHM) of around 100 nm. Their emission energies are in trend with their band gap values and the LUMO energies of the incorporated ligands. The internal quantum yields (IQYs) of staircase chain based structures have been determined at room temperature, and the values obtained with 360 nm as the excitation wavelength are 56%, 48%, 27% and 21% respectively. These results demonstrate that the varying functional groups on the *py* ligands significantly influence the quantum yield of the hybrid structures. Electron donating groups, such as methyl groups, enhance the emission, while electron-withdrawing groups, such as chlorine or bromine, lower the emission efficiency. The structures' band gaps, emission energies, IQY and ligand LUMO energies are highly related to each other and are in agreement with our previous studies on 1D-CuBr(*L*). The optical properties of these structures can be tuned by ligand design and selection.

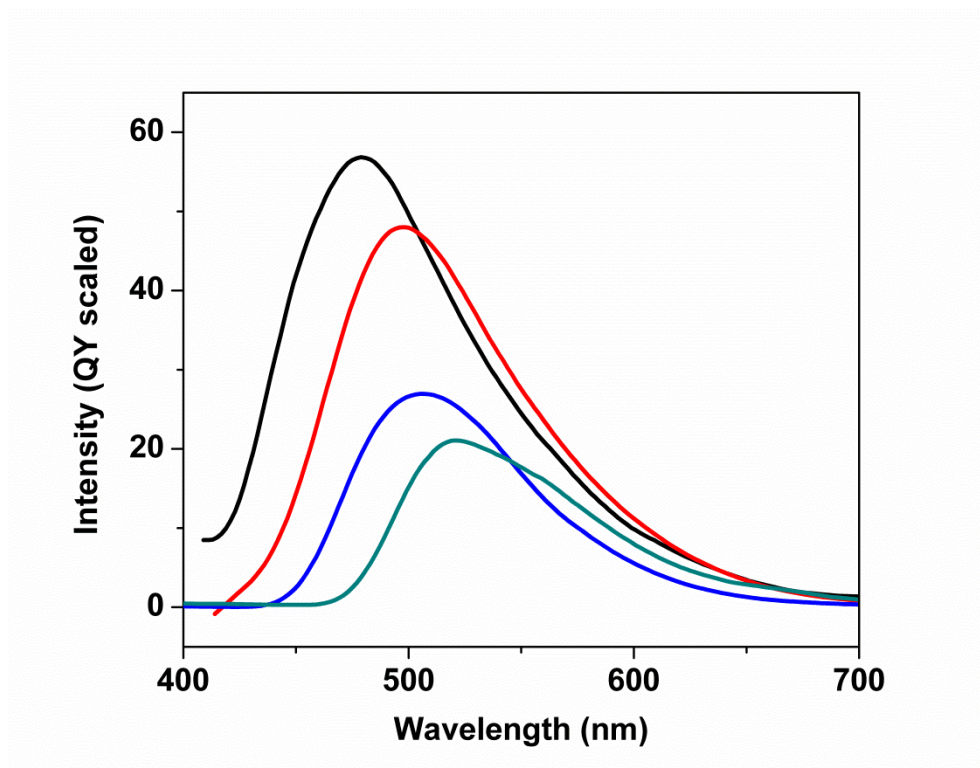


Figure 19. QY scaled PL spectra of 1D-CuBr(3,5-dm-py) (black), 1D-CuBr(py) (red), 1D-CuBr(3-Cl-py) (blue) and 1D-CuBr(3-Br-py) (green).

Table 4. Estimated Band Gaps, Emission Energies, IQYs, Emission Color.

Structure	Band gap (eV)	λ_{em} (nm) (298K)	Emission color	IQYs (%) 360nm
1D-CuBr(<i>3,5-dm-py</i>)	3.1	482	Blue	56
1D-CuBr(<i>py</i>)	2.8	494	Cyan	48
1D-CuBr(<i>3-Cl-py</i>)	2.7	505	Blue-green	27
1D-CuBr(<i>3-Br-py</i>)	2.5	514	Green	21
0D-Cu ₂ Br ₂ (<i>3,5-dm-py</i>) ₄	2.6	523	Green	70
1D-Cu ₂ Br ₂ (<i>5-Br-pm</i>) ₂	2.1	610	Red	3.2

The temperature-dependent emission spectra of doped structures show that they all display thermochromic behavior (Fig. 20). The intensity of LE band was completely quenched when the sample was dipped in liquid nitrogen (77 K), while the intensity of HE band becomes much stronger. After removing the crystals from liquid nitrogen, the initial emission intensities of the two bands returned to original at room temperature, indicating that the thermochromic luminescence is fully reversible. Though thermochromic behavior for copper halide cubane cluster-based hybrid materials is well studied which relates to shorter Cu to Cu bond distances (smaller than 2.8Å),^{34,61-63} as far as we know such behavior in extended staircase chain based structures is not reported. For example, a typical cubane structure 0D-Cu₄I₄(*py*)₄, it emits LE (yellow) emission at room temperature originated from “cluster centered” (CC) luminescence mechanism, and at low temperature (77 K), the LE emission gets quenched and the HE (blue) emission emerges as a combination of metal-to-ligand and halide-to-ligand charge transfer (MLCT and XLCT).³⁴ The LE band emissions in those doped samples behaves similar as that from cubane based structures, indicating they

might also be attributed to CC luminescence mechanism. One possible explanation to that is the possible shortening of Cu-Cu bond distance around the dopant sites as a result of doping. We attempted to identify this through single crystal X-ray diffraction analyses, however the crystal data obtained is exactly the same as the parent structure and the dopants could not be identified since the doping level is too low. We also found out that the dopants have to be multidentate ligands in order to achieve the broadening of the spectra. Other multidentate ligands include pyrimidine (*pm*) and 1,3,5-triazine (*tz*) were tried and exhibit the similar broaden effect as *pz* derivatives (Fig. 21). However, when replacing the dopant with monodentate ligands with lower LUMO energies, such as *3-cyano-py* and *4-cyano-py* (Table 2), no broadening effect was observed. Since multidentate ligands would generally connect single chains together to 2-D structures,^{64,65} the broaden effect from multidentate dopants might be related to chain-chain interaction and such interaction leads to the shortening of the Cu-Cu distance, resulting in the emergence of the LE band at room temperature. At lower temperature, such interaction is terminated and the LE band gets quenched. The full understanding of the broaden effect through doping is still limited, and further in-depth investigation of the luminescence mechanism is now underway.

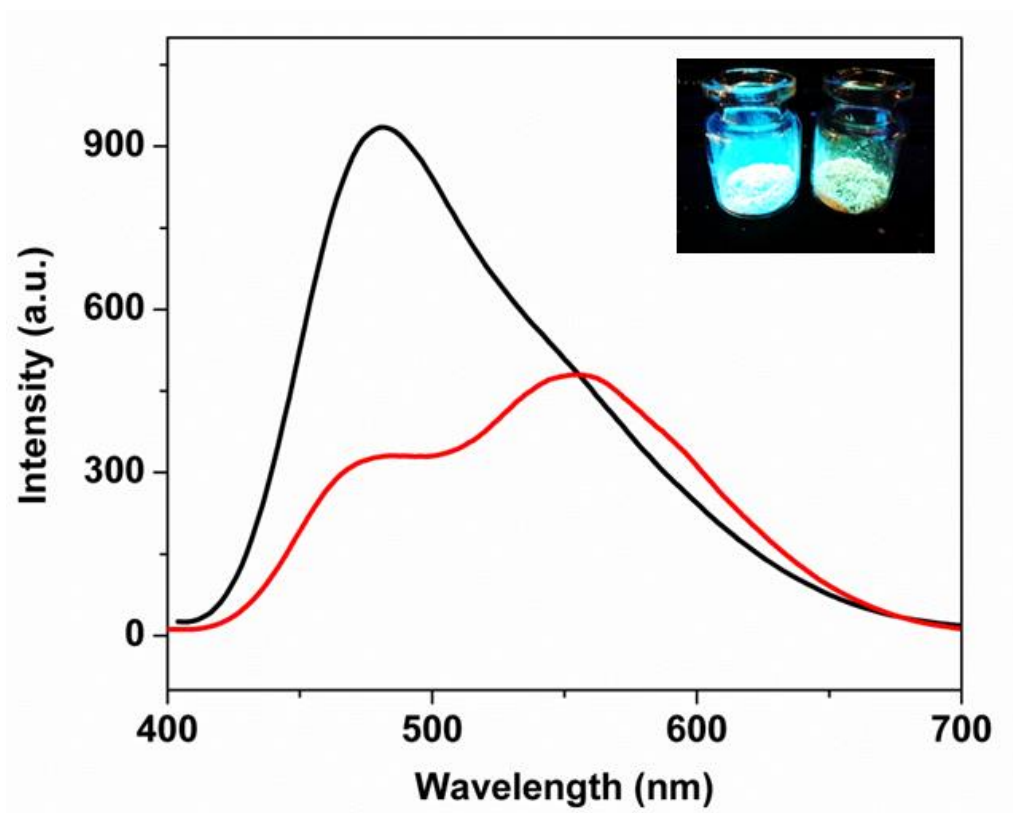


Figure 20. PL spectra of 0.12% doped sample at room temperature (red) and at 77K (black). Inset: Images of the sample taken out immediately from liquid nitrogen (left) and at room temperature (right).

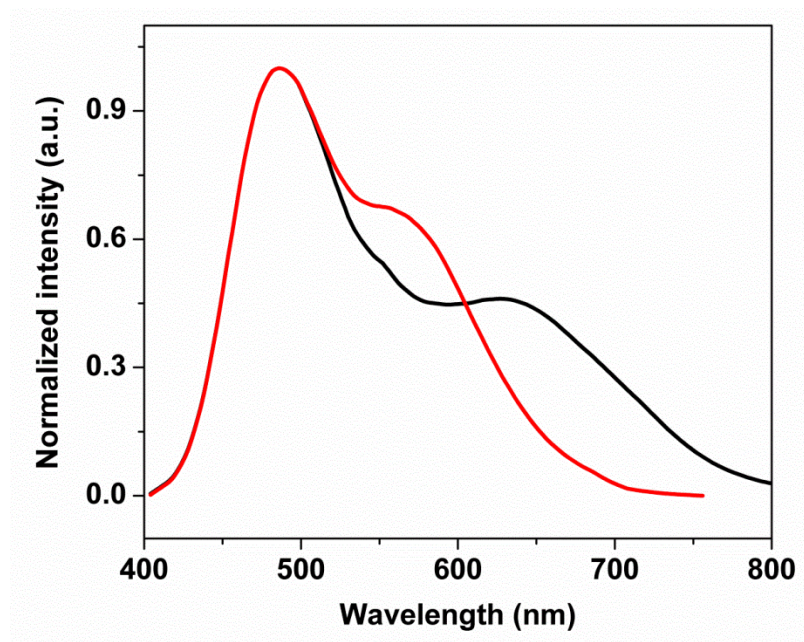


Figure 21. PL spectra of *pm* (black) and *tz* (red) doped 1D-CuBr(*py*). $\lambda_{\text{ex}}=360\text{nm}$.

The direct application of these white-lighting-emitting materials is the potential usage as lighting phosphors. The fact that the energy of the LE band is highly dependent on the selection of the dopants and the intensities of both bands vary with the doping level leads to the tunable white light qualities of these materials. Their performances as lighting phosphors were evaluated by internal quantum yield (IQY) measurements, Chromaticity color coordinates (CIE), Color Rendering Index (CRI) and CCT under the excitation of near-ultraviolet light (365 nm) and the results are summarized in Table 3. It is interesting that the IQYs of most of the doped structures are higher than that of their parent structure, with the highest value of 68%. Compared to other reported direct white light emitting phosphors which generally suffer from low IQYs, most of these compounds have IQYs higher than 60%, and based on our knowledge, they are among the highest IQYs for direct single-phase white-light-emitting materials. More interestingly, the color temperature could

also be tuned, from bluish (cold) to yellowish (warm) white light based on their CCT values (Fig. 22). The current commercial white light LEDs made from YAG:Ce produce “cold” white light with CCT values higher than 5000 K and might not be suitable for indoor illumination.⁶⁶ The color temperatures of these materials range from 3360 K to 5792 K, making these materials usable under various environments.

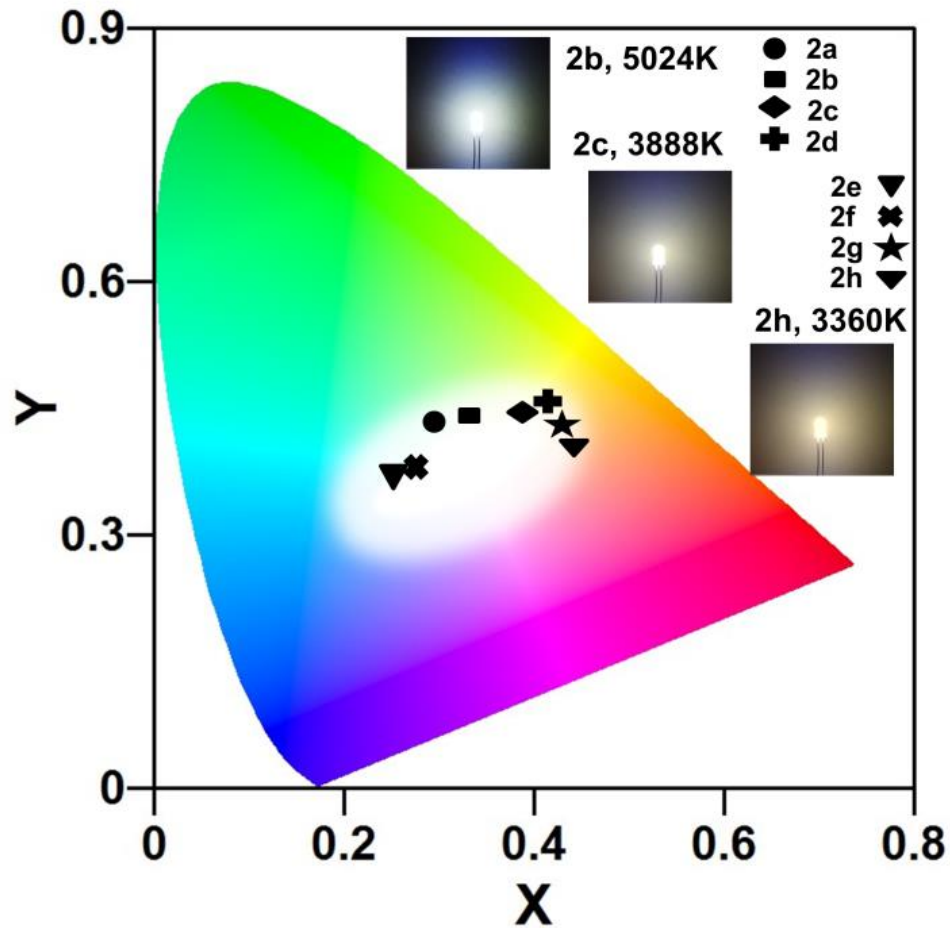


Figure 22. CIE coordinates of all white-light-emitting structures. Inset: photos of the LED bulbs under working condition. 2a-2h are labeled as increasing $p\chi$ doping level.

Moreover, the water stability of these materials ensures their solution processability and they could be used together with commercial binder for coating onto the substrates. 5 mm 365 nm LED chips were used and materials with various CCT values were uniformly coated onto their surface, displaying the white light from “cold” to “warm” as shown in Fig. 22 inset.

2.7 Summary

In summary, a series of copper bromide inorganic-organic hybrid semiconductors have been obtained and they exhibit intrinsic white light from single crystals upon a secondary ligand doping. The white light of these materials are tunable based on the selection of the dopants and the doping level, generating the white light from “cold” to “warm”. Further investigation was on their dual emission mechanism and thermochromic properties were observed. This work is a step further towards understanding the doping effect of copper halide based hybrid structures.

3. Precursor approach for the synthesis of Cu_2I_2 dimer based structures and their applications

3.1 Background

There have been some difficulties that need to be resolved for the practical usages of copper iodide based materials as lighting phosphors. First of all, the quantum yield (QY) of these phosphors needs to be high enough for practical applications. Our group have reported a series of 1D-CuI(L) structures based on staircase chain as LED phosphors and the highest QY we got is only 37.2% for 1D-CuI(*3-pc*), which is too low compared to commercial phosphors (usually higher than 70%).⁴⁵ In addition, copper iodide hybrid materials are majorly built by three inorganic motifs: Cu_2I_2 dimer, Cu_4I_4 tetramer and $\text{Cu}_\infty\text{I}_\infty$ staircase chain. Rational construction of the target materials with designed motifs remains challenging. It is hard to predict the compound formed, and in some cases, the formation of other type of compounds at the same time is unavoidable.

In this chapter, a family copper halide rhomboid dimer based hybrid materials as promising candidates as LED phosphors obtained by a novel bottom-up precursor approach will be discussed. These materials generally have the formula of $\text{Cu}_2\text{I}_2(\text{L}_1)_m(\text{L}_2)_n$ ($\text{L} = \text{organic ligand}$) and was synthesized by a 0D- $\text{Cu}_2\text{I}_2(\text{L})_4$ dimer based precursor. The newly developed precursor approach facilitates the reaction process, efficiently controls the construction based on the same-type inorganic motifs and prevents the formation of other types of products. These hybrid structures has high quantum yield (up to 90%), which is comparable to the commercial phosphors. These compounds are all air and moisture stable. The ligands used are all commercial available inexpensive organics without further modification and all of these phosphors could be obtained at room temperature in solution. Real light bulbs

based these phosphors combined with LED chips inside have been fabricated and show similar performance as the one based on commercial phosphors. Because of these, we believe that this type of materials are promising candidates for future commercial LED phosphors and the precursor approach will be a powerful blueprint for rational design of copper halide based structures.

3.2 Precursor synthesis of dimer based structures and single crystal data

Synthesis of $0D-Cu_2I_2(3-pc)_4$: 1.9g (10mmol) CuI was first well-dispersed in 50ml acetone and 3-pc(40mmol)/acetone solution was slowly added in under magnetic stirring at room temperature. Pure phase of the sample was collected by filtration after 3 hours of continuous stirring. This was used as the precursor the synthesis of other structures. (Yield is 95% based on Cu).

Synthesis of $0D-Cu_2I_2(3,5-dm-py)_4$: 0.29g (0.05mmol) $0D-Cu_2I_2(3-pc)_4$ was fully dissolved in 10ml acetone to form a clear solution in a glass vial. Then excess 3,5-dm-py (4mmol) in 2ml acetone solution were slowly added under magnetic stirring at room temperature. Precipitate formed as the acetone evaporated and was collected before the acetone completely dried. Single crystal of this could be obtained by leaving the mixed acetone solution in the open air undisturbed instead of stirring. Rod-shaped crystals would form as the acetone slowly evaporated. (Yield is 66% based on Cu).

Synthesis of $0D-Cu_2I_2(3-Cl-py)_4$ ($3-Cl-py=3-chloro-pyridine$): 0.29g (0.05mmol) $0D-Cu_2I_2(3-pc)_4$ was fully dissolved in 10ml acetone to form a clear solution in a glass vial. Then excess 3-Cl-py was added. The reaction vial was left open to let the acetone slowly evaporated. Pure

phase of powder sample, along with some rod-shaped crystals would form as the acetone was almost dried. (Yield is 36% based on Cu).

Synthesis of $0D-Cu_2I_2(tpp)_2(3-pc)_2$: 0.29g (0.05mmol) $0D-Cu_2I_2(3-pc)_4$ was fully dissolved in 10ml acetone to form a clear and stoichiometric *tpp* was slowly added in. The solution remained clear and was left in the open air for the acetone to evaporate slowly. After several hours, cubic shaped crystals formed at the bottom, which were suitable for single-crystal X-ray diffraction. Pure powder sample were obtained by directly mixing $0D-Cu_2I_2(3-pc)_4$ /acetone solution with stoichiometric *tpp* under magnetic stirring. Precipitate formed in several hours and was collected by filtration. This compound was used as the precursor for other *tpp* based structures. (Yield is 45% based on Cu).

Synthesis of $0D-Cu_2I_2(tpp)_2(4,6-dm-pm)_2$: 1.11g (1mmol) $0D-Cu_2I_2(tpp)_2(3-pc)_2$ was first dissolved 10 ml toluene and excess *4,6-dm-pm* (2mmol)/acetone solution was slowly added. Single crystals suitable for single X-ray diffraction were formed after 1 day. Pure phase of powder was synthesized by directly mixing $0D-Cu_2I_2(tpp)_2(3-pc)_2$ /toluene with excess *4,6-dm-pm* in acetone under stirring. Precipitate formed after several hours and was collected by filtration. (Yield is 57% based on Cu).

Synthesis of $1D-Cu_2I_2(tpp)_2(dps)$: Single crystal of $1D-Cu_2I_2(tpp)_2(dps)$ was obtained by the precursor method similar as above. $0D-Cu_2I_2(tpp)_2(3-pc)_2$ was used as the precursor and was first dissolved in toluene. Then *dps* was added in to the solution and the reaction was kept at 60 °C for 12h. Rod-shape crystals formed overnight. Pure phase of powder sample was obtained by mixing stoichiometric $0D-Cu_2I_2(tpp)_2(3-pc)_2$ with *dps* under stirring. The right product formed in 3 hours and was collected by filtration. (Yield is 81% based on Cu).

Synthesis of $1D-Cu_2I_2(tpb)_2(4,4'-bpy)$: Precursor method was used for synthesis of this compound, which is different as the method reported. Detail synthetic procedure was similar as the $1D-Cu_2I_2(tpb)_2(dps)$. (Yield is 90% based on Cu).

Synthesis of $1D-Cu_2I_2(tpb)_2(pz)$: Pure powder sample were obtained by precursor method similar as above. $0D-Cu_2I_2(tpb)_2(3-pc)_2$ was used as the precursor and excess pz was added to exchange $3-pc$. (Yield is 50% based on Cu).

Synthesis of $2D-Cu_2I_2(bpe)_2$: ($bpe=1,2-bis(4-pyridyl)ethane$): Different from traditional solvothermal method, pure phase of powder sample was obtained by precursor approach. $0D-Cu_2I_2(3-pc)_4$ was used as the precursor for this compound. First, 0.19g (1mmol) $0D-Cu_2I_2(3-pc)_4$ was fully dissolve in 10ml acetone and was slowly added to excess bpe /acetone solution at room temperature under stirring. Precipitate formed quickly and was collected. (Yield is 42% based on Cu).

Synthesis of $2D-Cu_2I_2(bpp)_2$: Pure powder sample was prepared by precursor method similar as $2D-Cu_2I_2(bpe)_2$. Excess bpp was used and the product formed immediately after mixing $0D-Cu_2I_2(3-pc)_4$ /acetone with bpp . (Yield is 74% based on Cu).

Synthesis of $2D-Cu_2I_2(dps)_2$: Single crystal of $2D-Cu_2I_2(dps)_2$ was prepared by mixing $0D-Cu_2I_2(3-pc)_4$ /acetone with excess dps /acetone and leaving the reaction mixture in the open air. Rod-shaped crystals formed in 2 days. Pure phase of powder sample was prepared by mixing the ligand with the precursor under magnetic stirring. (Yield is 68% based on Cu).

Synthesis of $2D-Cu_2I_2(5-me-pm)_2$: Single crystal of $2D-Cu_2I_2(5-me-pm)_2$ was prepared by mixing $0D-Cu_2I_2(3-pc)_4$ /acetone with excess $5-me-pm$ /acetone and leaving the reaction mixture in the open air. Rod-shaped crystals formed in 3 days. Pure phase of powder sample

was prepared by mixing the ligand with the precursor under magnetic stirring. (Yield is 60% based on Cu).

Table 5a. Summary of crystal data of new compounds

Compou nd	0D-Cu ₂ I ₂ (<i>β</i> -C/ <i>l</i> - <i>pp</i>) ₄	0D-Cu ₂ I ₂ (<i>tp</i> <i>p</i>) ₂ (<i>β</i> - <i>pc</i>) ₂	0D-Cu ₂ I ₂ (<i>tp</i> <i>p</i>) ₂ (<i>4,6-dm-pm</i>) ₂	1D-Cu ₂ I ₂ (<i>tp</i> <i>p</i>) ₂ (<i>bpp</i>)	1D-Cu ₂ I ₂ (<i>tp</i> <i>p</i>) ₂ (<i>4,4'-dps</i>)
Empirical Formula	C ₂₀ H ₁₆ Cu ₄ I ₂ N ₄	C ₂₄ H ₂₂ CuIN	C ₄₈ H ₄₆ Cu ₂ I ₂ N ₄	C ₄₉ H ₄₄ Cu ₂ I ₂ N	C ₉₂ H ₇₆ Cu ₄ I ₄ N ₄
FW	835.05	545.83	1121.71	1103.68	2187.32
Space Group	P-1	C2/c	P-1	P2 ₁ /c	C2/c
<i>a</i> (Å)	7.8020(4)	25.9199(15)	9.3886(3)	13.2151(5)	26.0237(10)
<i>b</i> (Å)	8.6628(4)	14.9505(9)	11.5199(4)	13.5525(5)	9.3012(4)
<i>c</i> (Å)	9.4711(5)	11.5468(7)	11.5849(4)	25.3512(9)	20.2799(8)
α (°)	90.919(2)	90	79.129(2)	90	90
β (°)	94.251(3)	97.115(2)	69.089(2)	94.613(2)	117.533(2)
γ (°)	102.751(2)	90	72.439(2)	90	90
<i>V</i> (Å ³)	622.28(5)	4440.1(5)	1111.29(7)	4525.6(3)	4352.8(3)
<i>Z</i>	1	8	1	4	2
<i>T</i> (K)	100(2)	150(2)	100(2)	298(2)	230(2)
λ (Å)	0.7749	0.71073	0.71073	0.7749	0.7085
<i>R</i> ₁	0.0388	0.0735	0.0421	0.0435	0.0503
w <i>R</i> ₂	0.1046	0.1725	0.0692	0.0652	0.0775

Table 5b. Summary of crystal data of new compounds.

Compound	1D-Cu ₂ I ₂ (<i>lpp</i>) ₂ (5- <i>Br-pm</i>)	1D-Cu ₂ I ₂ (5- <i>me-pm</i>) ₂	1D-Cu ₂ I ₂ (5- <i>Br-pm</i>) ₂	2D-Cu ₂ I ₂ (3,3'- <i>lpp</i>) ₂
Empirical Formula	C ₈₀ H ₆₆ Br ₂ Cu ₄ I ₄ N ₄ P ₄	C ₅ H ₆ CuIN ₂	C ₄ H ₃ BrCuIN ₂	C ₁₀ H ₈ CuIN ₂
FW	2128.82	284.56	349.43	346.62
Space Group	C2/c	Cmca	Cmca	P2 ₁ /n
<i>a</i> (Å)	17.2033(7)	8.4063(4)	8.437(2)	9.4898(13)
<i>b</i> (Å)	17.7719(7)	21.6785(10)	21.875(6)	9.7370(18)
<i>c</i> (Å)	14.9470(6)	16.5331(7)	16.757(4)	12.2051(18)
α (°)	90	90	90	90
β (°)	122.467(2)	90	90	111.784(2)
γ (°)	90	90	90	90
<i>V</i> (Å ³)	3855.6(3)	3012.9(2)	3092.6(14)	1047.2(3)
<i>Z</i>	2	16	16	4
<i>T</i> (K)	100(2)	100(2)	296(2)	150(2)
λ (Å)	0.7293	0.71073	0.71073	0.71073
R _p	0.0295	0.0384	0.0305	0.0445
R _w p	0.0478	0.0678	0.0655	0.0675

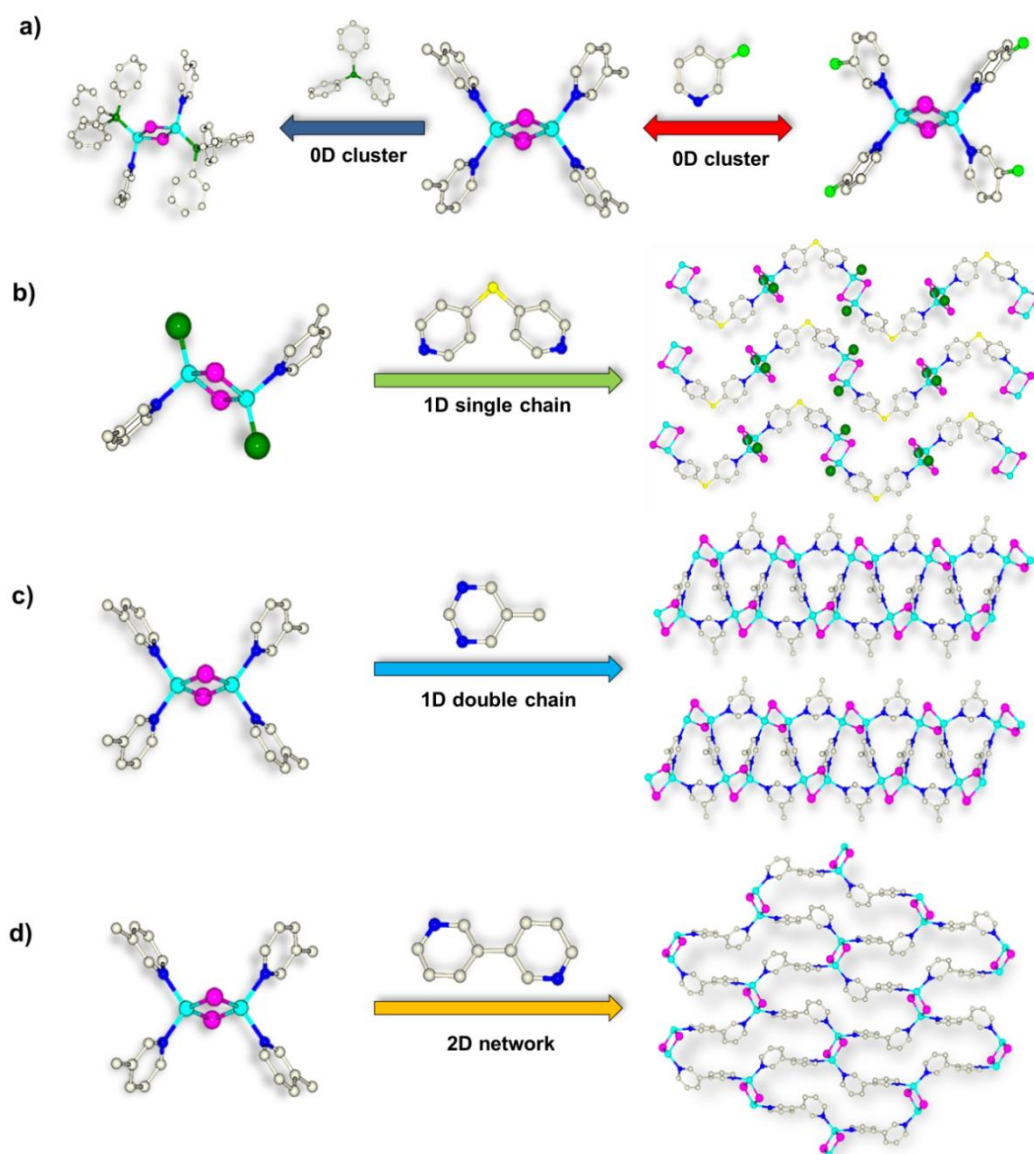


Figure 23. Schematic illustrating the design and construction of CuI(L) hybrid structures with a Cu_2I_2 molecular dimer precursor: (a) 0D cluster, (b) 1D single chain, (c) 1D double chain, and (d) 2D layered network. Color scheme of the balls: purple, I; cyan, Cu; dark blue, N; grey, C; light green, Cl; small green, P; big green, *tpp* molecule.

3.3 “Bottom-up” approach

One important requirement for LED phosphors is their quantum efficiency. Lower band gap is also favored since most of bulbs are fabricated by violet and blue LEDs, which means the band gaps should be less than 3.1eV (400nm) to be excited. However, the synthesis procedures of these six compounds are almost identical. All of the six compounds could be synthesized by directly mixing of CuI with the ligand at room temperature. It is difficult to deliberate construct the structure based on dimer and avoid the formation of other type of structures. Interestingly, we have discovered that ligand exchange could take place for most of the inorganic-organic hybrid materials. Usually by adding one similar type of ligand into the parent hybrid structure, the ligand in the parent structure would be replaced by the new ligand introduced while the inorganic motifs remain the same. The replacement always reaches to completion by adding excess new ligand. Based on these considerations, a new precursor approach was proposed that in order to keep the Cu_2I_2 dimer inorganic motif to maintain its high photoluminescence property while avoid the formation of other chain or cubane phases, a $0\text{D-Cu}_2\text{I}_2(\text{L})_4$ was used as a precursor for the construction of other dimer based compounds by ligand exchange (Fig. 23).

To verify the approach, $0\text{D-Cu}_2\text{I}_2(3\text{-}pc)_4$ was synthesized at first as precursor and then well-dissolved in acetone. Acetone was chosen as the solvent because it could well-dissolve $0\text{D-Cu}_2\text{I}_2(3\text{-}pc)_4$, but not for $0\text{D-Cu}_4\text{I}_4(3\text{-}pc)_4$ and $1\text{D-CuI}(3\text{-}pc)$. To prove that the dimer structure maintain in the solution, the dissolved solvent was evaporated and the precipitate after the solvent was dried is the pure phase of $0\text{D-Cu}_2\text{I}_2(3\text{-}pc)_4$ (Fig. 24). Introducing of other ligands into the dissolved acetone solution would lead to the ligand exchange process. When excess amount of other mono-dentate ligand was introduced, pure phase of 0D-

$\text{Cu}_2\text{I}_2(\text{L})_4$ of the new ligand would form after evaporation of the acetone. Single crystal would form if the evaporation process is relatively slow. Take $0\text{D-Cu}_2\text{I}_2(3\text{-Cl-py})_4$ as an example. $0\text{D-Cu}_2\text{I}_2(3\text{-py})_4$ was first dissolved completely in acetone in a glass vial and excess 3-Cl-py was slowly added into the acetone solution. After the mixing, the solution remains clear. Then the acetone solution was slowly evaporated until almost dry which lead to the formation of yellow cubic shaped crystals at the bottom of the vial. Traditional method, including mixing CuI/saturated KI solution or CuI/acetonitrile solution with 3-Cl-py would never form pure phase $0\text{D-Cu}_2\text{I}_2(3\text{-Cl-py})_4$, instead forms chain structures or mixtures of various phases. 2D network based on Cu_2I_2 dimer could be obtained by using bidentate ligand instead of mono-dentate ligand. Ligand exchange of $0\text{D-Cu}_2\text{I}_2(3\text{-py})_4$ with excess bidentate ligand forms a 2D framework, such as $2\text{D-Cu}_2\text{I}_2(bpe)_2$, $2\text{D-Cu}_2\text{I}_2(bpp)_2$, $2\text{D-Cu}_2\text{I}_2(dps)_2$ and $2\text{D-Cu}_2\text{I}_2(5\text{-me-pm})_2$. 2D frameworks have lower solubility under acetone, so it would precipitate out quickly when the new ligand is added. Usually excess ligand is needed in order to ensure complete transformation.

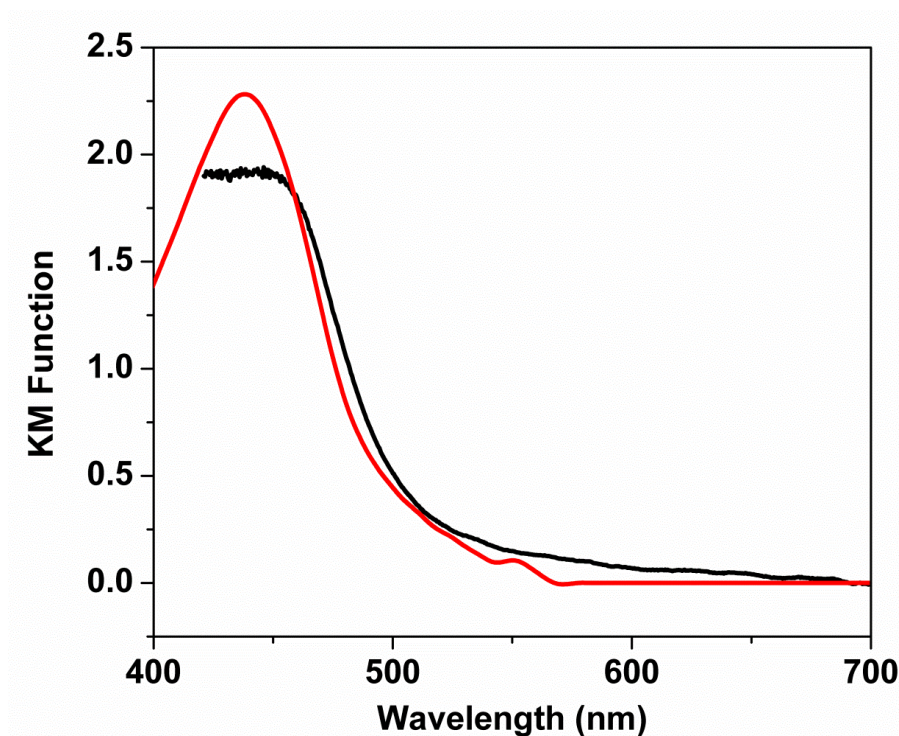


Figure 24. Optical absorption spectra of the precursor at solid state (red) and dissolved in acetone solution (black).

The *3-pc* ligand in $0D-Cu_2I_2(3-pc)_4$ could be partially replaced by triphenylphosphine (*tpp*) ligand and form a mixed ligand compound $0D-Cu_2I_2(tpp)_2(3-pc)_2$. Single crystals of $0D-Cu_2I_2(tpp)_2(3-pc)_2$ were grown by slowly adding *tpp*/acetone into $0D-Cu_2I_2(3-pc)_4$ /acetone solution. Cubic colorless crystals formed in several days. $0D-Cu_2I_2(tpp)_2(3-pc)_2$ could be treated as precursor for other $0D-Cu_2I_2(tpp)_2(L)_2$. $0D-Cu_2I_2(tpp)_2(4,6-dm-pm)_2$ were synthesized by ligand exchange of *4,6-dm-pm* with $0D-Cu_2I_2(tpp)_2(3-pc)_2$. The TG analyses shows that the *tpp* ligand has stronger P-Cu bonding compared to N-Cu bonding, so as a result, when $0D-Cu_2I_2(tpp)_2(3-pc)_2$ was exchanged with bidentate N-ligand, *tpp* could not be

replaced. As a result, a series of 1D-Cu₂I₂(*tpp*)₂(L)₂ were formed. *Tpp* was acted as a terminator in controlling the dimensionality, cutting the network from 2D to 1D. As we adding excess *bpp* in to 2D-Cu₂I₂(*dps*)₂, 2D-Cu₂I₂(*bpp*)₂ would form. In the similar pattern, adding excess *dps* into 1D-Cu₂I₂(*tpp*)₂(5-Br-pm) would lead the formation of 1D-Cu₂I₂(*tpp*)₂(*dps*) as *tpp* is hard to be replaced. Adding excess *dps* into 1D-Cu₂I₂(*tpp*)₂(*dps*) would not form 2D-Cu₂I₂(*dps*)₂, but on the contrary, adding *tpp* into the 2D-Cu₂I₂(*dps*)₂ would form 1D-Cu₂I₂(*tpp*)₂(*dps*). Based on these observations, using the precursor approach, a family of copper iodide dimer based inorganic organic hybrid structures from 0D to 2D could be synthesized by a 0D-Cu₂I₂(3-*pc*)₄ precursor.

Different from the traditional crystallization method, our new strategy based on ligand exchange has two obvious advantages. First of all, it keeps the basic inorganic motifs during the whole reaction process, which effectively eliminate the possibility of forming other type of products. As far as we know, the products obtained by this method are purer than the one prepared by traditional method. Secondly, this approach facilitates the reaction process. All of the compounds obtained could be synthesized within several hours, and in some cases, in several minutes, at room temperature. Compared to the literature of some of these compounds that requires high temperature for several days, this method is much more facile and energy efficient. We believe that this approach could be further used for other unreported Cu₂I₂ dimer based structures and facilitates the reaction procedure of reported structures.

3.4 Enhanced thermal stability by formation of extended structures

Stability is also an important factor for evaluating the LED phosphors. Thermal stability of these phosphors was determined by TG analysis. 0D structures could usually be stable up to 60°C. The decomposition of the structure starts by losing the organic ligand. The residue, which is copper iodide, could stable up to 400°C. As a result, the stability of the compound depends on the bonding of the copper and the ligand (Fig. 25). Because of this, 1D and 2D structures have much better thermal stability compared to 0D structures due to the formation of framework. The organic ligand was stabilized in the structure by two adjacent copper iodide inorganic motifs. Most of the 1D or 2D structures could be stable above 150°C, which meet the basic stability requirement in LED industry. Also these compounds are air and moisture stable. Leaving the sample under air for several months would not change the structures and the emission intensity. As we disperse a portion of 200 mg of 1D- $\text{Cu}_2\text{I}_2(\text{tpp})_2(\text{dps})$ and 2D- $\text{Cu}_2\text{I}_2(\text{dps})_2$ into water for 24h and recollected the samples, the powder PXRD shows the structure maintains and the QY drop is less than 5%.

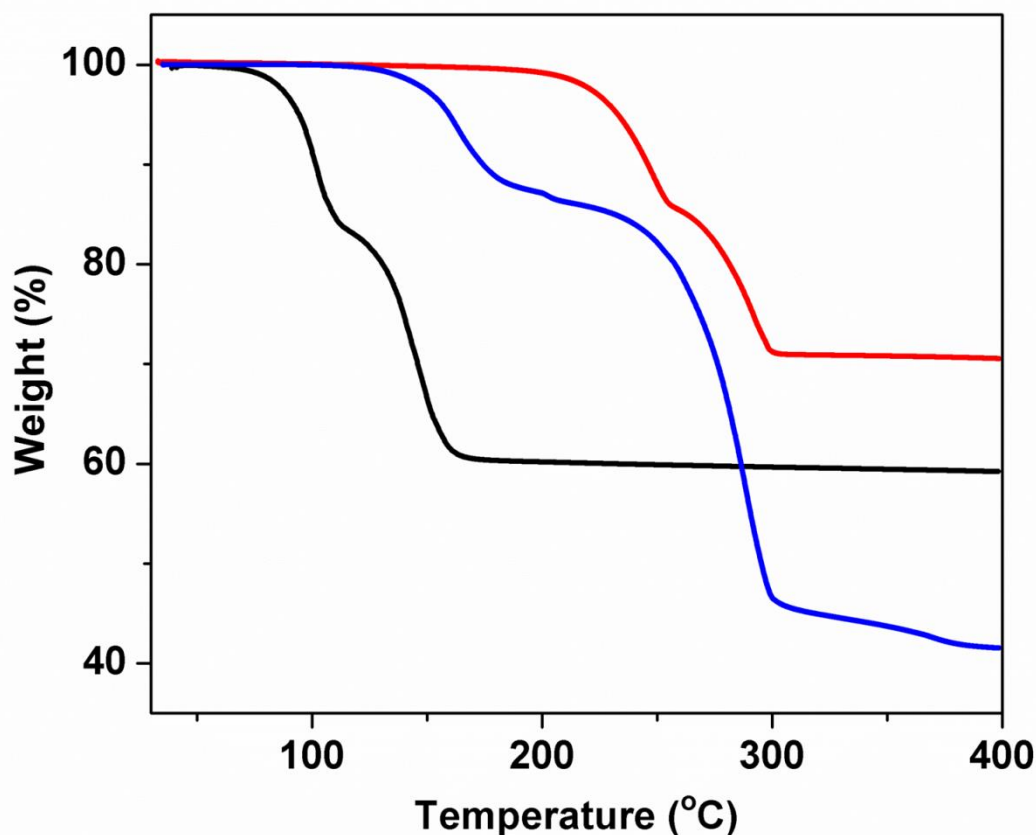


Figure 25. TG profiles of selected 0D (black), 1D (blue) and 2D structures (red).

3.5 Optical properties and luminescence mechanism

DFT calculation was conducted on selected structures and the results indicate similar density of states pattern. The valence band maximum majorly consists of inorganic copper iodide while the conduction band minimum is majorly contributed from the organic ligand. As we incorporated ligand with different LUMO energies into the structures with the same dimensionality, their band gaps change accordingly. For *tpp* based compound, both the phosphate based and the nitrogen based ligand contribute to the conduction band. As *tpp* has higher LUMO energy than most of the common N-ligands, introduction of *tpp* into the

structure usually leads to a blue shift in their optical performance. As a result, *tpp* acts not only a dimensionally controller, but an optical modulator. It is worth mentioning that, all of the compounds we obtained have band gaps that are lower than 3.1eV, usually between 2.3eV (540nm) to 2.8 eV (442nm), which means that all of the compounds could be excited by blue or violet light, even green light. The photoluminescence study shows that the emission of these compounds covers the whole visible light region, from blue to red. Their emission energy is in trend with their band gap value with a stoke shift of 30-60nm. Their quantum yields

Traditional phosphors based on Eu^{3+} , Tb^{3+} or Mn^{2+} , whose transitions are forbidden has long decay times ($>1\text{ms}$). This will cause the phosphor quenching due to the saturation from the high LED radiation flux on the phosphor. Lifetimes of these phosphors are usually within micro-second range, which prevent the saturation-based quenching. So the photoluminescence behavior of these compounds should be classified as phosphorescence.

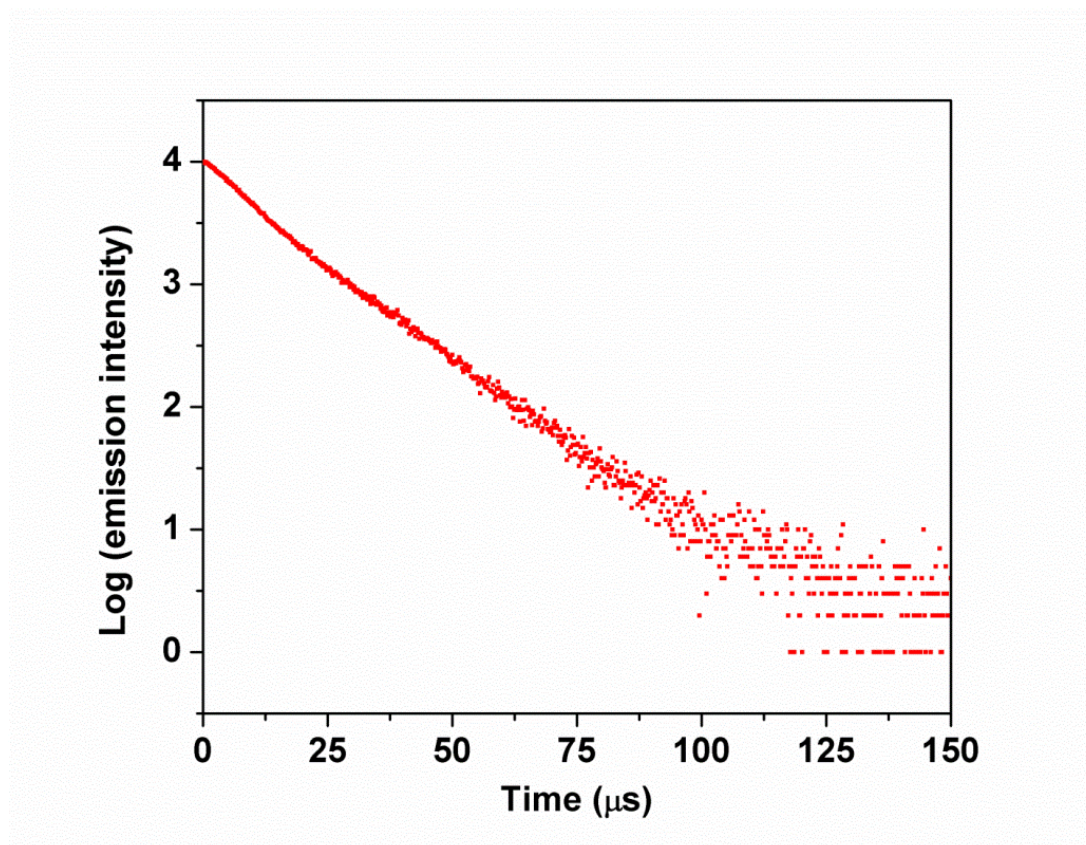


Figure 26. Luminescence decay profile (log scale) of 1D-Cu₂I₂(tpb)₂(bpp).

Table 6. Estimated band gaps, emission energies and internal quantum yields (IQY), emission color of Cu₂I₂ based compounds, and LUMO energies of organic ligands calculated at the level of B3LYP/6-311++G(3df,3pd).

Compounds	Band Gap (eV)	λ_{em} (nm)	Emission color	CIE	IQY (%)	T _D
0D-Cu ₂ I ₂ (<i>3-pc</i>) ₄	2.6	496	Blue-green	0.21, 0.40	95.2±1.4	60
0D-Cu ₂ I ₂ (<i>3,5-dm-py</i>) ₄	2.8	479	Blue	0.17, 0.24	81.5±1.1	60
0D-Cu ₂ I ₂ (<i>3-Cl-py</i>) ₄	2.5	530	Green	0.38, 0.58	85.6±1.2	50
0D-Cu ₂ I ₂ (<i>tpp</i>) ₂ (<i>3-pc</i>) ₂	3.0	455	Blue	0.14, 0.15	90.3±0.4	135
0D-Cu ₂ I ₂ (<i>tpp</i>) ₂ (<i>4,6-dm-pm</i>) ₂	2.9	465	Blue	0.15, 0.17	72.3±0.2	120
1D-Cu ₂ I ₂ (<i>tpp</i>) ₂ (<i>bpp</i>)	2.8	458	Blue	0.15, 0.15	91.7±0.5	180
1D-Cu ₂ I ₂ (<i>tpp</i>) ₂ (<i>4,4'-dps</i>)	2.6	532	Green	0.33, 0.54	80.0±1.2	150
1D-Cu ₂ I ₂ (<i>tpp</i>) ₂ (<i>4,4'-bpy</i>)	2.4	540	Yellow	0.38, 0.58	76.2±0.9	160
1D-Cu ₂ I ₂ (<i>tpp</i>) ₂ (<i>pz</i>)	2.1	631	Red	0.55, 0.30	26.1±0.3	120
1D-Cu ₂ I ₂ (<i>5-mc-pm</i>) ₂	2.3	570	Orange	0.43, 0.53	30.8±0.8	130
2D-Cu ₂ I ₂ (<i>bpe</i>) ₂	2.8	494	Blue-green	0.20, 0.37	82.3±0.4	170
2D-Cu ₂ I ₂ (<i>3,3'-bpy</i>) ₂	2.6	515	Green	0.26, 0.50	77.3±0.6	210
2D-Cu ₂ I ₂ (<i>4,4'-dps</i>) ₂	2.5	547	Yellow	0.40, 0.54	70.8±0.3	160
Two-component white phosphor	--	458, 540	White	0.31, 0.36	62.6±0.2	160

Special attention has been paid on blue excitable yellow phosphors that could be used in combine with blue LEDs to generate white light. Currently, the commercial yellow phosphor is predominately Ce doped yttrium aluminum garnet (YAG: Ce), which require the rare-earth metal Y and Ce. $2\text{D-Cu}_2\text{I}_2(\text{dps})_2$ was found to be yellow phosphor and was chosen to further evaluate the performance of this type of materials compared with commercial yellow phosphor YAG: Ce. Their emission spectra (Figure 3a) show that they have comparable broad emission bands with a full width at half maximum (FWHM) of 100nm in the green-yellow light region with almost identical λ_{em} . The CIE value calculated from it spectra, (0.40, 0.54) for $2\text{D-Cu}_2\text{I}_2(\text{dps})_2$, is also very close to that from YAG (0.41, 0.56). Its absorption curve shows that its absorption maximum is at around 450nm, indicating a strong absorption efficiency of blue light (Figure 3a). TG analysis indicates that it could be thermally stable up to 150. A series of stability experiments were further carried out on the suitability of $2\text{D-Cu}_2\text{I}_2(\text{dps})_2$ as yellow phosphor for white LED. After leaving this sample at room temperature in the air for six month, the structures still remains and the emission intensity drop is less than 5%. Dispersing the sample in water, leaving it there for one month and recollecting it would not change the structure and its emission property. These prove its high water and air stability. To mimic the working conditions, the sample was exposed under blue light (450nm) for a week; the structure maintains and no obvious decrease in emission was observed. Heating the sample in the oven for at 80°C for a week would lead to an emission intensity drop of 4.8% (Figs. 27-30).

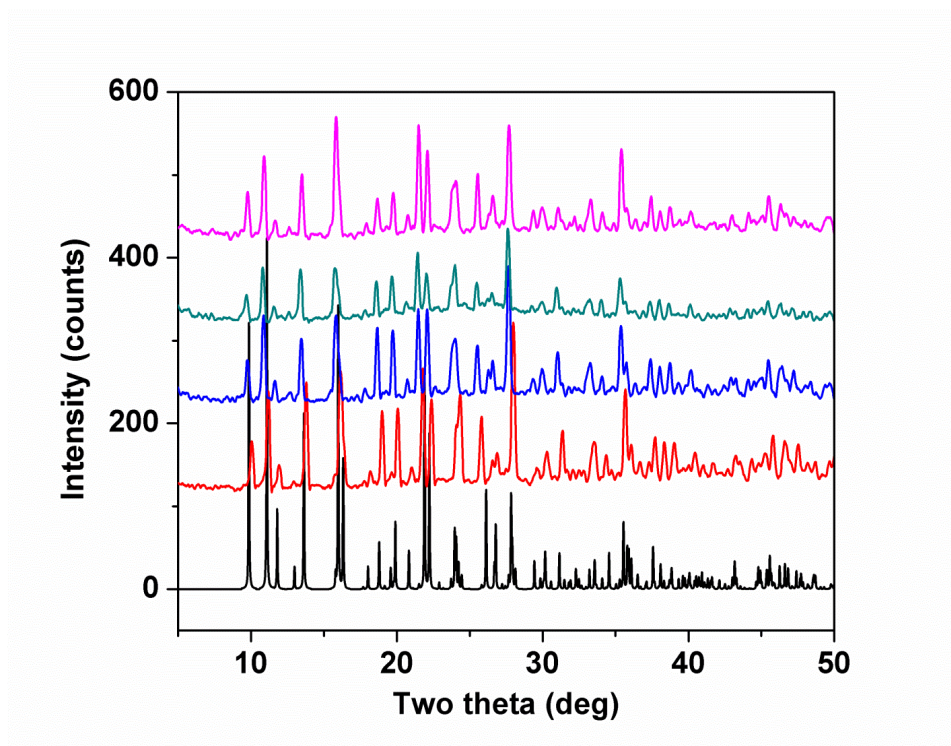


Figure 27. PXRD patterns of $2D-Cu_2I_2(4,4'-dps)_2$ after various treatments. From bottom to top: simulated, freshly made, in air for six month, under blue light for a week, heated at 80 °C for a week.

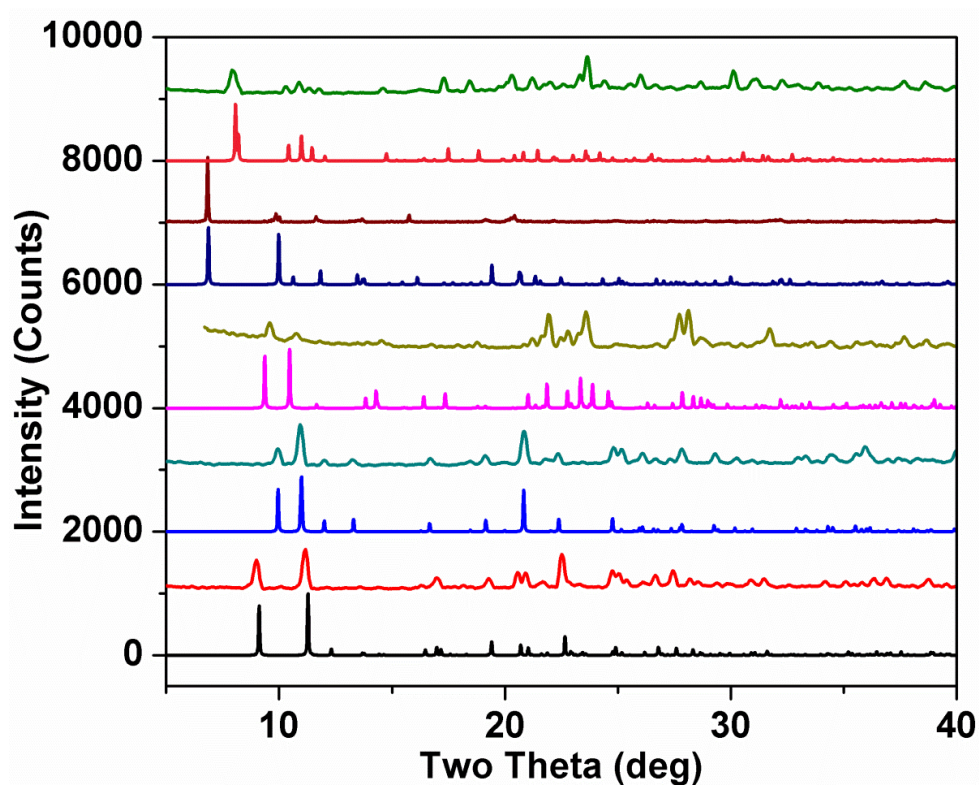


Figure 28. PXRD patterns of compounds from bottom to top: 0D- $\text{Cu}_2\text{I}_2(3\text{-pc})_4$, 0D- $\text{Cu}_2\text{I}_2(3,5\text{-dm-py})_4$, 0D- $\text{Cu}_2\text{I}_2(3\text{-Cl-py})_4$, 0D- $\text{Cu}_2\text{I}_2(\text{tpp})_2(3\text{-pc})_2$, 0D- $\text{Cu}_2\text{I}_2(\text{tpp})_2(4,6\text{-dm-pm})_2$, 1D- $\text{Cu}_2\text{I}_2(\text{tpp})_2(\text{bpp})$.

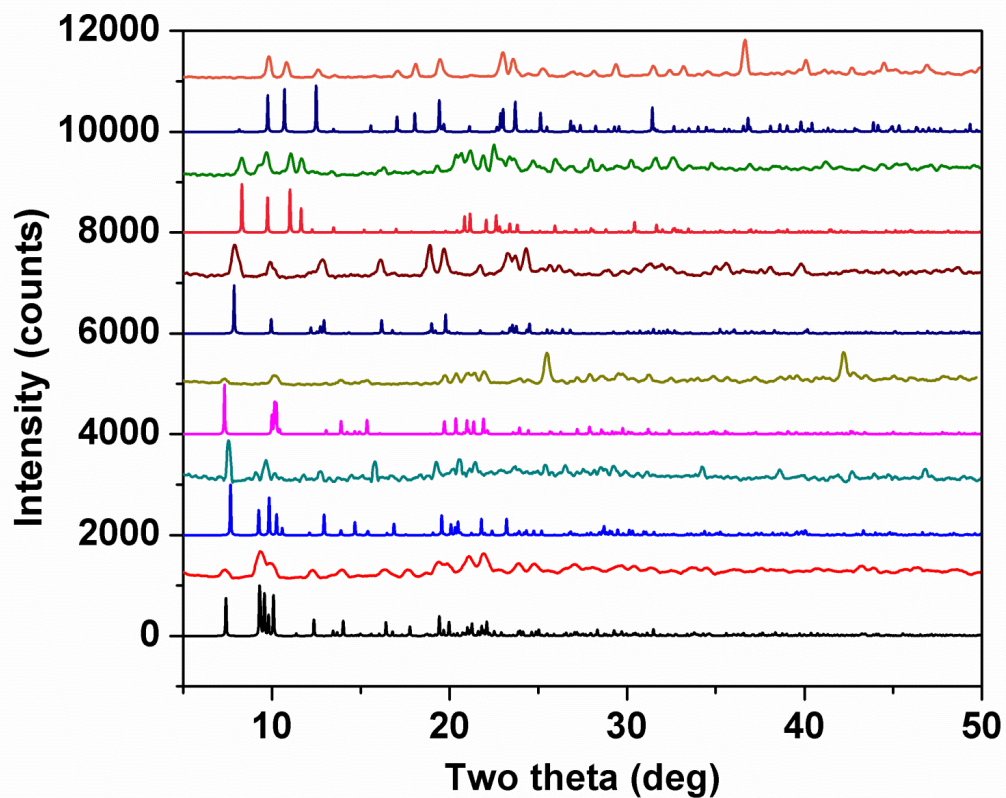


Figure 29. PXRD patterns of compounds 1D-Cu₂I₂(tpp)₂(4,4'-dps), 1D-Cu₂I₂(tpp)₂(4,4'-bpy), 1D-Cu₂I₂(tpp)₂(pz), 1D-Cu₂I₂(5-me-pm)₂, 2D-Cu₂I₂(bpe)₂, 2D-Cu₂I₂(3,3'-bpy)₂, 2D-Cu₂I₂(4,4'-dps)₂.

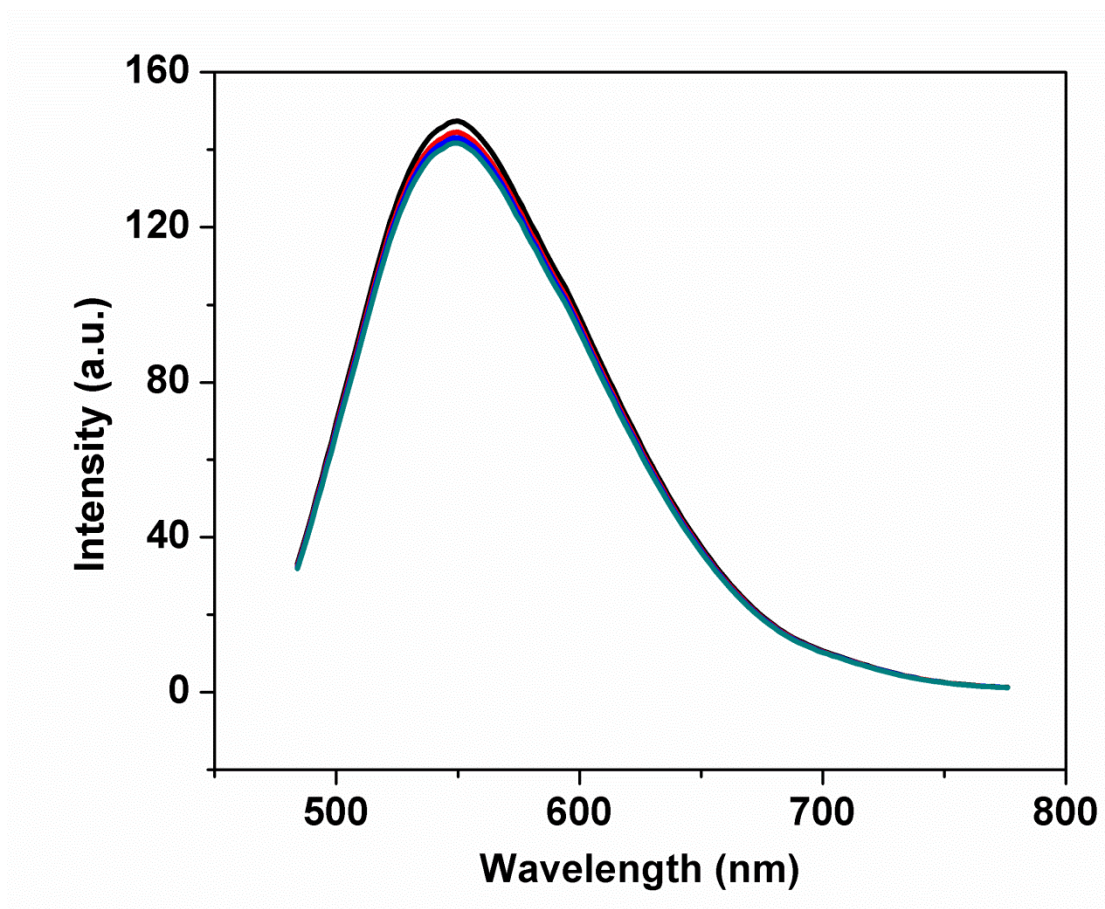


Figure 30. Emission spectrum of $2\text{D-Cu}_2\text{I}_2(4,4'\text{-dps})_2$ after various treatments. From bottom to top: freshly made (black), in the air for six month (red), under blue light for a week (blue), at 80 °C for a week (cyan). λ_{ex} is 455 nm.

In addition to yellow phosphors, phosphors with other colors are also in demand in industry, such as blue phosphors which are commonly used as emitters for fluorescent lamps, and red phosphors which are usually used in combined with YAG to improve the light quality to make warmer white light. This type of phosphors has the unique advantage of optical tunability that could achieve various colors by proper phosphor designs (Fig. 31). Pure white light mixed phosphor has been made by directly mixing a blue phosphor 1D-

$\text{Cu}_2\text{I}_2(\text{tpp})_2(\text{bpp})_2$ and a yellow phosphor $1\text{D-Cu}_2\text{I}_2(\text{tpp})_2(\text{bpy})$. The quantum yield obtained is 61.2%.

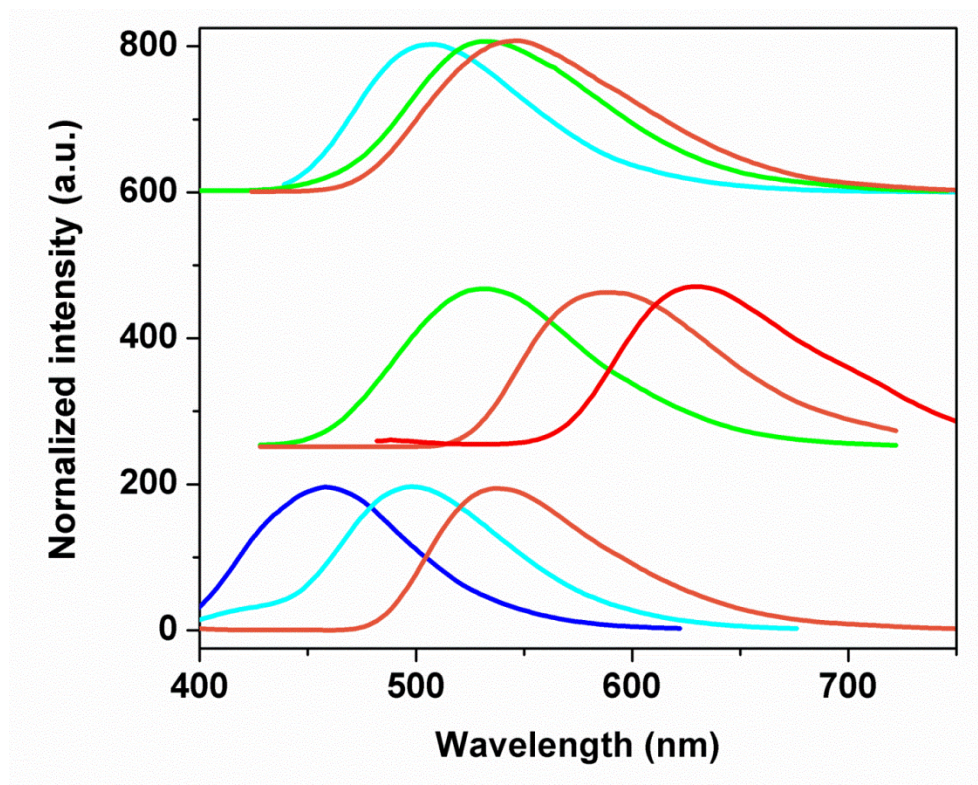


Figure 31. Photoluminescence spectra ($\lambda_{\text{ex}} = 360 \text{ nm}$) of selected compounds.

3.6 Performance as lighting phosphors

To further evaluate their performance, LED bulbs were fabricated by remote phosphor coating approach (Figs 32-33). Integrated coating, which the phosphor has direct contact with the LED, is not suitable. One reason for this is the light from the phosphor would be absorbed by the LED chip and also the heat from the LED would lead to the decomposition of the phosphor. As a result, the remote phosphor approach overcome the

issue of temperature increase caused by the LED chip and could maintain a friendly working environment for the phosphor. A water soluble binder was used for the coating to ensure optimum performance. The phosphors were coated on the inner shell of 25mm diameter glass globes. Detailed coating procedure was described in the supporting information. Violet LEDs (405nm) or blue LEDs (450nm) were fabricated inside the bulbs as the excitation source. Schematics of this system were illustrated in Figure X. Figure X is the image taken at the working condition. Keeping the light bulbs on for weeks would not cause any obvious change of their emitting brightness.

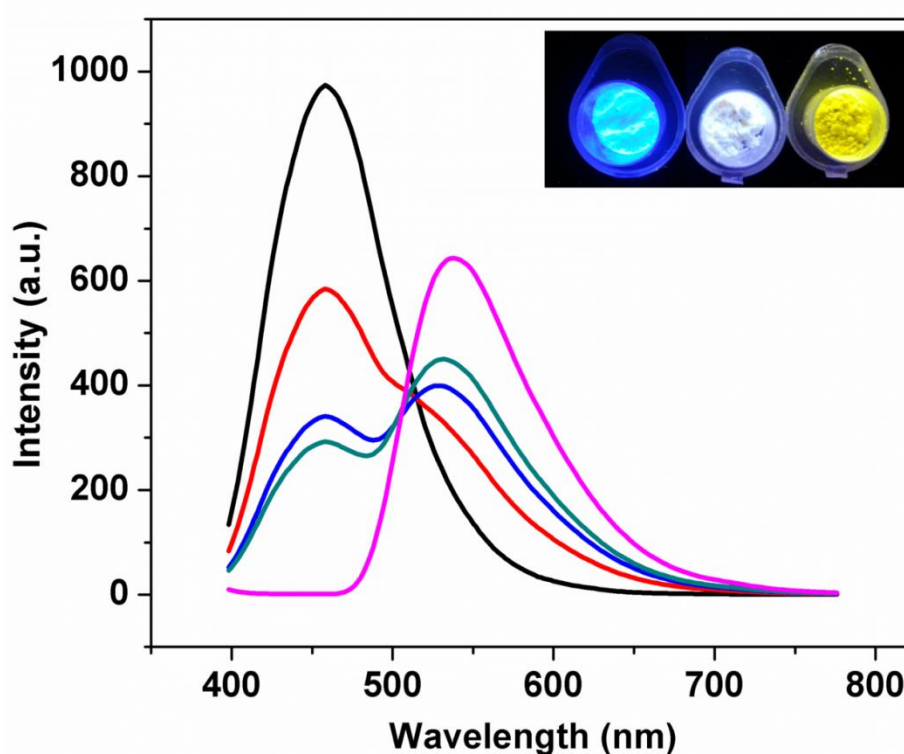


Figure 32. Luminescence spectra of the two-component phosphors with the following weight percentage of $1D-Cu_2I_2(tpp)_2(dps)$: 0 wt% (black), 5 wt% (red), 15 wt% (blue), 25 wt% (green), 100 wt% (pink).



Figure 33. LED bulbs design and displayed at working condition.

3.7 Summary

In summary, a precursor approach has been developed as a rational design pathway for copper iodide based complexes. Based on this approach, a series of 0D to 2D inorganic-organic hybrid materials based on copper halide dimer have been synthesized as promising LED phosphors with tunable emissions. Comparing with the current commercially available phosphors and previously reported non-rare-earth phosphors, they have several obvious advantages. First of all, this type of materials has genuinely high quantum efficiency that is

comparable to the commercial phosphors. All of these emissions are tunable and could be predicted by computation. Secondly, most of these phosphors are synthesized by common cost effective inorganic and organic raw materials, and could be easily synthesized at low temperature in solution. Moreover, these materials are rare-earth free, which will release the pressure of rare-earth supply shortage. This work is a pioneering work of highly efficient copper iodide based non-rare-earth phosphors and will open up a new approach in designing phosphors with specific requirement.

4. Mechanochemical synthesis of high-performance hybrid materials

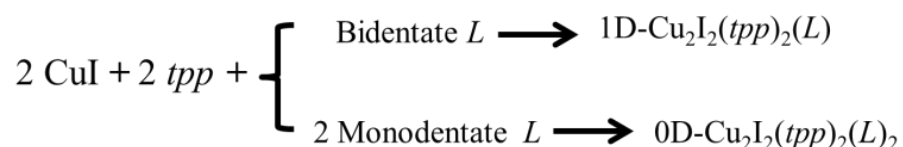
4.1 Background

Traditional solvothermal method has been developed extensively in laboratory as the synthetic approach for preparing a series of novel materials, such as graphene, metal-organic frameworks (MOFs), inorganic-organic hybrid materials, and nanocrystals (NCs).^{25,27-29,43,67-71} However, the usage of large amount of solvents (often organic-based), the complicated reaction procedure and the relatively long reaction time make this method not favorable for industrial production since large-scale synthesis generally requires the reaction under environmental friendly conditions with minimum usage of auxiliary substances. The concept of auxiliary substances has been brought up by green chemistry, meaning all substances required for a chemical synthesis and subsequent product purification, including solvents, drying agents, column packing agents, etc., either for chemical synthesis or product purification.⁷² Since functional materials such as MOFs and NCs exhibit significant potentials for commercialization,^{73,74} developing greener approach which could limiting the usage of auxiliary substances and simply the reaction procedures for the syntheses of these materials in large quantity is becoming highly relevant.

Recently, copper halide based inorganic-organic hybrid materials have attracted much attention due to their structural diversity, remarkable luminescence properties, facile syntheses, as well as earth abundancy and low cost. In particular, they are considered as promising potential phosphor candidates to replace traditional REE based materials for general lighting devices.^{32,45,47} Among them, certain types of structures, such as those built on CuI monomers, Cu₂I₂ dimers and Cu₄I₄ cubane

tetramers, have shown high internal quantum yields (IQYs) that are comparable to those of the commercial phosphors.^{33,46} However, many CuI based materials are synthesized in organic solvents including acetonitrile, dichloromethane, etc., which are classified as volatile organic compounds (VOCs) and lead to environmental damage and human health risks.^{45,46} The complicated separation, purification and drying processes cause more auxiliary substance usage and additional loss of the product.

Scheme 1. Stoichiometric syntheses with anticipated structure and composition.



The mechanochemical technique, such as manual grinding or ball milling, have been reported as greener approaches for various materials' syntheses, such as organic compounds and metal complexes, with the advantages of high reaction yield, low pollution, and shorter reaction times compared to conventional methods.⁷⁵⁻⁷⁹ However, there are scant literature reports demonstrating this approach for copper halide hybrid materials, mainly because of the difficulties in isolating targeted phases, as various types of structures may simultaneously form upon simple grinding.⁸⁰ Moreover, washing and separation procedures are usually needed in order to remove unreacted starting materials, which require the use of additional solvent and lowers the yields of the final products. To address these concerns, in this study, I developed a green synthetic route that involves stoichiometric mixing of reactants by mechanochemical approach. In order to achieve high-quality single-phase products,

triphenylphosphine (*tpp*) was introduced as a second ligand in addition to the nitrogen containing ligands (N-ligands), which limits the reaction products to dimers, and prevents the formation of side products. Both CuI and *tpp* were added in stoichiometric quantities based on their ratio in the anticipated products (see Scheme 1). The selected N-ligands are liquids and were added in excess to ensure reaction completion. Employing this approach, all of the solid starting materials were transformed into product and the excess liquid ligand simply evaporates out during grinding. As a result, the reaction proceeds to full completion, with no discreet waste formed and no washing or purifying steps needed. This green chemistry route provides a means to overcome the negative environmental and health related impacts typically associated with material synthesis (Fig. 34).

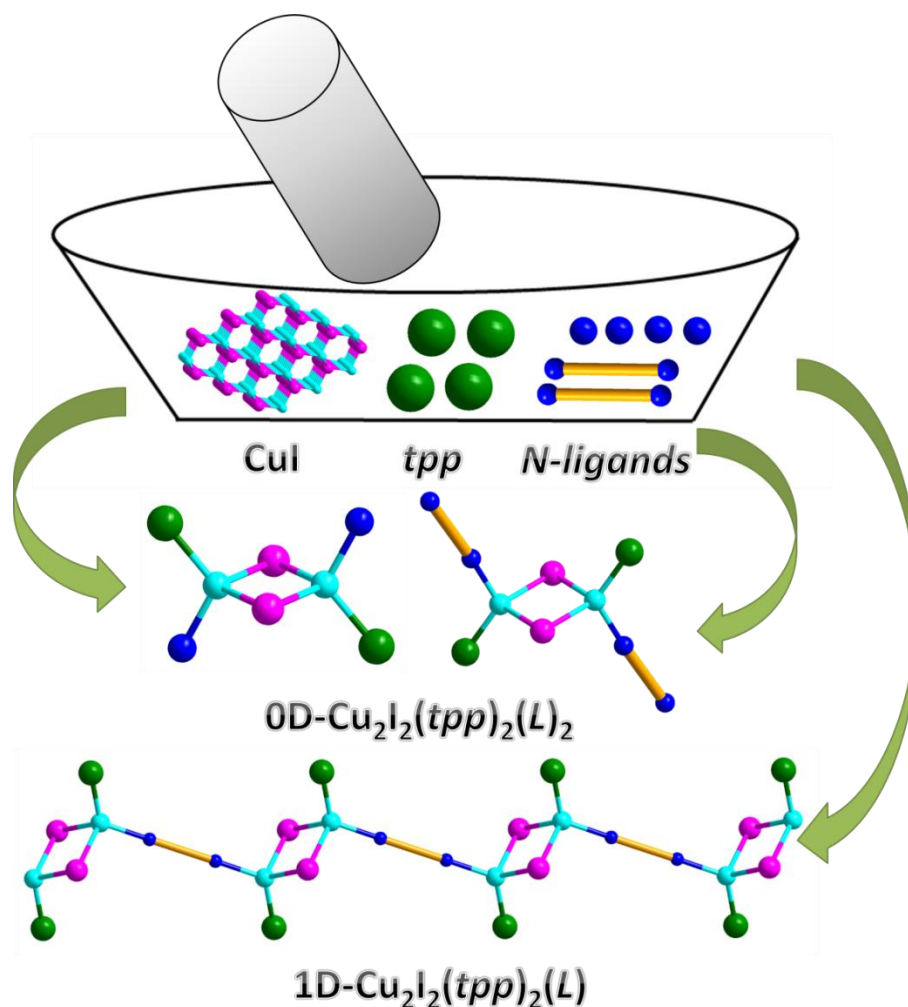


Figure 34. Illustration of the grinding synthesis.

4.2 Solvent-free synthesis

$0\text{D-Cu}_2\text{I}_2(tpp)_2(4\text{-}pc)_2$, $0\text{D-Cu}_2\text{I}_2(tpp)_2(3\text{-}pc)_2$, $0\text{D-Cu}_2\text{I}_2(tpp)_2(py)_2$, $0\text{D-Cu}_2\text{I}_2(tpp)_2(4,6\text{-}dm\text{-}pm)_2$, $0\text{D-Cu}_2\text{I}_2(tpp)_2(4\text{-}me\text{-}pm)_2$, $0\text{D-Cu}_2\text{I}_2(tpp)_2(3\text{-}Br\text{-}py)_2$, $1\text{D-Cu}_2\text{I}_2(tpp)_2(pm)$, $1\text{D-Cu}_2\text{I}_2(tpp)_2(2,5\text{-}dm\text{-}pz)$, $1\text{D-Cu}_2\text{I}_2(tpp)_2(2\text{-}pr\text{-}pz)$, $1\text{D-Cu}_2\text{I}_2(tpp)_2(2\text{-}me\text{-}pz)$ were synthesized by manual grinding method in a similar manner. CuI and tpp were added stoichiometrically based on the composition of the product and liquid based N-

ligands were added in excess. Reactants were placed in a simple agate mortar and were ground with a regular pestle. After grinding, the reaction mixture was dried for several minutes and was collected by scraping the product off of the mortar. No further washing or separation was needed and the reaction yields are quantitative. For a typical synthesis of $0D-Cu_2I_2(tpp)_2(3-pc)_2$, CuI (0.19 g, 1.0 mmol) and *tpp* (0.28 g, 1.0 mmol) and *3-pc* (1.0 ml) were added to mortar and ground with the pestle manually. The reaction mixture started to emit blue under UV light upon grinding. The whole reaction mixture was ground for 5 min and the reaction powder was dried under vacuum for 15 min. The powder in the mortar was scraped off and was used directly for characterization. The whole process should be conducted in the hood.

$0D-Cu_2I_2(tpp)_2(1-me-bzim)_2$ was prepared by solvothermal synthesis. CuI (0.019g, 0.1 mmol) and *tpp* (0.028 g, 0.1 mmol) and 1-methyl-benzimidazole (*1-me-bzim*) (0.013g 0.1 mmol) were added into a mixture of CH_2Cl_2 /toluene (1:1/v:v) and were heated at 80 °C. Single crystals along with pure phase powder were formed overnight. The yield was 57% based on Cu.

Ball milling of $0D-Cu_2I_2(tpp)_2(3-pc)_2$ was conducted on Spex 8000m mixer/mill. CuI (0.19 g, 1.0 mmol), *tpp* (0.28 g, 1.0 mmol) and *3-pc* (80 μ l) was added to a stainless steel reaction canister. The total milling time was 5 min. Afterwards, the white powder product was scraped out of the canister.

Crystals suitable for single crystal X-ray diffraction were obtained by heating a mixture of $0D-Cu_2I_2(tpp)_3$ precursor and N-ligands in mixed CH_2Cl_2 /toluene (1:1/v:v) solvent system at 80 °C. Crystals typically form within 24 h. For a typical synthesis of $0D-Cu_2I_2(tpp)_2(4-mr-pm)_2$, $0D-Cu_2I_2(tpp)_3$ precursor (0.062g, 0.1 mmol) and *4-me-pm* (0.1 ml) were added to a CH_2Cl_2 /toluene mixture and were heated at 80 °C overnight.

Colorless cubic crystals were filtered via vacuum filtration for further characterizations.

The one-pot synthesis of direct white light emitting blends was achieved by grinding CuI (0.19 g, 1.0 mmol), *tpp* (0.28 g, 1.0 mmol), *3-pc* (0.6 ml) and *2,5-dm-pz* (1.0 ml). After grinding for 5 min, both 0D-Cu₂I₂(*tpp*)₂(*3-pc*)₂ and 1D-Cu₂I₂(*tpp*)₂(*2,5-dm-pz*) formed together as a white-light blend of a blue phosphor and a yellow phosphor, respectively.

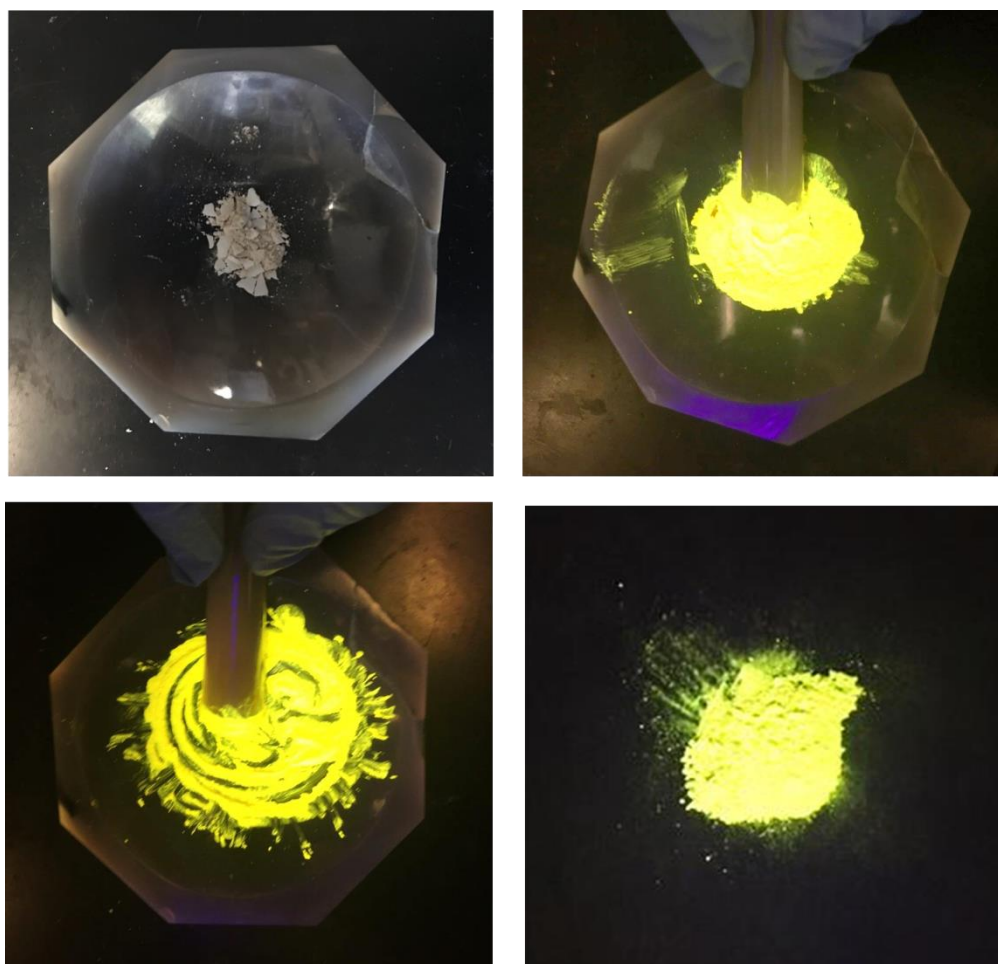


Figure 35. Images taken of grinding 1D-Cu₂I₂(*tpp*)₂(*2-pr-pz*) under UV light.

4.3 New structures and phase purity analysis

Ten pure-phase CuI compounds were obtained using the manual grinding method described in the Experimental section (Fig. 34). The grinding syntheses and structure formation can be directly monitored under UV light (Fig. 35); reactions were typically complete within ten minutes. In the case of several compounds, a few drops of dichloromethane were added during grinding in order to achieve thorough homogenization of the reaction mixture. The purities of the obtained products were confirmed by PXRD analyses. Based on PXRD patterns of the as-made samples compared with simulated patterns, pure phases of all these compounds were obtained. The PXRD patterns were also compared with those of the starting materials and possible intermediates, including CuI, *tpb*, and $0D-Cu_2I_2(tpb)_3$, the results of which indicate that all of the reactants were consumed and no intermediates exist in the final products. The unreacted N-ligands (liquid) together with the small amount of solvent (if used) were evaporated during the grinding process or after evacuation. As a result, the obtained powders are pure phase and require no additional separation or purification. Single crystals of the new compounds were obtained by dissolving the $0D-Cu_2I_2(tpb)_3$ precursor with the N-ligands in a mixture of dichloromethane and toluene (v : v = 1 : 1) followed by mild heating.

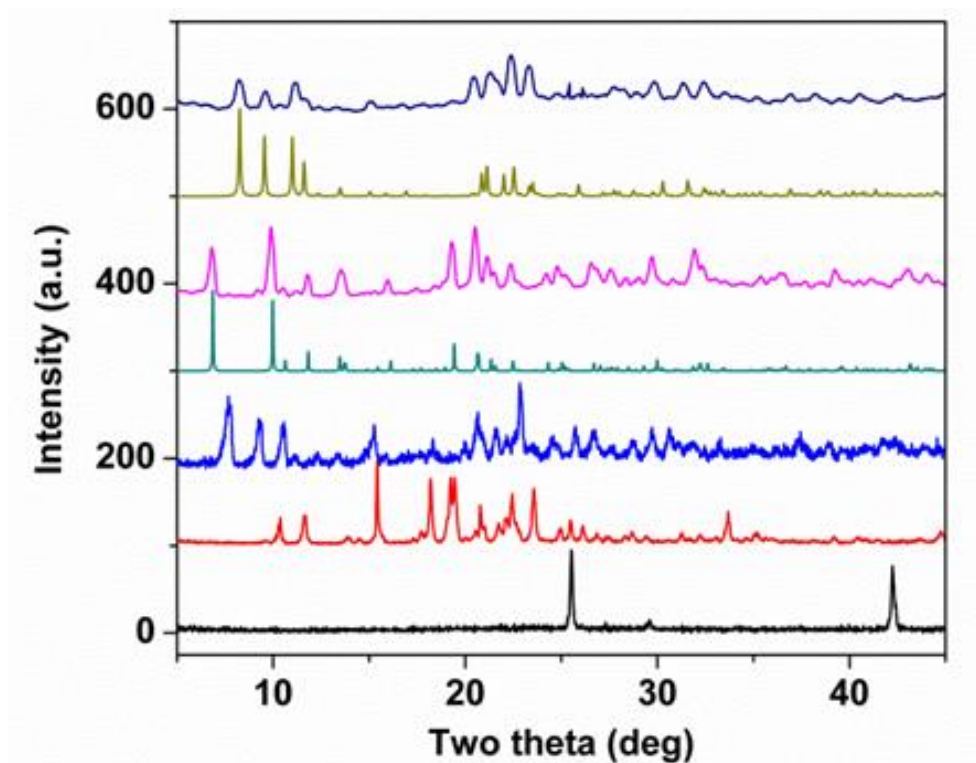


Figure 36. PXRD patterns of selected structures compared with the starting materials. From bottom to top: commercial CuI, commercial *tpp*, as made 0D-Cu₂I₂(*tpp*)₃, simulated 0D-Cu₂I₂(*tpp*)₂(3-*pc*)₂, as made 0D-Cu₂I₂(*tpp*)₂(3-*pc*)₂, simulated 1D-Cu₂I₂(*tpp*)₂(2-*me-pz*), as made 1D-Cu₂I₂(*tpp*)₂(2-*me-pz*).

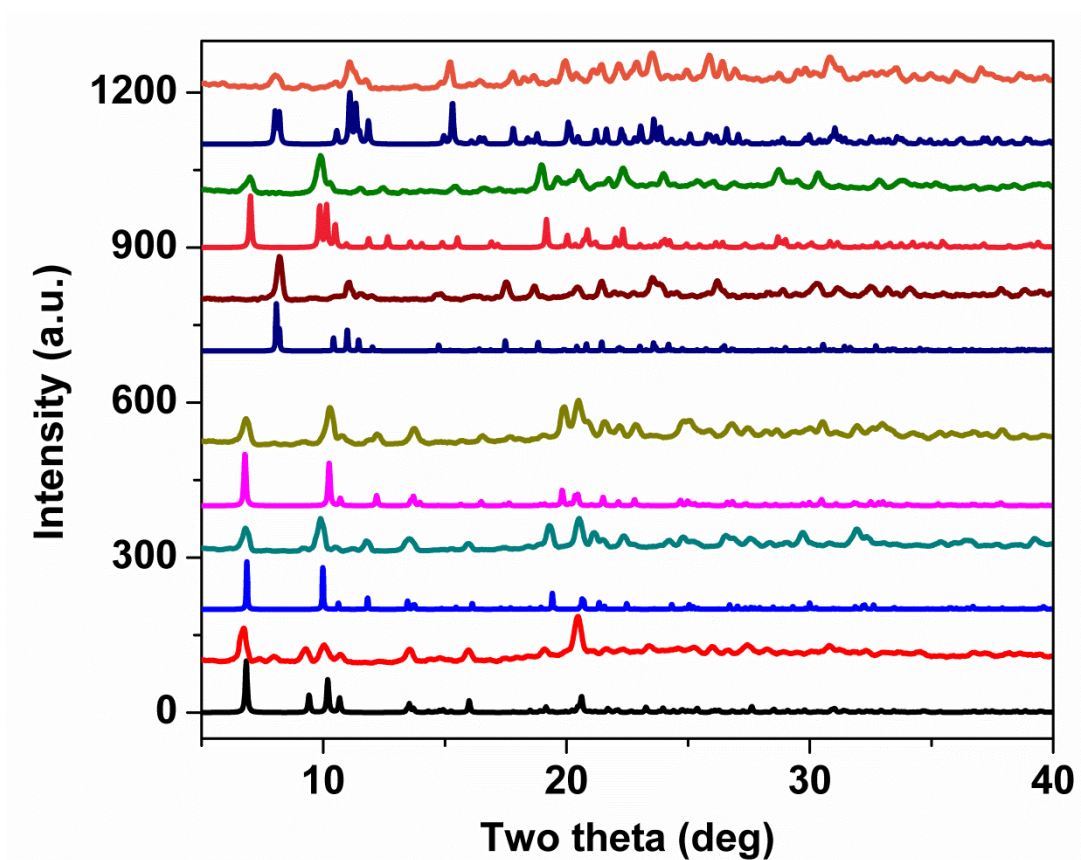


Figure 37. PXRD patterns. From bottom to top: 0D-Cu₂I₂(*tpb*)₂(4-*pc*)₂, 0D-Cu₂I₂(*tpb*)₂(3-*pc*)₂, 0D-Cu₂I₂(*tpb*)₂(*py*)₂, 0D-Cu₂I₂(*tpb*)₂(4,6-*dm-pm*)₂, 0D-Cu₂I₂(*tpb*)₂(4-*me-pm*)₂, 0D-Cu₂I₂(*tpb*)₂(3-*Br-py*)₂.

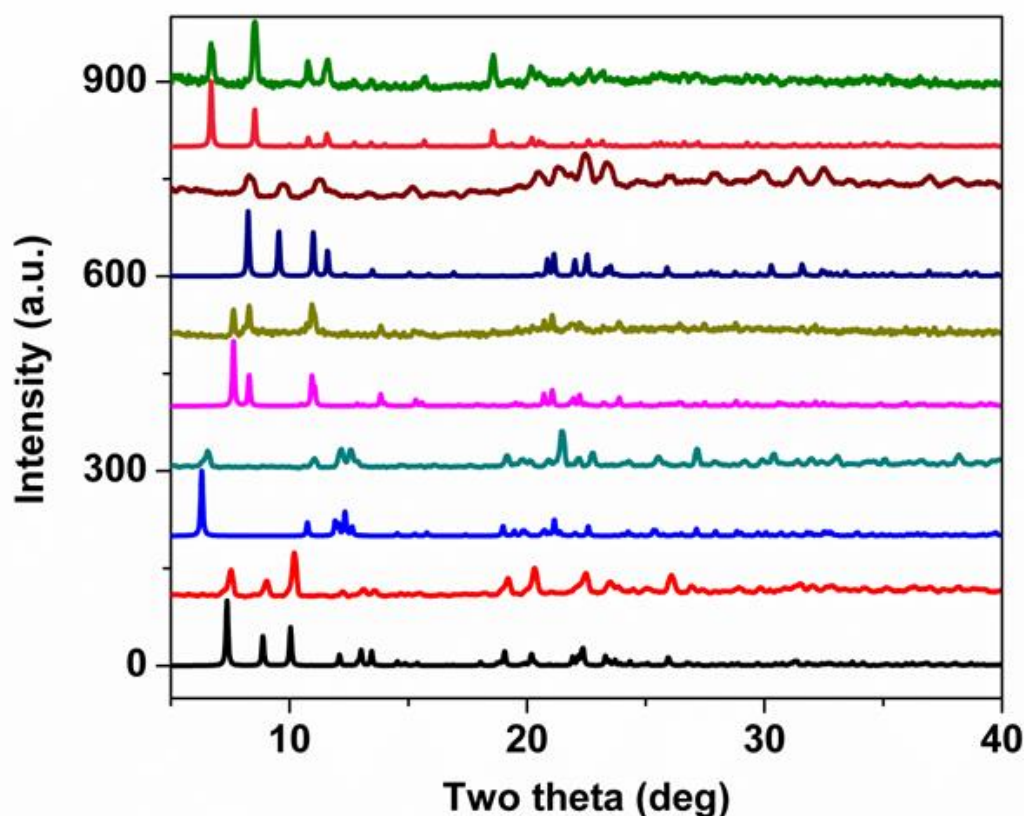


Figure 38. PXRD patterns. From bottom to top: $1\text{D-Cu}_2\text{I}_2(\text{tpp})_2(\text{pm})$, $1\text{D-Cu}_2\text{I}_2(\text{tpp})_2(2,5\text{-dm-pz})$, $1\text{D-Cu}_2\text{I}_2(\text{tpp})_2(2\text{-pr-pz})$, $1\text{D-Cu}_2\text{I}_2(\text{tpp})_2(2\text{-me-pz})$, $0\text{D-Cu}_2\text{I}_2(\text{tpp})_2(1\text{-me-bzim})_2$.

The reaction of CuI with organic ligands generates a variety of structures affected by solvent type and reaction conditions. Simply grinding the CuI with the N-ligand leads to a mixture of many types of structures. For example, when CuI was ground with 3-pc, the $0\text{D-Cu}_2\text{I}_2(3\text{-pc})_4$, $0\text{D-Cu}_4\text{I}_4(3\text{-pc})_4$, and $1\text{D-CuI}(3\text{-pc})$ all formed with no means of separation. However, when tpp was introduced, the final product was pure phase dimer based $0\text{D-Cu}_2\text{I}_2(\text{tpp})_2(3\text{-pc})_2$, suggesting the tpp containing structure is the most thermodynamically stable phase. This can be attributed to the Cu-P bonds being stronger than Cu-N, which was evidenced in the TG profile; the tpp in these

structures has much higher decomposition temperature compared to that of the N-ligands. The steric hindrance of bulky *tpp* molecules can also restrict the structures to Cu_2I_2 dimer based.

To confirm that the *tpp* Cu_2I_2 dimer based structures are the most thermodynamically stable phase, we ground pre-made *tpp*-free CuI structures with their corresponding ligand but introduced *tpp* to the mixture to see if the *tpp* phase would dominate the final product. When mixtures of 0D- $\text{Cu}_2\text{I}_2(3\text{-}pc)_4$, 0D- $\text{Cu}_4\text{I}_4(3\text{-}pc)_4$, or 1D-CuI(*3-pc*) were ground with *tpp* and *3-pc* for 10 min, 0D- $\text{Cu}_2\text{I}_2(tpp)_2(3\text{-}pc)_2$ is the only product (Fig. 36). Based on this finding, we can conclude that even if kinetically stable by-product phases form during the grinding process, they eventually transform to 0D- $\text{Cu}_2\text{I}_2(tpp)_2(3\text{-}pc)_2$. As a result, *tpp* plays a vital role in achieving clean synthesis of the target product and preventing the formation of mixed phases.

To confirm the mechanochemical nature of the reactions, comparison reactions were conducted by mixing the starting materials in a uniform manner avoiding any mechanical forces. Taken 0D-CuI(*tpp*)₂(*4,6-dm-pm*)₂ as an example. After the carefully placing the CuI, *tpp* and *4,6-dm-pm* in the mortar without any disturbance until the ligand was dried, the reaction was monitored under a UV bar and only a very small portion of the reaction mixture showed blue emission under the UV light (Fig. 39), indicating that most of the starting materials remain unreacted. This provides strong evidence that the mechanical energy provided by grinding is the major cause for the breaking and forming of bonds. Generally, grinding increases the reactants' contact surface areas and creates more reactive centers that drive the reaction to completeness.⁸¹

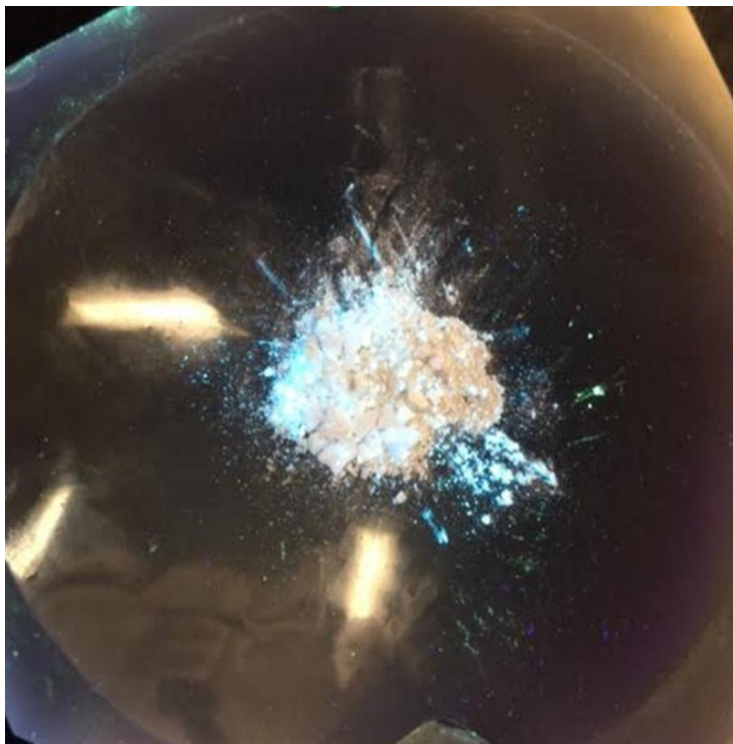


Figure 39. Mixture of CuI, *tpp* and 4,6-*dm-pm* without applying mechanochemical force. Image was taken under UV bar (365nm) after the liquid N-ligand was completely dried.

4.4 Reaction process analysis

Another advantage of this method is that the reaction progress is often visible and can be monitored due to the emissive nature of the products. The reaction progress of 0D-Cu₂I₂(*tpp*)₂(3-*pc*)₂ was investigated in detail using PXRD analyses at different stages of grinding. The grinding process was stopped at specific intervals and the reaction was dried for characterization. Based on PXRD data, several “transition states”, such as 0D-Cu₂I₂(*tpp*)₃ and 0D-Cu₂I₂(3-*pc*)₄, may form at early stages, which would completely transform to 0D-Cu₂I₂(*tpp*)₂(3-*pc*)₂ after 10 min of grinding, since it

is the most thermodynamically stable phase (Fig. 40). As a result, the reaction might go through two pathways (Fig. 41). CuI can first react with *tpb* to form $0D-Cu_2I_2(tpb)_3$, and then react with surrounding *3-pc* to form the final product. Or, the $0D-Cu_2I_2(3-pc)_4$ forms first in the ligand excess environment and then reacts with *tpb*. Both pathways finally lead to the formation of the desired product, $0D-Cu_2I_2(tpb)_2(3-pc)_2$. It is worth mentioning that grinding syntheses may not be suitable for single crystal growth, which can be achieved by conventional solvothermal methods.

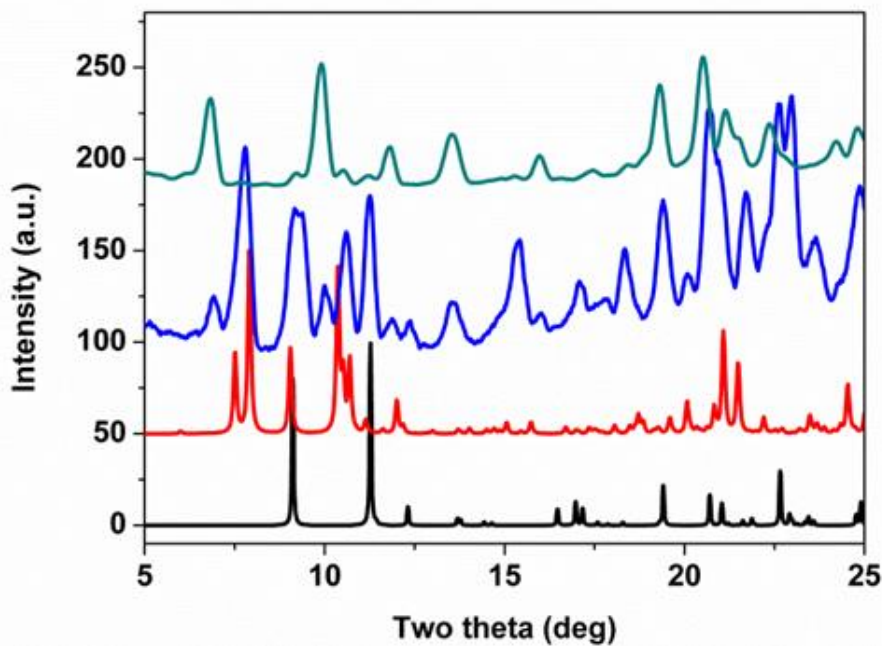


Figure 40. PXRD patterns of various phases. From bottom to top: simulated $0D-Cu_2I_2(3-pc)_4$, as made $0D-Cu_2I_2(3-pc)_4$, simulated $0D-Cu_4I_4(3-pc)_4$, as made $0D-Cu_4I_4(3-pc)_4$, simulated $1D-CuI(3-pc)$, as made $1D-CuI(3-pc)$, simulated $0D-Cu_2I_2(tpb)_2(3-pc)_2$, and final product $0D-Cu_2I_2(tpb)_2(3-pc)_2$, after grinding of the three-phase mixture.

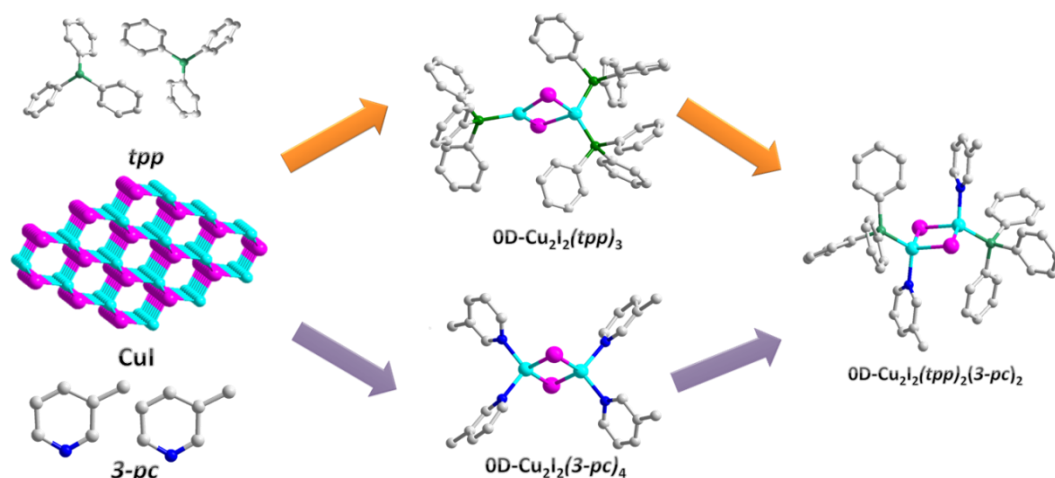


Figure 41. Two possible reaction pathways for the formation.

Green chemists categorize the solvents and other materials required for the syntheses as auxiliary substances. Limiting the usage of auxiliary substances is a major task for green chemistry. Though people usually associate grinding synthesis with “solvent free”, it generally means that no solvent was intentionally added into the reaction mixture. In fact, most of the mechanochemical reactions of coordination polymers, including metal-organic frameworks (MOFs), have reported grinding with the aid of a small amount of solvents.⁸² Fluidity has to be considered for these reactions to proceed. In these cases, the expression “minimal usage of solvent” instead of “solvent free” is used, and such grinding approaches are called “liquid assisted grinding” (LAG).⁸³ For other cases, one of the reactants is often liquid or the moisture in the air aids the reactions.⁸⁴ In this work, we focused on liquid ligands that play the role of “solvent”. As a result, no discreet solvent is needed for most of the syntheses. However, this does not mean that the use of exclusively solid ligands would make the grinding syntheses of these materials unachievable. We have tried to

use *1-me-bzim*, a solid organic, as the ligand and by simple grinding, blue emitting 0D- $\text{Cu}_2\text{I}_2(\text{tpp})_2(1\text{-me-bzim})_2$ forms in high quality. However, the ligand has to be added in excess and solvent needs to be added in order to ensure the reaction goes to completion. The unreacted portion of the ligand also needs to be washed by solvents, such as ethanol. When solid *1-me-bzim* was ground stoichiometrically with CuI without solvent, unreacted CuI and *tpp* peaks are present in the PXRD pattern, even after long periods of grinding. In both cases, further purification is necessary in order to obtain pure phase and this would add to more labor and auxiliary substance usage.

In order to show the possibility of industrial production, balling milling synthesis was also performed to generate 0D- $\text{Cu}_2\text{I}_2(\text{tpp})_2(3\text{-pc})_2$. After 5 min of milling, pure phase 0D- $\text{Cu}_2\text{I}_2(\text{tpp})_2(3\text{-pc})_2$ was obtained with better quality compared to manual grinding, judging from the PXRD patterns (Fig. 42). This shows the potential of this method for industrial milling, which could further lower manufacturing costs.

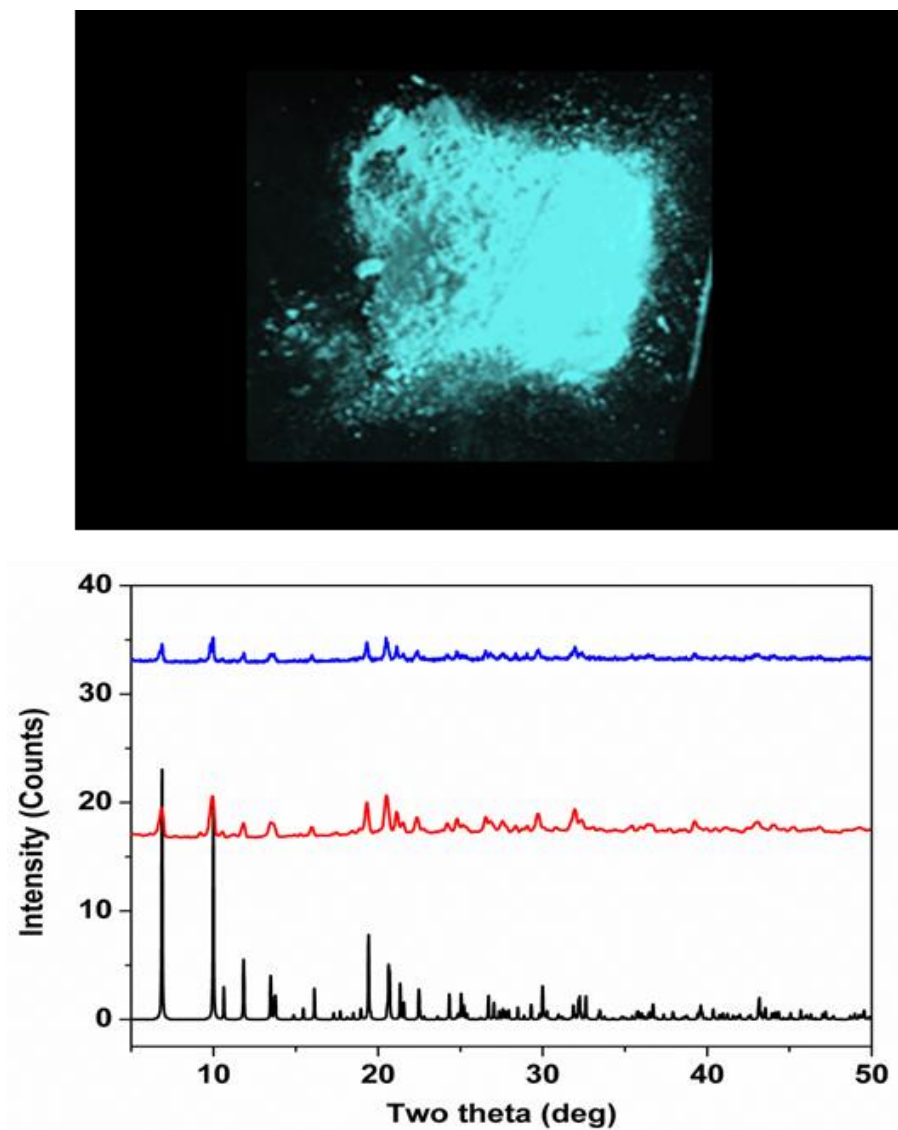


Figure 42. Top: Product of $0\text{D-Cu}_2\text{I}_2(\text{tpb})_2(3\text{-pc})_2$, prepared by ball-milling under UV radiation. Bottom: PXRD patterns of $0\text{D-Cu}_2\text{I}_2(\text{tpb})_2(3\text{-pc})_2$, from bottom to top: simulated pattern, sample prepared by manual grinding, and sample prepared by ball milling.

4.5 Optical properties and application as lighting phosphors

The optical absorption spectra were recorded at room temperature and converted using the Kubelka-Munk function. Band gaps of the products were estimated from the absorption edges (Fig. 43) and are listed in Table 8. DFT calculations on Cu_2I_2 dimer structures indicate that the band gaps of these structures are tunable via incorporation of ligands with different LUMO energies.⁴⁶ Based on these findings, ligands with varying LUMO energies were selected, which lead to products with band gap values varying from 2.2 eV to 3.1 eV (Table 8). The solid state PL emission spectra were measured on powder samples at room temperature (Fig. 44). All compounds exhibit intense luminescence in the visible light region (400-700 nm), and have emission energies that are in trend with their band gap energies. The emission spectra are all single band emission with a full width at half maximum (FWHM) of ~100 nm. The luminescence mechanism of CuI based dimers are proposed to be a combination of halide-to-ligand charge transfer (XLCT) metal-to-ligand charge transfer (MLCT), and halide-to-metal charge transfer (XMCT).^{33,34} The IQYs of these structures were measured and are listed in Table 8; most of the products have IQYs higher than 70%, comparing favorably to the values of commercial phosphors.

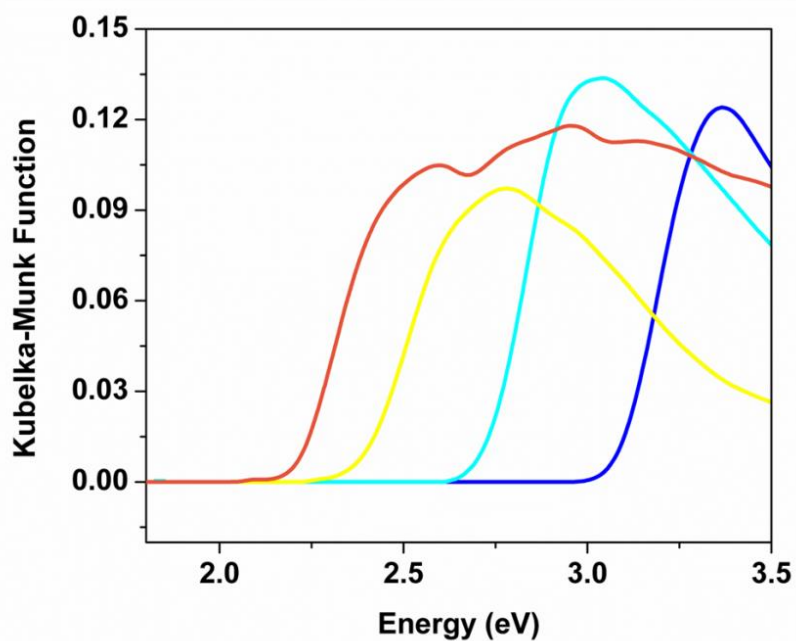


Figure 43. Optical absorption spectra of 0D-Cu₂I₂(tpp)₂(3-pc)₂, (blue), 0D-Cu₂I₂(tpp)₂(4-me-pm)₂ (cyan), 1D-Cu₂I₂(tpp)₂(2,5-dm-pz) (yellow), 1D-Cu₂I₂(tpp)₂(2-me-pz) (orange) at room temperature.

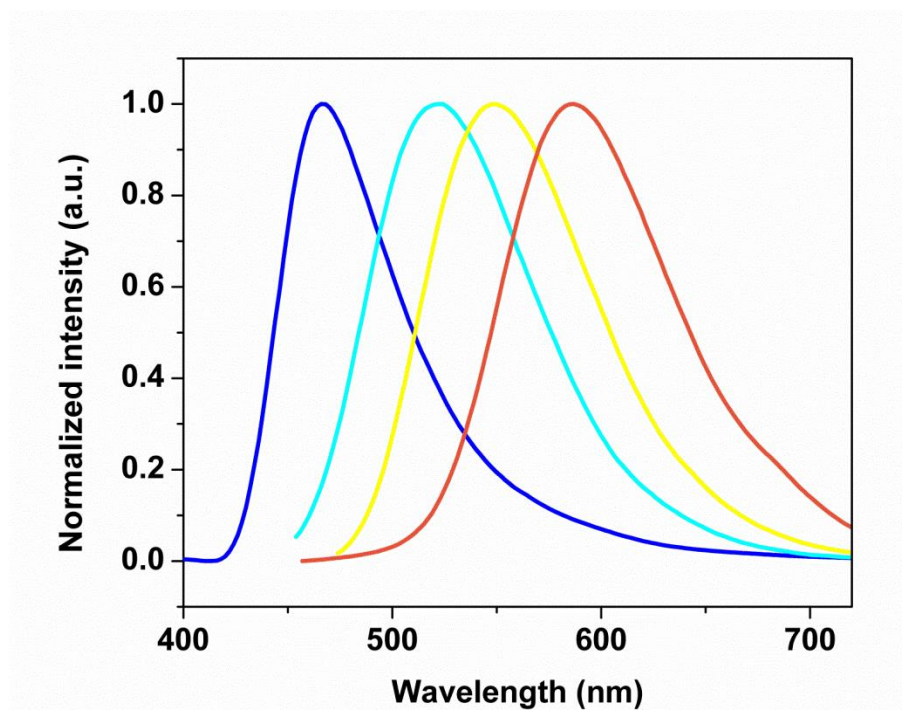


Figure 44. PL spectra of 0D-Cu₂I₂(*tpp*)₂(*3-pc*)₂, (blue), 0D-Cu₂I₂(*tpp*)₂(*4-me-pm*)₂ (cyan), 1D-Cu₂I₂(*tpp*)₂(2,5-dm-pz) (yellow), 1D-Cu₂I₂(*tpp*)₂(2-me-pz) (orange) at room temperature; $\lambda_{\text{ex}} = 360$ nm.

Table 7. Summary of crystal data of new structures.

	0D-	0D-	1D-	1D-	1D-	0D-Cu ₂ I ₂ (<i>tpp</i>) ₂
Compou nd	Cu ₂ I ₂ (<i>tpp</i>) ₂ (<i>4-me- pm</i>) ₂	Cu ₂ I ₂ (<i>tpp</i>) ₂ (<i>3-Br-py</i>) ₂	Cu ₂ I ₂ (<i>tpp</i>) ₂ (<i>2,5-dm- pz</i>)	Cu ₂ I ₂ (<i>tpp</i>) ₂ 2 (<i>2-pr-pz</i>)	Cu ₂ I ₂ (<i>tpp</i>) ₂ (<i>2-me-pz</i>)	(<i>1-me-bz-im</i>) ₂
Empirical	C ₄₆ H ₄₂ Cu ₂ I ₂	C ₄₆ H ₃₈ Br ₂ Cu ₂ I ₂	C ₂₁ H ₁₉ CuI	C ₅₇ H ₅₆ Cu ₂ I	C ₄₅ H ₄₂ Cu ₂ I ₂	C ₅₂ H ₄₆ Cu ₂ I ₂ N ₄
Formula	N ₄ P ₂	N ₂ P ₂	NP	₂ N ₂ P ₂	N ₄ P ₂	P ₂
FW	1093.65	1221.42	506.78	1211.85	1081.64	1169.75
Space Group	P-1	P-1	P-1	P2 ₁ /n	P2 ₁ /n	P-1
a (Å)	9.2967(4)	9.3013(3)	8.3000(3)	15.1834(7)	8.9262(4)	11.9531(4)
b (Å)	9.6556(4)	11.5128(4)	9.2088(4)	21.2369(9)	18.4737(7)	14.6004(5)
c (Å)	13.6494(6)	11.6191(5)	14.4351(6)	17.6739(7)	13.1212(5)	15.7384(6)
α(°)	71.076(2)	80.231(2)	79.195(2)	90	90	113.6280(10)
β(°)	72.817(2)	71.464(2)	76.687(2)	115.349(2)	94.020(2)	102.747(2)
γ(°)	73.955(2)	69.554(2)	63.524(2)	90	90	94.386(2)
V (Å ³)	1084.95(8)	1102.95(7)	956.50(7)	5150.2(4)	2158.36(15)	2412.23(15)
Z	1	1	2	4	2	2
T (K)	100(2)	150(2)	150(2)	150(2)	150(2)	100(2)
λ(Å)	0.7749	0.7749	0.7749	0.7749	0.7749	0.7749
R ₁	0.0197	0.0270	0.0271	0.0287	0.0328	0.0273
wR ₂	0.0449	0.0582	0.0606	0.0563	0.0649	0.0603
CCDC #	1510195	1510193	1510192	1510194	1510196	1510191

Table 8. Estimated band gaps, emission energies, IQY, emission color of compound.

Compound	Band		Emission Color	CIE Coordinates	IQY (%) $\lambda_{\text{ex}} =$ 360nm
	Gap (eV)	λ_{em} (nm)			
0D-Cu ₂ I ₂ (<i>tpp</i>) ₂ (<i>4-pc</i>) ₂	3.1	450	blue	0.13, 0.14	86.7±0.8
0D-Cu ₂ I ₂ (<i>tpp</i>) ₂ (<i>3-pc</i>) ₂	3.0	455	blue	0.14, 0.15	90.3±0.4
0D-Cu ₂ I ₂ (<i>tpp</i>) ₂ (<i>py</i>) ₂	2.9	495	blue-green	0.23, 0.40	69.5±0.5
0D-Cu ₂ I ₂ (<i>tpp</i>) ₂ (<i>4,6-dm-pm</i>) ₂	2.9	465	blue	0.15, 0.17	72.3±0.2
0D-Cu ₂ I ₂ (<i>tpp</i>) ₂ (<i>4-me-pm</i>) ₂	2.7	485	blue-green	0.20, 0.23	92.2±1.2
0D-Cu ₂ I ₂ (<i>tpp</i>) ₂ (<i>3-Br-py</i>) ₂	2.6	505	blue-green	0.22, 0.43	75.3±0.3
1D-Cu ₂ I ₂ (<i>tpp</i>) ₂ (<i>pm</i>)	2.5	530	green-yellow	0.32, 0.52	66.5±0.7
1D-Cu ₂ I ₂ (<i>tpp</i>) ₂ (<i>2,5-dm-pz</i>)	2.3	545	yellow	0.39, 0.55	52.0±0.5
1D-Cu ₂ I ₂ (<i>tpp</i>) ₂ (<i>2-pr-pz</i>)	2.2	570	orange	0.44, 0.49	48.5±0.3
1D-Cu ₂ I ₂ (<i>tpp</i>) ₂ (<i>2-me-pz</i>)	2.2	585	orange	0.52, 0.47	35.7±0.6
0D-Cu ₂ I ₂ (<i>tpp</i>) ₂ (<i>1-me-bzim</i>) ₂	2.9	465	blue	0.15, 0.18	74.3±0.5
White light blend	N.A.	455, 545	white	0.30, 0.36	72.2±0.7

The thermogravimetric (TG) analyses of these compounds were performed on their powder samples. Based on their TG profile, a two-step weight loss is usually observed for all patterns. The first step typically starts between 100 °C to 200 °C, and is ascribed to the loss of the N-ligand. The second step, which usually occurs around 250 °C, is the loss of *tp* and the remaining residue is comprised of CuI. In all cases the experimental weight losses are in agreement with the calculated values from the structural formulae.

The one-pot synthesis of a direct white light emitting blend was achieved by grinding CuI, *tp* and two N-ligands instead of one. *3-pc* and *2,5-dm-pz* were selected as the N-ligands and after grinding, both 0D-Cu₂I₂(*tp*)₂(*3-pc*)₂ and 1D-Cu₂I₂(*tp*)₂(*2,5-dm-pz*) form as a white-light blend of a blue and a yellow phosphor, respectively. Their phases were confirmed by the PXRD analysis of the white-light blend. The light quality was easily tuned by the ratio of the ligand added; an optimum molar ratio was found to be 1:1.6 (Fig. 45). The IQY of the blend is as high as 72% under 360 nm excitation. The CIE, CRI and CCT of this blend were calculated to be (0.30, 0.36), 63.6, and 8001 K, respectively.

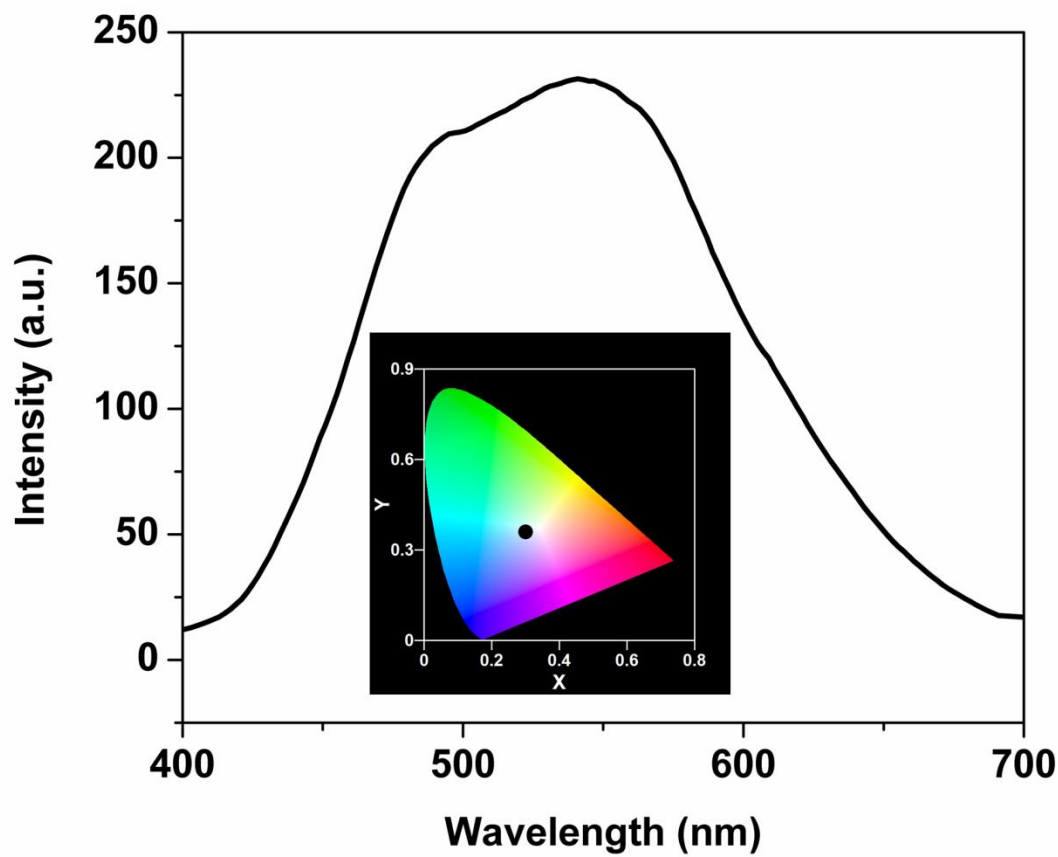


Figure 45. Emission spectrum of the white phosphor composite obtained by one-step synthesis. Inset: CIE coordinates of the composite.

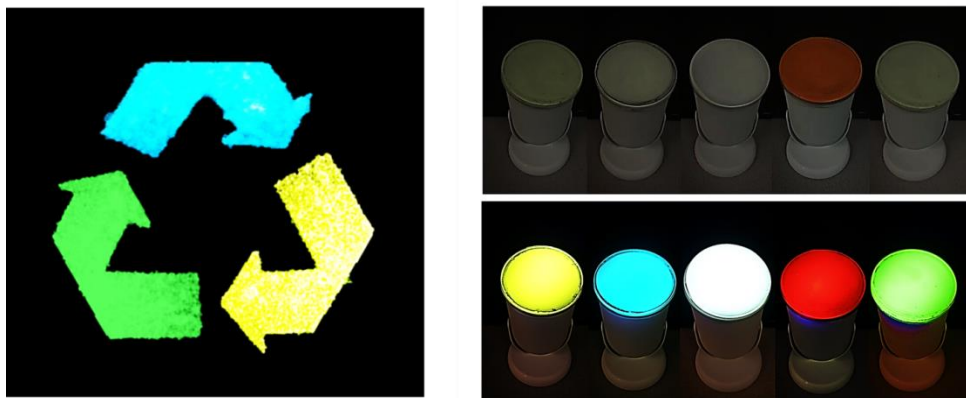


Figure 46. Green chemistry logo prepared by spray coating of the samples on black plastic substrate. (left) and prototype LED lamps at “off” (top) and “on” (bottom) conditions (right).

Spray coating is a well-developed technique for the fabrication of LEDs and was applied for to uniformly coat the phosphors onto various substrates. The phosphor layer has to be very thin and uniform to avoid self-absorption. $0D-Cu_2I_2(tpp)_2(4,6-dm-pm)_2$, $1D-Cu_2I_2(tpp)_2(pm)$, $1D-Cu_2I_2(tpp)_2(2,5-dm-pz)$, were selected as cyan, green and yellow phosphors respectively, and were dissolved organic solvents, such as CH_2Cl_2 . The solution was placed in a commercial sprayer and was sprayed onto the substrates using a mask to display the green chemistry symbol (Fig. 46). The CH_2Cl_2 dried quickly, leaving the uniformly dispersed thin layer.

Prototype lamps were prepared by a remote coating approach, as the phosphors have a certain distance from the excitation source. A water-soluble binder (PolyOx N-750) was added to the phosphor spray mixture to adhere the phosphor coating onto the plastic plate caps for the lamps. These caps were then placed on top of UV chips

as the excitation source in the commercial lighting lamps and they display various colors of light including white light in the working condition (Fig. 46). After keeping the light on for a week, no obvious decrease of the intensity was observed, and the temperature of the plates is similar to room temperature, indicating the heat from the LED chips has been dissipated.

4.6 Summary

In summary, a simple mechanochemical (e.g. manual grinding and ball milling) method has been developed in this study to prepare copper iodide based inorganic-organic hybrid phosphor materials. Washing and separation procedures are not needed as the solid starting materials transform completely to the targeted products, while excess liquid N-ligands evaporate out after grinding/ball milling. As a result, no excess waste is formed and the reactions generate quantitative yields. The targeted final products are Cu_2I_2 dimer based structures with impressively high IQYs, often comparable with commercial phosphors. The inclusion of triphenylphosphine effectively prevents the formation of other by-products. This green and low-cost synthetic route introduces a new and systematic approach for large-scale preparation of inorganic-organic hybrid materials, bringing these phosphors one step closer towards commercialization.

5. Copper halide monomer based structures with exceptionally high quantum efficiencies

5.1 Background

The structural diversities of copper halide based inorganic-organic hybrid structures and luminescence dependent on their structures encourage scientist to study their structure-optical relationships and to design new structures with better performances. A variety of inorganic building motifs have been reported for these structures, with the most common being CuX monomer, Cu₂X₂ rhomboid dimer, Cu₄X₄ cubane tetramer, and (CuX)_∞ staircase chain. The ratios of copper to coordinated ligands are 3:1, 1:1, 1:3, and 1:3 respectively. Compared to the other three, compounds with copper halide mononuclear motif have been much little investigated. Possible reason of that is their extremely low thermal and moisture stability, which hinder the development of this structure family.^{15,80}

Due to the importance of these materials, in the past few years, we have been devoted to developing new methods to enhance the stability of them and trying to make them more suitable for real applications. Based on our earlier investigation, these structures could be synthesized rationally with the designed inorganic motif by precursor approach to keep the emissive core intact. Enhancing the stability of the overall structures could be achieved with proper ligand selection to form stronger Cu-ligand bond or incorporation of the emissive core into frameworks. Under the guideline of these approaches, a family of strongly luminescent copper halide monomer based structures has been obtained, with 0D-CuI(3-*pc*)₃, 0D-CuBr(3-*pc*)₃, 0D-CuI(1,2-*dm-im*)₂ synthesized by traditional method, and 0D-CuI(*tpp*)₂(1-

et-im), 0D-CuI(*tpb*)₂(2-*eto*x-*pz*), 0D-CuI(*tpb*)₂(2-*pr*-*pz*), 0D-CuI(*tpb*)₂(*dipe*)_{0.5}, 0D-CuBr(*tpb*)₂(*dipe*)_{0.5}, 1D-CuI(*tpb*)(*bbipe*)_{0.5}, 1D-CuBr(*tpb*)(*bbipe*)_{0.5} by using 0D-CuX(*tpb*)₃ (X = I, Br) as the precursor. Extended structures exhibit significantly enhanced chemical and thermal stability compared to that of molecular clusters, with maintained internal quantum yields (IQYs) higher than 70 %, exhibiting promises as phosphor candidates for general lighting applications.

5.2 Ligand preparation and precursor approach for the synthesis

Synthesis of 1,5-bis(1H-benzo[d]imidazol-1-yl)pentane (*bbipe*): A mixture of 1.2 g (30 mmol) NaOH, 1.18 g (10 mmol) benzimidazole in 20 ml DMSO was stirred at 70 °C for 2 hours, and then 540 μ l (4 mmol) 1,5-dibromopentane was injected into the solution. The reaction mixture was heated around 100 °C for 24 h. After that, the solution was cooled to room temperature and poured into 150 ml cold water. The mixture was extracted with methylene chloride for three times and *bbipe* was obtained as white solid by concentrating the organic phase in vacuum. Pure product of high yield (90%) was obtained after recrystallization with acetone/hexanes. ¹HNMR (300MHz, CDCl₃) δ (ppm): 1.31-1.42(m, 2H), 1.86-1.96(m, 4H), 4.12-4.17(m, 4H), 7.26-7.32(m, 6H), 7.80-7.84(m, 4H).

Synthesis of 1,5-di(1H-imidazol-1-yl)pentane (*dipe*): The synthetic procedure of *dipe* is similar as that of *bbipe* except the starting material is imidazole instead of benzimidazole, affording *dipe* as colorless oil. The yield is 75 %. ¹HNMR (400MHz, CDCl₃) δ (ppm): 1.26-1.30(m, 2H), 1.59-1.81(m, 4H), 3.88-3.92(m, 4H), 6.89-7.07(m, 4H), 7.34-7.44(m, 2H).

Synthesis of 0D-CuI(*3-pc*)₃: The synthesis was carried out according to the reported method. CuI (0.02 g, 0.1 mmol) was first dissolved in 5.0 ml acetonitrile and was added dropwise into *3-pc* (5.0ml) in a reaction vial at room temperature. Green crystalline powder formed in a few minutes and has to be filtered out immediately after they formed. (12 % yield based on Cu).

Synthesis of 0D-CuBr(*3-pc*)₃: The synthesis was conducted similarly as above. Single crystals were obtained by slow diffusion method. CuBr (0.015g, 0.1 mmol) was dissolved in 5.0 ml acetonitrile and was added slowly into *3-pc* (5.0ml) in a reaction vial. Green powder along with fine rod-shaped single crystals was formed in a few minutes at room temperature and was collected immediately by filtration (17 % yield based on Cu).

Synthesis of 0D-CuI(*1,2-dm-im*): Single crystals were obtained by slow diffusion method similar as above. CuI (0.02 g, 0.1 mmol) was first dissolved in 5.0 ml acetonitrile and *1,2-dm-im* (1.0ml) was added. The reaction mixture was kept at room temperature. Colorless cubic crystals formed in 1 day (40 % yield based on Cu).

Synthesis of 0D-CuI(*tp*)₃ and 0D-CuBr(*tp*)₃: Syntheses of these two precursors were conducted the same as reported method. The yield of them are 89 % and 75 % based on Cu, respectively

Synthesis of 0D-CuI(*tp*)₂(*1-et-im*): Precursor approach was applied for the syntheses. Pure phase of powder product was prepared by solvothermal method. 0D-CuI(*tp*)₃ was chosen as the precursor. In a typical synthesis, 0D-CuI(*tp*)₃ (0.1g, 0.1 mmol), *1-et-im* (0.1 ml) was added into a CH₂Cl₂/toluene (1:1, v:v) in a close reactional vial and the reaction mixture was kept at 80 °C for 24h. Colorless cubic crystals formed along with pure phase of power products at the bottom of the vial. They were collected by filtration, washed with ethanol for three times and dried in the vacuum oven for 3 h before further characterization (62 % yield

based on Cu). The following compounds were synthesized in a similar manner unless stated otherwise.

Synthesis of 0D-CuI(*tpp*)₂(2-*etxo-pz*) was prepared in a similar way as above. Greenish cubic crystals formed in 24 h (67 % yield based on Cu).

Synthesis of 0D-CuI(*tpp*)₂(2-*pr-pz*) is the same as above except the N-ligand is 2-*pr-pz*. Yellowish plate-shaped crystals formed in 24 h (59 % yield based on Cu).

Synthesis of 0D-CuI(*tpp*)₂(*dipe*) is similar as above. Colorless cubic crystals formed in 24 h (48 % yield based on Cu).

Synthesis of 0D-CuI(*tpp*)₂(*dipe*) is similar as above except 0D-CuBr(*tpp*)₃ was used as the precursor. Colorless cubic crystals formed in 24 h (57 % yield based on Cu).

Synthesis of 0D-CuI(*tpp*)₂(*bbipe*) was synthesized similarly as above. Colorless cubic crystals formed in 24 h (39 % yield based on Cu).

Synthesis of 0D-CuBr(*tpp*)₂(*bbipe*) is similar as above except 0D-CuBr(*tpp*)₃ was used as the precursor. Colorless cubic crystals formed in 24 h (45 % yield based on Cu).

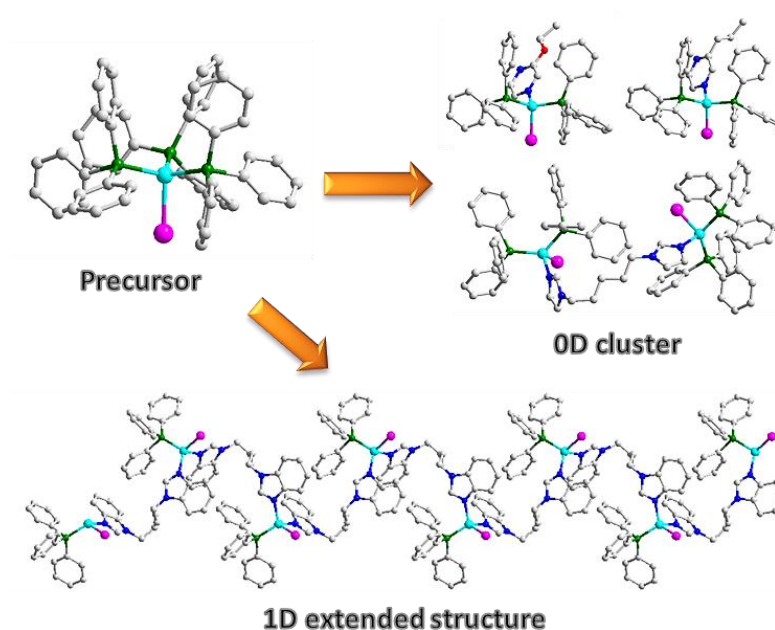


Figure 47. Illustration of precursor approach for the syntheses of monomer based structures.

5.3 Structure and optical characteristics

It is well-understood that the inorganic motifs of these structures determine the overall luminescence mechanism, and their optical properties could be tuned by the selection of different organic ligands. For copper halide monomers, dimers and chains, the luminescence mechanism is generally a combination of metal-to-ligand-charge-transfer (MLCT) and halide-to-ligand-charge transfer (XLCT); while for cubane tetramers, their emission is majorly from a cluster-centered (CC) luminescence mechanism.⁸⁵ Based on the data, 0D- $\text{CuI}(\text{py})_3$ monomer has the highest IQY compared to the other three, and this is also in agreement with other reported work on strongly emissive monomers. However, monomers are extremely unstable even at room temperature. Though the emissive property of

monomers is interesting, a rough search has been done on the copper iodide based structures in the CCDC database, and the results show that the reported monomers only consist less than 5 % of all reported structures. The little investigation on these structures is highly due to their “fragile” characteristics, which would severely limit their real applications.

Syntheses of the molecular clusters were conducted in the same manner as conventional method. The synthesis of them needs to be very carefully to avoid the formation of mixture phase as the transformation of those structures sometime happens very quickly. They have to be synthesized by direct mixing of the ligand with copper halides in acetonitrile and the products formed must to be separated immediately, or otherwise they will decompose. Their phases of the as-made samples were confirmed by powder X-ray diffraction (PXRD) analyses. They are extremely unstable even in the air and would completely lose structure in a week exposing to air. They also lose structures immediate when in contact with water, indicating they are very sensitive to moisture. All these three samples exhibit intense emission at room temperature under ultraviolet light excitation, with green, green and blue respectively. Quantum yield measurements were conducted, and the results indicating that they all have extremely high IQYs.

Monomer based structures are hard to synthesize, since most likely, the more stable dimer, cubane tetramer or staircase chain based structures would form under the same synthetic condition. Rational design of keeping the copper halide mononuclear motif in the products was achieved by using a monomer precursor $0D-CuX(tpp)_3$ ($X = I$ or Br) as starting material instead of bulk copper halides. A variety of N-heterocyclic ligands (N-ligands) have been used for ligand exchange, including *py* derivatives, *pz* derivatives and *im* derivatives, leading to the formation of ten other structures. By introducing the N-ligands into the reaction mixture, one of the *tpp* in the cluster was replaced by the N-ligands forming new structures,

while the other two *tpb* would stay in the new structures. The replacement would generally stop at this point without further replacing. As the result, in those structures obtained, each copper atom bonds to one halide atom, two *tpb* molecules and one N-ligand. This method might also be applicable to copper chloride based structures, but they generally have significantly lowered quantum yields, which are out of our research interests.

Table 9. Summary of optical and thermal measurement results

#	Structures	Band gap (eV)	λ_{em} (nm, R.T.)	Emission color	IQY(%, 360 nm)	Decom. Temp. (°C)
1	0D-CuI(<i>3-pc</i>) ₃	2.3	505	Blue-green	97	Room Temp.
2	0D-CuBr(<i>3-pc</i>) ₃	2.2	520	Green	96	Room Temp.
3	0D-CuI(<i>1,2-dm-im</i>) ₂	3.1	470	Blue	88	Room Temp.
4	0D-CuI(<i>tp</i>) ₂ (<i>1-et-im</i>)	3.1	460	Blue	76	150
5	0D-CuI(<i>tp</i>) ₂ (<i>2-eto-x-pz</i>)	2.5	520	Green	85	100
6	0D-CuI(<i>tp</i>) ₂ (<i>2-pr-pz</i>)	2.4	550	Yellow	78	100
7	0D-CuI(<i>tp</i>) ₂ (<i>dipe</i>) _{0.5}	3.3	470	Blue	82	180
8	0D-CuBr(<i>tp</i>) ₂ (<i>dipe</i>) _{0.5}	3.1	495	Blue-green	79	170
9	1D-CuI(<i>tp</i>)(<i>bbipe</i>) _{0.5}	3.3	475	Blue	80	220
10	1D-CuBr(<i>tp</i>)(<i>bbipe</i>) _{0.5}	3.2	500	Blue-green	72	200

Several compounds in this family are *tpb* containing copper halide monomer based clusters, with the general formula of $0D-CuX(tpb)_2(L)$ ($X = I$ or Br , $L =$ monodentate N-ligands). In those structures, one copper atom is coordinated to one iodine atom, two *tpb* molecules and one monodentate N-ligand molecule, displaying mononuclear tetrahedral coordination geometry. Differently, some other compounds are formed with bidentate N-ligand with the formula of $0D-CuX(tpb)_2(L)_{0.5}$ ($X = I$ or Br , $L =$ bidentate N-ligands). PXRD analyses reveal that they are iso-structures to each other with different halides. In these structures, two inorganic cores were connected by *dipe* forming an overall 0D molecular cluster.

5.4 Optical properties and strong luminescence

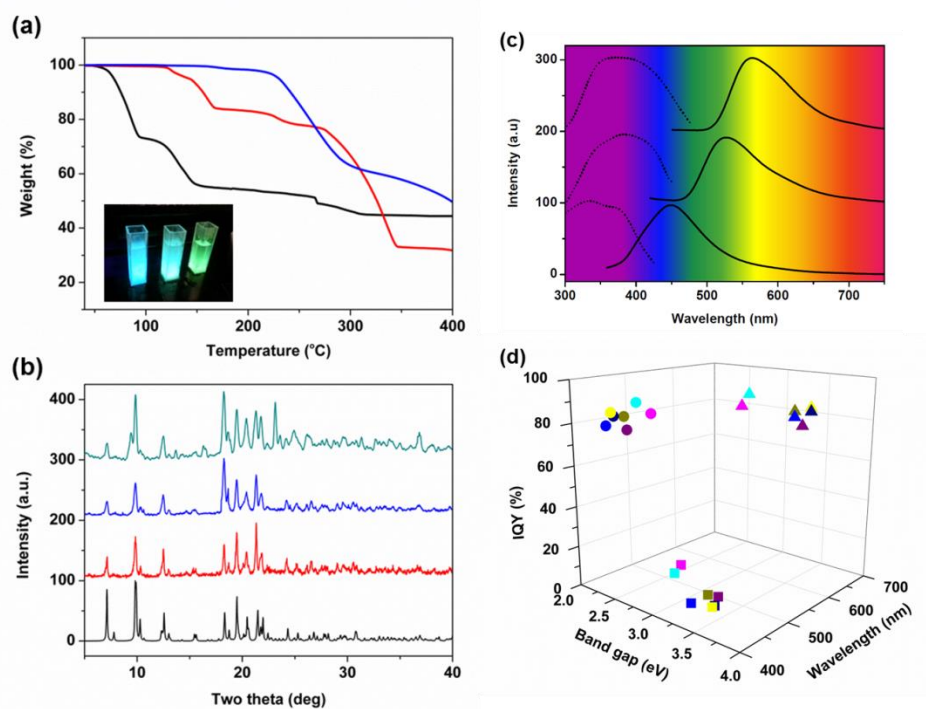


Figure 48. (a) TG profile of 0D-CuI(3-*pc*)₃ (black), 0D-CuI(*tpb*)₂(1-*et-im*) (red), 1D-CuI(*tpb*)(*bbipe*)_{0.5} (blue). Inset: selected samples in water under UV irradiation (365nm). (b)

PXRD patterns. From bottom to top: simulated 1D-CuBr(*tpp*)(*bbipe*)_{0.5}, as made 1D-CuBr(*tpp*)(*bbipe*)_{0.5}, 1D-CuBr(*tpp*)(*bbipe*)_{0.5} soaked in water for 7 days. 1D-CuBr(*tpp*)(*bbipe*)_{0.5} heated at 100 °C for 7 days. (c) PL spectra of selected compounds. From bottom to top: excitation and emission spectra of 0D-CuI(*tpp*)₂(*1-et-im*), 0D-CuI(*tpp*)₂(*2-etox-pz*), 0D-CuI(*tpp*)₂(*2-pr-pz*). $\lambda_{\text{ex}} = 360 \text{ nm}$ λ_{em} = peak wavelengths of their emission spectra. (d) 3D plot of the optical data of 0D-CuI(*tpp*)₂(*1-et-im*) (blue), 0D-CuI(*tpp*)₂(*2-etox-pz*) (cyan), 0D-CuI(*tpp*)₂(*2-pr-pz*) (pink), 0D-CuI(*tpp*)₂(*dipe*)_{0.5} (dark blue), 0D-CuBr(*tpp*)₂(*dipe*)_{0.5} (purple), 1D-CuI(*tpp*)(*bbipe*)_{0.5} (yellow), 1D-CuBr(*tpp*)(*bbipe*)_{0.5} (dark yellow).

Two compounds are monomer based 1D extended structures with the general formula of 1D-CuX(*tpp*)(*L*)_{0.5} (X = I or Br, *L* = bidentate N-ligands. They are iso-structures to each other with different halides. In these structures, each copper is coordinated to one *tpp* molecules and the mononuclear core was connected by *bbipe* as the organic ligand. As we searched in the database, they are the first examples of copper halide monomer based extended structures. It is worth mentioning that the *tpp* molecules would be the key factor of stabilizing those structures and keeping the monomer intact in the products since direct mixing of the ligand with the copper iodide without the addition of *tpp* would form the stable Cu₄I₄ cubane tetramer based structure 1D-Cu₄I₄(*bbipe*)₂ immediately. Further expanding of the type of extended structures could be performed by using various bidentate imidazole derivatives.

The thermogravimetric (TG) analyses for all compounds were performed and their decomposition temperatures were estimated based on their TG profiles (Fig 48a, Table 9). The decomposition of the structures is due to the leaving of the organic ligands upon

heating. Compared to molecular clusters, which generally decompose at room temperature, extended structures have much better thermal stability, with all of them stable high than 100 °C and several members higher than 150 °C. To further evaluate their thermal stability, one extended structure 1D-CuBr(*tpb*)(*bbipe*)_{0.5} was selected and heated in the oven without protection at 100 °C for 7 days. PXRD measurement was conducted on the sample before and after heating, indicating their structures remain intact (Fig. 3b). Compound 1D-CuBr(*tpb*)(*bbipe*)_{0.5} were soaked in water for a long period of time (7 days) and no structural changes were observed in the PXRD patterns (Fig. 48b). The significantly enhanced water stability ensures the applications of materials under moist environment.

5.5 Summary

In summary, a family of copper halide monomer based structures has been obtained by precursor approach, and they exhibit strong luminescence and enhanced stability compared to traditional 0D-CuX(*py*)₃. This work might attract more attention to the study of copper halide monomer based structures.

6. Development of AIO type of structures and their unique properties

6.1 Background

Based on our earlier work, it has been found out the structures with cluster-based inorganic modules, such as Cu_2I_2 rhomboid dimer or Cu_4I_4 cubane tetramers, typically have much higher quantum yields compared to structures with extended inorganic modules, such as CuI infinite chain or layers.^{46,86} However, limitations still exist that need to be fully addressed before possible commercialization of these materials. Though the extended frameworks exhibit enhanced stability, molecular clusters generally have much higher quantum efficiency that are more ideal for lighting applications, but their stability is generally too low. Also the formation of stable frameworks always requires stricter reaction condition and more complicated synthesis of specially designed ligands, which may bring up cost issues unfavorably for large scale synthesis. Therefore, developing cost-effective synthetic route for more suitable candidates is still being pursued.

Recently, a new type of ionic copper iodide based hybrid structures has emerged, structurally similar as the lead halide perovskite based structures intensively studied nowadays.⁸⁷⁻⁹¹ In those structures, both the inorganic component and the organic component are ionic pairs, and the whole structures are formed by the electrostatic attraction between oppositely charged ions without coordinate bonds that connect the metal and the ligands. Interestingly, such structures show significantly enhanced thermal stability compared to that of neutral structures, demonstrating the potential of enhancing the stability by transforming the “fragile” coordinate bonds to stronger ionic bonds.^{87,88,92} However, those structures are typically considered as “ligand-free” structures, as there is no coordinate bond between the ligands and the Cu atoms.⁸⁷ Such structural change compared to the

original ligand-coordinated structures lead to the absence of organic-ligand-related excited states upon excitation, including metal-to-ligand charge transfer (MLCT), halide-to-ligand charge transfer (XLCT) etc., resulting in severe luminescence quench.^{87,92} Because of this, little attention has been paid on this type of structures, and nearly all of these structures reported up to now are with internal quantum yields (IQYs) less than 10 %, which is too low for any luminescence-related applications. To address these issues, we designed a new “all-in-one” (AIO) type of structures that combine all three features necessary for both high luminescence and stability, which are (i) molecular crystal, (ii) cation and anion pairs, and (iii) coordinate bond between the cation and the anion, into one structure type (Fig. 3). In those structures, both the inorganic modules and the organic ligands are ionic pairs, but they are connected by coordinate bonds, forming neutral molecular clusters. We expect that the stability of such materials could be enhanced due to their ionic nature, while their luminescence property maintains due to the coordination of the ligands to the metal in molecular crystals. The synthesis of this type of structures is achieved through the design of the ligand. Instead of using traditional neutral organic ligands, we used cationic ligands with free binding sites to template the synthesis. The cationic nature of the ligands would ensure the formation of anionic inorganic modules, while the free binding sites on the ligands could coordinate to Cu atoms forming coordinate bonds. Under such design, 10 new AIO type of structures were obtained, with the general formula of $\text{Cu}_m\text{I}_{m+n}(\text{L})_n$, L = organic ligands. Their design strategy, synthetic condition and structural characteristics are discussed in detail.

6.2 Synthetic design, ligand synthesis and compound preparations

Selected cationic organic ligands were prepared according to reported procedures with some modifications.⁹³⁻⁹⁵ For Route I, the alkylation was controlled at only one of the N atom alkylated of bidentate ligands while keeping the other N atom unalkylated. For Route III, the alkylation took place only at substituted group, keeping the N atoms on the aromatic ring intact for further coordination (Fig. 49).

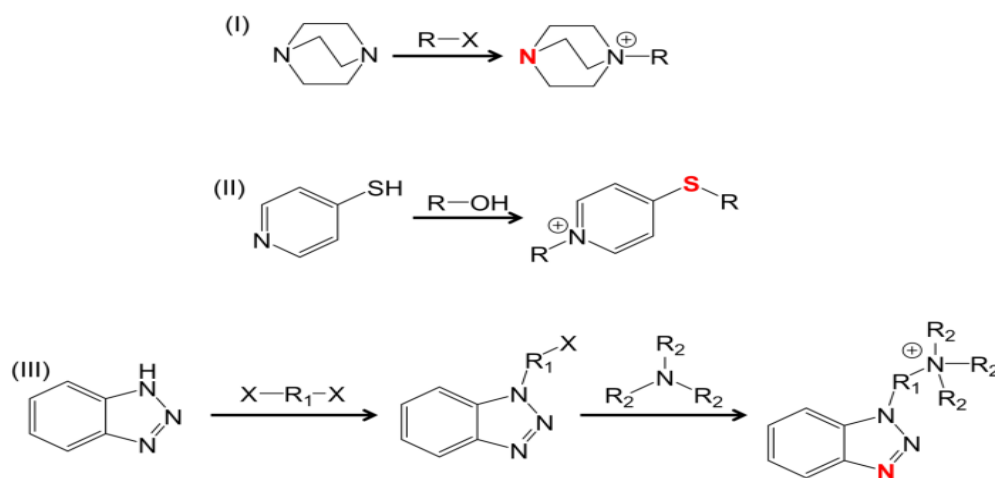


Figure 49. Synthetic approach I, II and III used to prepare cationic ligands with free binding sites marked in red.

Preparation of 1-benzyl-1,4-diazabicyclo[2.2.2]octan-1-ium (*bz_χ-ted*): *Ted* (1.12 g, 10 mmol) was first dissolved in acetone (50 ml) upon sonication and benzyl bromide (1.71 g, 10 mmol) was added dropwise into it under magnetic stirring. The solution remained clear after the mixing and white precipitate formed in a few hours. The precipitate was collected by filtration, washed with ethyl acetate, and dried under vacuum. The yield is 87%.

Preparation of 1-(3-chloropropyl)-1,4-diazabicyclo[2.2.2] octan-1-ium (*3-Cl-pr-ted*): *Ted* (1.12 g, 10 mmol) was dissolved in ethyl acetate (40 ml) upon sonication and 1-chloro-3-iodopropane (2.04 g, 10 mmol) was added slowly into it under magnetic stirring. The solution was stirred for two hours and the white precipitate formed was collected by filtration, washed with ethyl acetate, and dried under vacuum. The yield is 67%.

Preparation of 1-propyl-1,4-diazabicyclo[2.2.2]octan-1-ium (*pr-ted*): *Ted* (1.12g, 10 mmol) was first dissolved in acetone (50 ml) upon sonication and 1-bromopropane (1.23 g, 10 mmol) was added dropwise into it under magnetic stirring. The solution remained clear after the mixing and colorless oily precipitate formed in an hour. The precipitate was collected by centrifuge, washed with ethyl acetate, and dried under vacuum. The yield is 68%.

Preparation of 1-(2-bromoethyl)-1,4-diazabicyclo[2.2.2]octan-1-ium (*2-Br-et-ted*): 1-Bromo-2-iodoethane (2.34 g, 10 mmol) was added dropwise into acetone (50 ml) containing *ted* (1.12 g, 10 mmol) under magnetic stirring. White precipitate formed in a few hours, and the precipitate was collected by centrifuge, washed with ethyl acetate, and dried under vacuum. The yield is 70%.

Preparation of 1-isopropyl-1,4-diazabicyclo[2.2.2]octan-1-ium (*i-pr-ted*): *Ted* (1.12 g, 10 mmol) was first dissolved in acetone (50 ml) upon sonication and 2-bromopropane (1.23 g, 10 mmol) was added dropwise into it under magnetic stirring. The white precipitate formed in one day. The precipitate was collected by filtration, washed with ethyl acetate, and dried under vacuum. The yield is 75%.

Preparation of 1-butyl-1,4-diazabicyclo[2.2.2]octan-1-ium (*bu-ted*): *Ted* (1.12 g, 10 mmol) was first dissolved in acetone (50 ml) upon sonication and 1-bromobutane (1.37 g, 10 mmol) was added dropwise into it under magnetic stirring. White precipitate formed within an hour.

The precipitate was collected by filtration, washed with ethyl acetate, and dried under vacuum. The yield is 80%.

Preparation of (1H-benzo[d][1,2,3]triazol-1-yl)methanol (*btm*): A mixture of benzotriazole (*bta*) (3.4 g, 0.025 mol), distilled water (50 ml), and formaldehyde solution (36%, 10 ml) was first refluxed for 1.5 hours. After cooling to room temperature, the resulting white precipitate was collected by filtration, washed with water and dried under vacuum to give the corresponding *btm*. The yield is 92%.

Preparation of 1-(chloromethyl)-1H-benzo[d][1,2,3]triazole (*Cl-mbt*): *Btm* (3.7 g, 0.025 mol) was dissolved in a mixture of CH_2Cl_2 (60 ml) and dimethylformamide (DMF) (40 ml), and thionyl chloride (5 ml) in methylene chloride (10 ml) was added dropwise into it under magnetic stirring at room temperature. The reaction mixture was kept stirring for 2 h, then its pH was adjusted by saturated NaHCO_3 solution to 7. The organic layer was separated and was evaporated under reduced pressure, giving white crystalline powder as 1-(chloromethyl)-1H-benzotriazole. The yield is 85%.

Preparation of 1-(1H-benzo[d][1,2,3]triazol-1-yl)-N,N,N-trimethylmethanaminium (*btmm*): *Cl-mbt* (3.8 g, 0.025 mol) was then fully dissolved in acetone (20 ml) and KI (5 g) was added. The reaction mixture was kept under stirring for 2 h before the solution was filtered. The filtrate was then added with trimethylamine (2 ml) and the precipitate was formed after stirring at room temperature overnight. The white precipitate was filtered, washed with acetone and dried under vacuum as the final product. The yield is 62%.

Preparation of N-((1H-benzo[d][1,2,3]triazol-1-yl)methyl)-N,N-dimethyl ethanaminium (*btmdme*): The synthetic procedure is similar as that of *btmm*, except the trimethylamine was replaced by N,N-dimethylethylamine. The yield is 57%.

Preparation of N-((1H-benzo[d][1,2,3]triazol-1-yl)methyl)-N,N-dibutylbutan-1-aminium (*btmdb*): The synthetic procedure is similar as that of *bttmm*, except the trimethylamine was replaced by N,N-dimethylethylamine. The yield is 69%.

Synthesis of AIO structures: The reaction conditions used to prepare AIO type of compounds were similar to those developed for the synthesis of CuI(L) structures containing only Cu-N dative bonds. Single crystals can be obtained by slow diffusion at room temperature. For *tpp* containing structures, a molecular precursor $0D-Cu_2I_3(tpp)_3$ was used.

Synthesis of $Cu_3I_5(bz\text{-}ted)_2$: CuI (0.19 g, 1 mmol) was first dissolved in KI saturated solution (2 ml) in a reaction vial. Acetonitrile (2 ml) was added as another layer and then the ligand (1mmol) in methanol (2 ml) was added slowly in to the vial. The reaction mixture was kept undisturbed at room temperature, and rod-shaped single crystals formed in one day and were collected by filtration. Yield is 74%.

Synthesis of $Cu_4I_6(3\text{-}Cl\text{-}pr\text{-}ted)_2$: Acetonitrile (2 ml) was added into KI saturated solution (2 ml) containing CuI (0.19 g, 1 mmol), and then the ligand (1 mmol) in methanol (2ml) was slowly added. Rod-shaped single crystals formed in one day and were collected by filtration. Yield is 68%.

Synthesis of $Cu_4I_6(pr\text{-}ted)_2$: Plate-shaped crystals were prepared similarly as above. Pure phase of powder samples could be synthesized by direct mixing of CuI in acetonitrile with ligand in methanol. Precipitate formed immediately and was collected by filtration. Yield is 81%.

Synthesis of $Cu_4I_6(2\text{-}Br\text{-}et\text{-}ted)_2$ is prepared similarly as above. Plate-shaped crystals were formed in 3 days and were collected by filtration. Yield is 65%.

Synthesis of $\text{Cu}_4\text{I}_6(i\text{-}pr\text{-}ted)_2$: was prepared in the same way as above. Rod-shaped single crystals formed in 3 days. Yield is 72%.

Synthesis of $\text{Cu}_6\text{I}_8(bu\text{-}ted)_2$ was synthesized by the method similar as above. Plate-shaped colorless single crystals could be obtained in 1 day. Yield is 83%.

Synthesis of $\text{Cu}_2\text{I}_4(mtp)_2$ was prepared by the solvothermal reaction of CuI, KI, 4-mercaptopyridine and methanol in a molar ratio of 1:6:2:1:300 at 150 °C for 48 h. pH of the reaction mixture were adjusted by 1M HCl to 2. Large amount of yellowish crystalline powder of 7 with the yield of 71% was generated. Rod-shaped crystals suitable for single-crystal X-ray analyses were together with the powder and were separated for structure determination.

Synthesis of $\text{Cu}_4\text{I}_6(tp)_2(bttmm)_2$: 0D- $\text{Cu}_2\text{I}_2(tp)_3$ (0.1 g) was first well dispersed in a mixture of toluene (2 ml) and CH_2Cl_2 (2 ml), and then was mixed with the ligand (0.1 g) in methanol (2 ml). The mixture was heated at 80 °C for 2 days, which afforded greenish crystalline powder along with plate-shaped single crystals. Yield is 59%.

Synthesis of $\text{Cu}_4\text{I}_6(tp)_2(btmdme)_2$: Yellowish rock shaped single crystals were obtained under the similar condition as above. Yield is 52%.

Synthesis of $\text{Cu}_6\text{I}_8(btmdb)_2$: Saturated KI solution (2 ml) containing CuI (0.19 g, 1 mmol) was mixed with methanol (2 ml) containing the ligand (8 mmol). Then acetone (5 ml) was added and the reaction mixture was kept in the open air for the solvent to slowly evaporate. Yellowish rhombohedral-shaped single crystals formed in 3 days and were collected by filtration. Yield is 65%.

6.3 Design strategy and structural characteristics

The AIO type structures can be regarded as the combination of two previously reported structure types: the neutral molecular cluster and ionic structures. The pure ionic structures (no direct Cu-L bonds, “ligand-free”) are much more stable than those built on Cu-L coordinate (dative) bonds,^{87-90,92} however, their optical emission is very weak,^{87,88,92,96-99} with low luminescence internal quantum yields. On the other hands, nonionic molecular clusters with Cu-L dative bonds exhibit the highest IQYs but have poor structural stability. Our hypothesis is that incorporating both ionic and coordinate bonds into the same structure will produce compounds that are both highly emissive and robust.

To obtain the AIO structures we have designed a group of cationic ligands having free N (or S) binding sites. The cationic nature of the ligands will ensure the formation of ionic compounds with anionic inorganic modules, while the free binding sites enable their direct coordination to Cu atoms to form coordinate/dative bonds.

The general approach to synthesize a cationic N/S-ligand is by alkylation of a tertiary amine group of selected ligand to afford an ammonium salt by Menshutkin reaction.¹⁰⁰ Three types of reactions (I, II and III, Fig. 47) were designed. In Reaction I, alkylation occurs at one of the tertiary N site of a bidentate N-ligand (e.g. triethylenediamine). The unalkylated N atom serves as binding site for Cu metal. In Reaction II, alkylation takes place at the aromatic N while S atom acts as a binding site for Cu. While these reactions involve a single step, Reaction III is a two-step process, where alkylation happens at the NH site of an N-heterocyclic ring, making aromatic N atom available for binding to Cu metal center. Bidentate triethylenediamine (*ted*), 4-mercaptopyridine (*4-SH-py*), and benzotriazole (*bta*) derivatives were selected as starting ligands for route I, II and III, respectively, from which ten (10) cationic ligands were prepared, including one formed in-situ.

Direct reactions of these cationic ligands with CuI led to the formation of ten (10) new AIO type compounds with the general formula of $0D-Cu_mI_{m+n}(L)_n$ (L = cationic organic ligand) (Table 10 and 11). In some cases, triphenylphosphine (*tpp*) was introduced as terminal ligands to prevent the formation of high dimensional inorganic modules such as chains or layers. All compounds are molecular species containing inorganic clusters of various compositions (Fig. 48) with the following formulae: $Cu_3I_5(bz\text{-}ted)_2$, $Cu_4I_6(3\text{-}Cl\text{-}pr\text{-}ted)_2$, $Cu_4I_6(pr\text{-}ted)_2$, $Cu_4I_6(2\text{-}Br\text{-}et\text{-}ted)_2$, $Cu_5I_7(i\text{-}pr\text{-}ted)_2$, $Cu_6I_8(bu\text{-}ted)_2$, $Cu_2I_4(mtp)_2$, $Cu_4I_6(tpp)_2(bttmm)_2$, $Cu_4I_6(tpp)_2(btmdme)_2$, and $Cu_6I_8(btmdb)_2$.

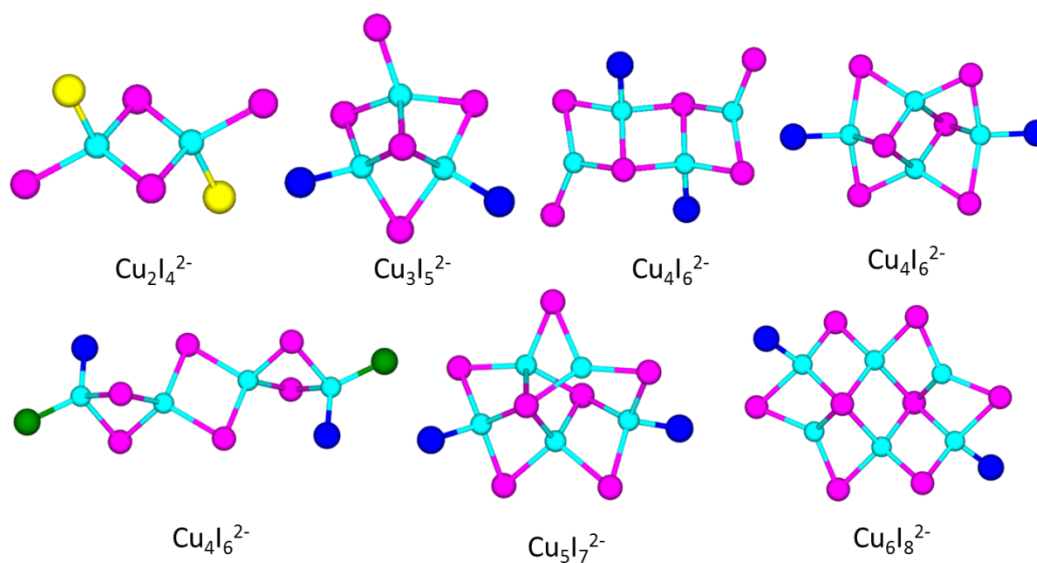


Figure 50. Examples of inorganic anionic cluster motifs obtained for AIO type of compounds.

Crystal structure analysis reveals that direct coordinate/dative bonds are formed between the free binding atom (N, P or S) of the cationic ligand and Cu atom of the anionic cluster in all 10 structures. The Cu–N distances in these compounds are similar to typical Cu–N bond lengths found in other CuI-based hybrid structures containing only dative bonds (2.0~2.2 Å).^{18,33,34,45,46} Based on the types of binding atoms these compounds can be categorized into two sub-groups. For sub-group I compounds, the N atom directly coordinated to metal has a sp^3 electron configuration (part of the aliphatic ring), whereas the coordinating N atom of the ligands in sub-group II compounds has a sp^2 configuration (part of the aromatic ring, Table 1). The Cu–Cu distances are generally much shorter in subgroup I (2.61–2.64 Å) than in sub-group II (2.86–3.09 Å). The common features of these AIO compounds are: (i) they are molecular crystals; (ii) the inorganic modules are anionic and the organic ligands are cationic; (iii) the anionic inorganic component and the cationic organic component are further connected by coordinate/dative bonds. Different from molecular crystals made of neutral inorganic modules, which are limited to a small group of clusters such as CuI monomers, Cu₂I₂ dimers, or Cu₄I₄ tetramers, a large variety of anionic inorganic modules can be obtained using similar ligands, suggesting a remarkably rich structural variation of this type of compounds. Among 10 structures included here, 7 different inorganic cluster are identified, from dimer (Cu₂) to hexamer (Cu₆), most of which are discovered for the first time. In addition, some of them have the same composition but are structurally different, adding yet another degree of diversity towards this family. For example, compounds Cu₄I₆(*pr-ted*)₂, Cu₄I₆(2-*Br-et-ted*)₂ and Cu₄I₆(*tpp*)₂(*bttmm*)₂ all contain (Cu₄I₆)²⁻, but their structures are very different (Fig. 1b). Structures with identical inorganic modules but coordinated to different ligands have also been obtained, such as Cu₄I₆(3-*Cl-pr-ted*)₂ and Cu₄I₆(*pr-ted*)₂; Cu₄I₆(*tpp*)₂(*bttmm*)₂ and Cu₄I₆(*tpp*)₂(*btmdme*)₂; indicating the formation of the

structure types is not completely random, but is related to the choice of ligands. Different from neutral molecular species where each Cu atom has tetrahedral coordination and bonds to at least one ligand molecule, some Cu atoms in ionic compounds are coordinated only to three iodine. The unsaturated coordination of Cu atoms is a unique property of this structure family.

6.4 Optical Properties and luminescence mechanism

Room temperature photoluminescence was measured on all AIO samples as well as selected pure ionic compounds. While the latter group are all thermally stable above 180 °C, they are poor emitters with IQY values typically less than a few percent. For example, $\text{Cu}_4\text{I}_8(1,4\text{-de-ted})_2$ ($1,4\text{-de-ted}$ = 1,4-diethyl-1,4-diazabicyclo[2.2.2] octane-1,4-diium) gives a very weak yellow-orange emission (Fig. 51) with a IQY (2%).⁹² On the contrary, all AIO compounds display intense luminescence with internal quantum yields (IQYs) greater than 60%. Some are as high as 92% (Table 11). Such differences suggest that metal-ligand bonds play a vital role in the electron transfer process upon excitation of these compounds.

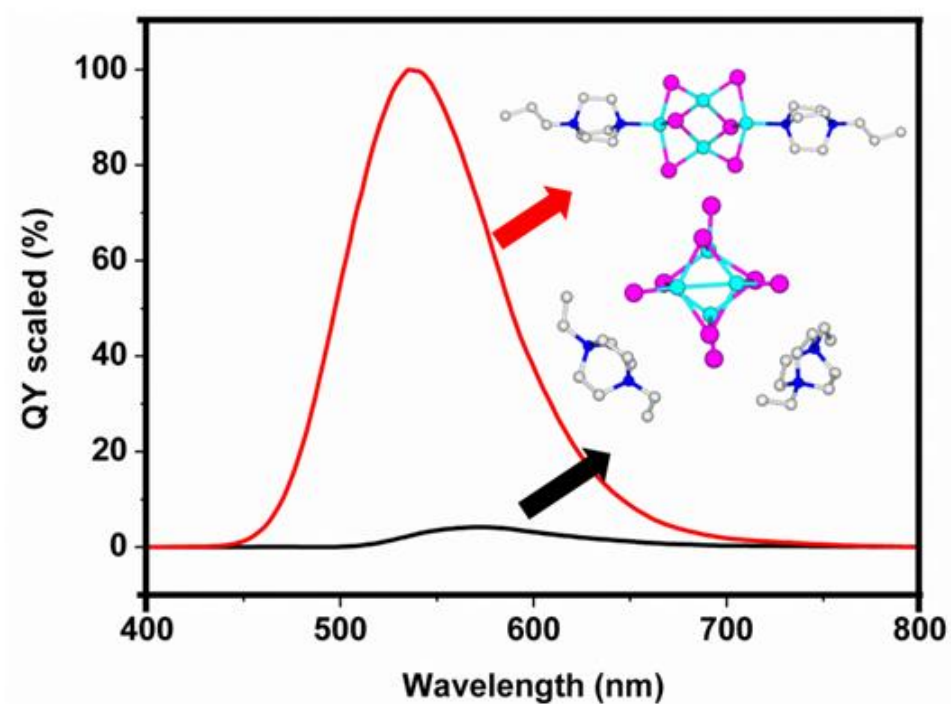


Figure 51. QY scaled emission spectra of $\text{Cu}_4\text{I}_6(\text{pr-td})_2$ (red) and $\text{Cu}_4\text{I}_8(\text{di-et-td})_2$.

It is also interesting to note the similarities and differences in the optical behaviors of the compounds in two sub-groups: While all of them emit at similar energies (within green to yellow region) and have a broad single emission band at room temperature (Fig. 52) the optical band gaps of sub-group I compounds are considerably higher than those of the sub-group II compounds (Table 11). Clearly, photoluminescence of sub-group I does not correlate with their optical band gaps (Fig. S24), which is similar to that of Cu_4I_4 cubane based structures. Like most of the cubane structures, the sub-group I compounds also have short Cu-Cu distances (less than 2.8 \AA), suggesting that they may follow the same emission mechanism. Sub-group II compounds, on the other hand, have emission energies close to their estimated optical band gaps, resembling those of $\text{Cu}_2\text{I}_2(\text{L})_m$ dimer- and 1D- $\text{CuI}(\text{L})$

chain-based structures.^{45,46} The Cu-Cu distances are generally longer in these compounds (with the exception of $\text{Cu}_6\text{I}_8(\text{btmdb})_2$). Note all members of this sub-group can be effectively excited by blue light, an important requirement for phosphors that can be used in conjunction with a blue LED chip in commercial WLED bulbs/lamps. Among them, compound **8** has a IQY of 71% under 450 nm excitation, compared favorably to that of a benchmark yellow phosphor YAG:Ce^{3+} . To the best of our knowledge, this is the highest IQY value among all blue-excitable copper iodide based phosphors reported to date.

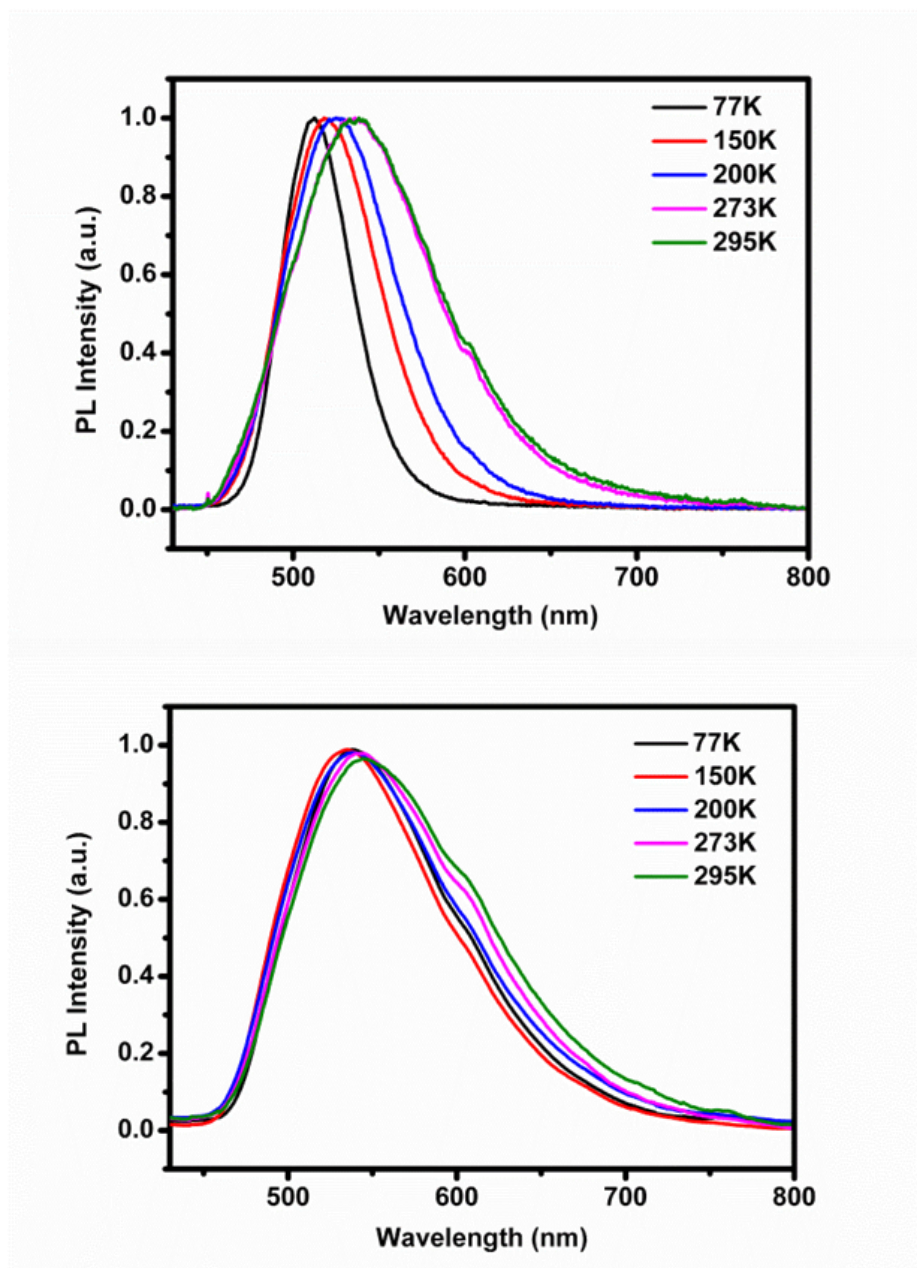


Figure 52. Emission spectra of $\text{Cu}_4\text{I}_6(\text{pr-td})_2$ (top) and $\text{Cu}_4\text{I}_6(\text{tp})_2(\text{bttmm})_2$ (bottom) at various temperatures ($\lambda_{\text{ex}} = 360 \text{ nm}$).

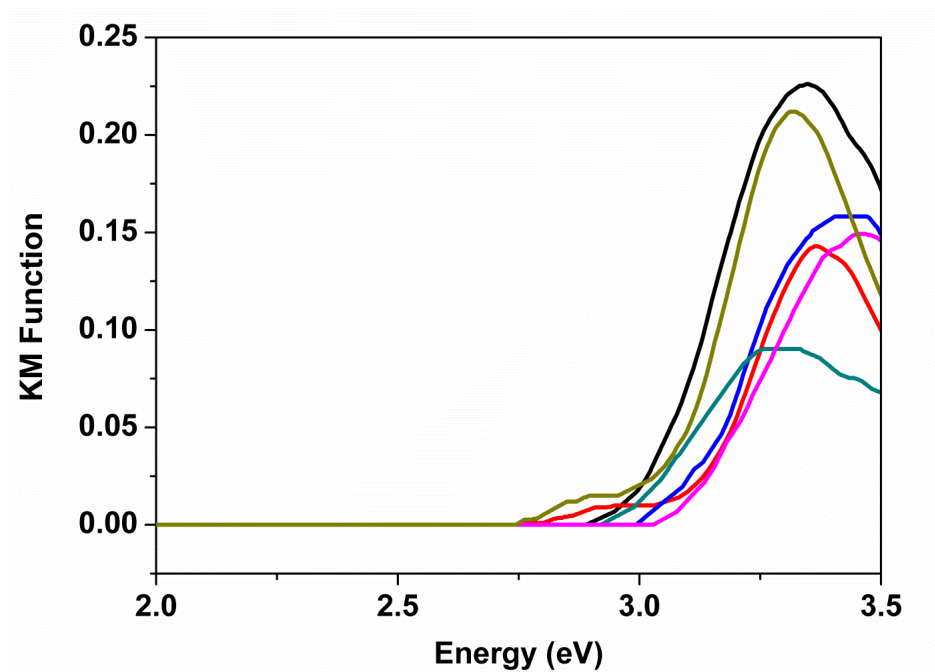


Figure 53. Optical absorption spectra of compounds in sub group (I).

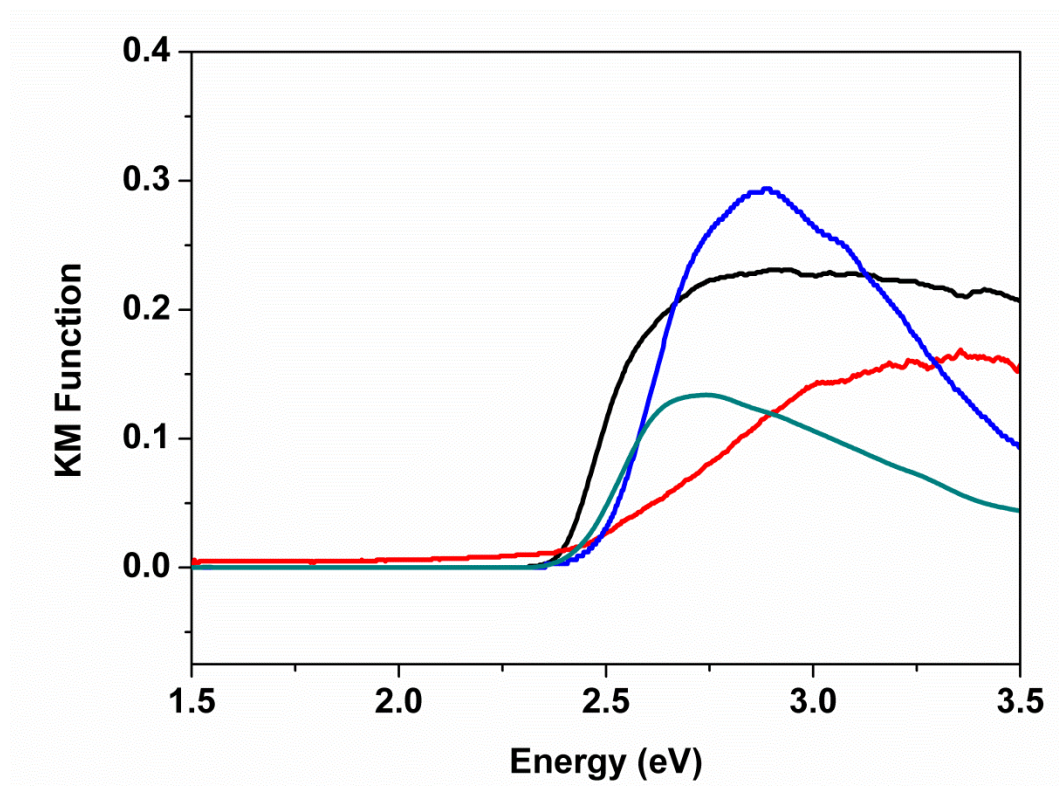


Figure 54. Optical absorption spectra of compounds in sub group (II).

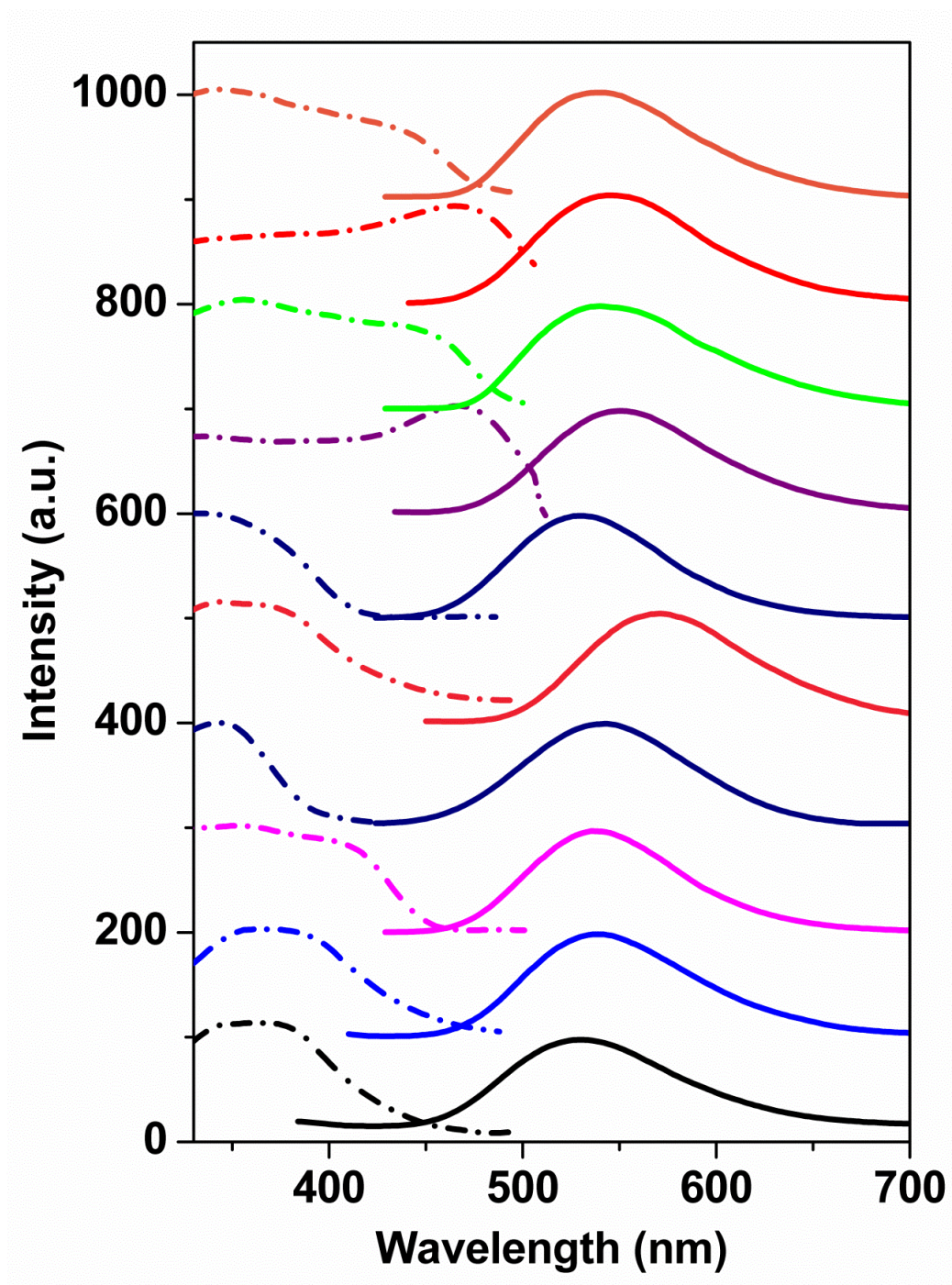


Figure 55. Excitation and emission spectra of all compounds.

The sub-group I compounds exhibit thermochromic behavior, as illustrated in Fig. 52. For compound $\text{Cu}_4\text{I}_6(\text{pr-}t\text{ed})_2$, lowering temperature results in a small blue shift in its emission peak accompanied by a peak width narrowing. This behavior can be attributed to reduced structural torsion at low temperatures and increased localization of the excited state on the molecular structure.¹⁰¹⁻¹⁰³ On the other hand, sub-group II compounds do not show clear thermochromism. There is very little temperature dependence in their emission energies (Fig. 52). The PL lifetimes of sub-group I compounds (e.g. $\text{Cu}_4\text{I}_6(\text{pr-}t\text{ed})_2$ and $\text{Cu}_6\text{I}_8(\text{bu-}t\text{ed})_2$) show very little or no dependence on temperature, which is characteristic of phosphorescence. Their PL lifetime decay curves are best fit with a single exponential decay function, with an average amplitude-weighted PL lifetime decay constant (τ) about 5 μs (Fig. 56). For sub-group II compounds, however, the PL lifetimes have strong temperature dependence, with values decreasing from 23-24 μs at 77 K to 1.3-1.6 μs at 295 K. Their PL lifetime decay curves are best fit by a double exponential decay function indicating that two separate processes may be contributing to the emission. For $\text{Cu}_4\text{I}_6(\text{tpp})_2(\text{btmm})_2$, as temperature increases there is generally an increase in the fraction of the short lifetime decay constant, τ_1 , and at 295 K, almost 50% of the PL lifetime decay is attributed to a relatively fast 380 ns component. This suggests that in addition to phosphorescence ($\sim 50\%$), a substantial fraction of the emission at room temperature originates from thermally-activated delayed fluorescence (TADF) (Fig. 56). TADF has been observed previously in organic-inorganic hybrid materials and is associated with small singlet to triplet energy differences (Fig. 56) allowing exchange of electrons between the lowest excited triplet state (T_1) and the lowest excited singlet state (S_1) prior to radiative recombination. The lack of emission peak shifts with increasing temperature is also consistent with TADF and a small energy difference between S_1 and T_1 . On the other hand, the absence of TADF for compound $\text{Cu}_4\text{I}_6(\text{pr-}t\text{ed})_2$

(and other sub-group I compounds) is attributed to a large energy separation between S_1 and T_1 excited states which inhibits reverse intersystem crossing (RISC, Fig. 56). This large energy difference is due to a higher lying S_1 state compared to sub-group II compounds and is consistent with the generally higher optical band gaps or shorter wavelength (higher energy) absorption onset observed in the optical absorption spectra of sub-group I compounds.

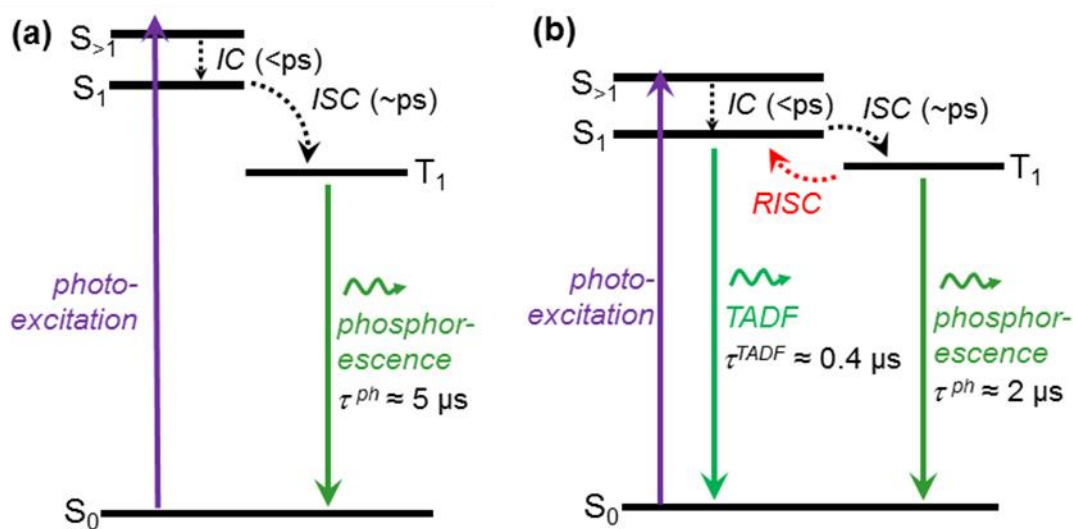


Figure 56. Energy diagrams of (a) compound $\text{Cu}_4\text{I}_6(\text{pr-td})_2$ indicating phosphorescence and (b) compound $\text{Cu}_4\text{I}_6(\text{tp})_2(\text{bttmm})_2$ indicating TADF and phosphorescence emission processes. The approximate time constants for internal conversion (IC) and intersystem crossing (ISC) are indicated along with the approximate time constants for TADF and phosphorescence which are extracted from the measured PL lifetime decay times.

DFT calculations were performed on selected structures from sub-group I (compounds $\text{Cu}_5\text{I}_7(\text{i-pr-td})_2$ and sub-group II $\text{Cu}_2\text{I}_4(\text{mt})_2$ (Fig. 52). The calculations correctly captured the trend that compounds in sub-group I have higher band gaps than those in sub-group II,

although the calculated values are systematically lower than experiment by about 0.7 eV.¹⁰⁴ This error range is consistent with recent calculations on a series of semiconductors and insulators using hybrid functionals.¹⁰⁵ The calculations correctly capture the experimental observation that optical band gaps of sub-group I are significantly larger than those of sub-group II (Fig. 52). The valence bands of all four compounds share common features - the primarily contributions are from the inorganic components (Cu 3d and I 5p atomic orbitals). However the contributions to the conduction bands are very different for compounds from the two sub-groups. For sub-group I compounds, they are mainly from Cu and I atomic orbitals (Cu 3d and I 5p), supporting a “cluster-centered” (CC) charge transfer mechanism for the observed luminescence.^{34,106,107} For sub-group II compounds, they are mostly from organic ligands (C 2p and N 2p atomic orbitals), and therefore, the emission is largely due to a metal-to-ligand charge transfer (MLCT) and iodine-to-ligand charge transfer (XLCT).

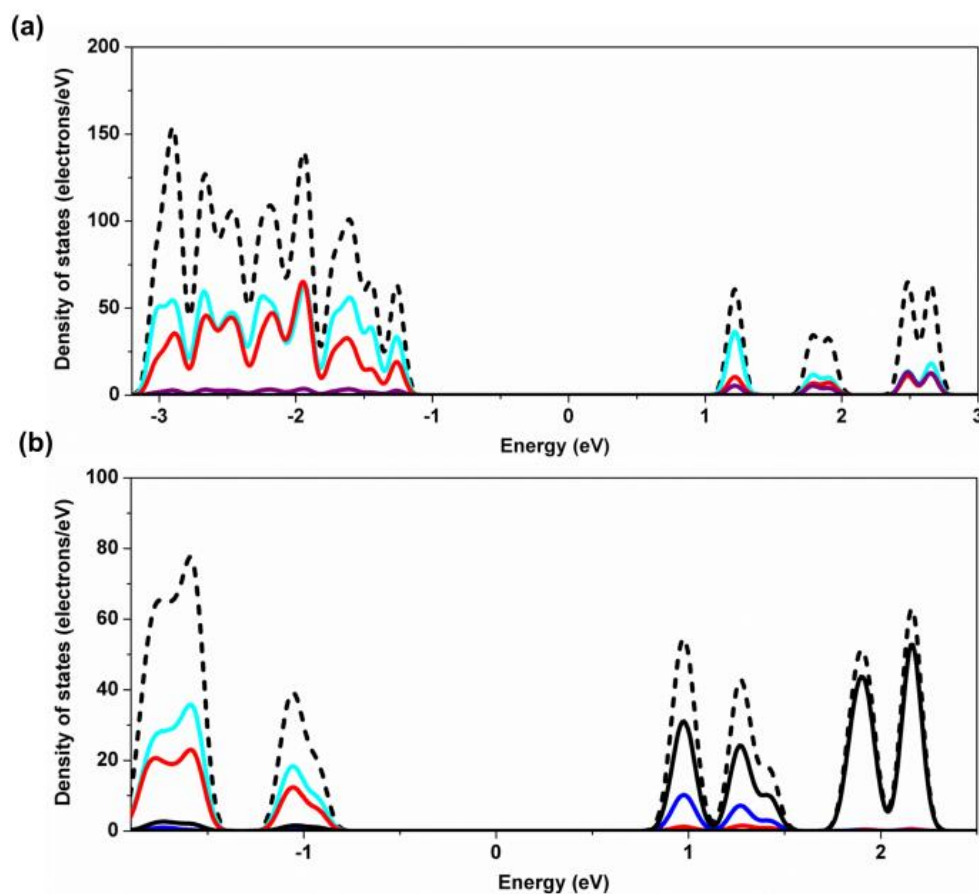


Figure 57. Density of states (DOS) plots for compounds $\text{Cu}_5\text{I}_7(i\text{-}pr\text{-}td)_2$ and $\text{Cu}_2\text{I}_4(mtp)_2$. Line color scheme: dashed black: total; cyan: Cu (3d); pink Cu (4s); red: I (5p); purple I (5d); blue: N (2p); black: C (2p).

6.5 Significantly improve thermal-/photostability

The greatly enhanced thermal stability of these AIO structures is reflected from thermogravimetric (TG) analysis results. The decomposition temperatures of sub-group I compounds are as high as 300 °C, (Fig. 58). Most sub-group II compounds are stable up to 200 °C (Fig. 59). Compared to Cu_mI_n -based charge-neutral molecular clusters, which

generally decompose below 80 °C, the addition of ionic bonding stabilizes AIO structures by at least 100 °C.

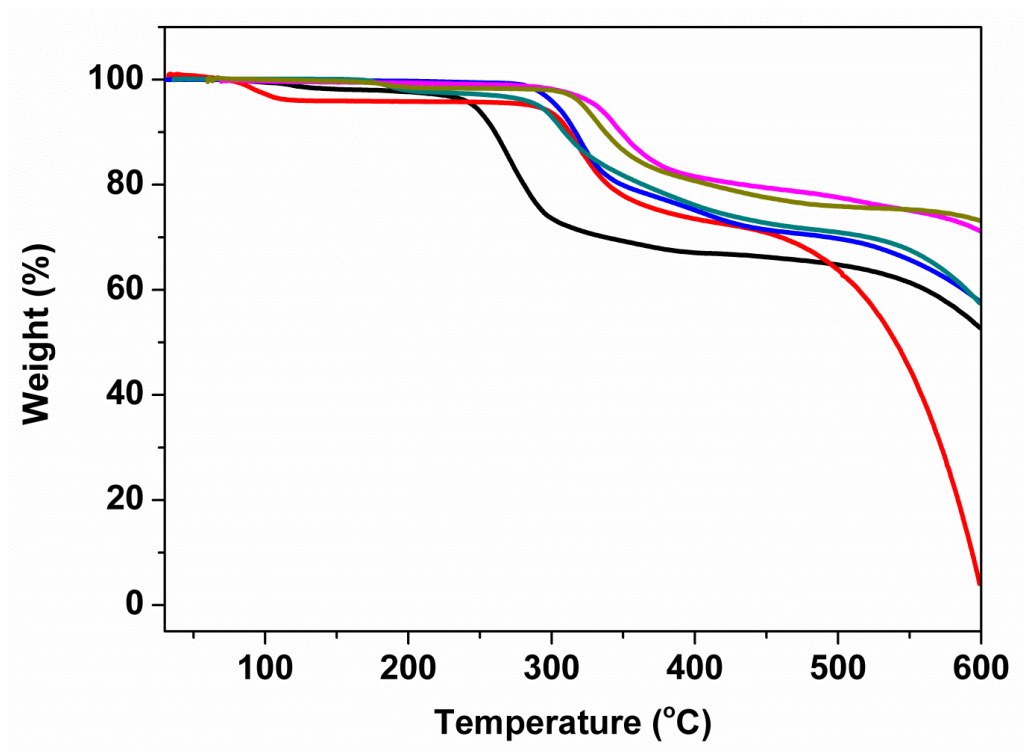


Figure 58. TG plots of structures in sub group (I). $\text{Cu}_3\text{I}_5(\text{bz-ted})_2$ (black), $\text{Cu}_4\text{I}_6(3\text{-Cl-pr-ted})_2$ (red), $\text{Cu}_4\text{I}_6(\text{pr-ted})_2$ (blue), $\text{Cu}_4\text{I}_6(2\text{-Br-et-ted})_2$ (green), $\text{Cu}_5\text{I}_7(i\text{-pr-ted})_2$ (pink), $\text{Cu}_6\text{I}_8(\text{bu-ted})_2$ (gold).

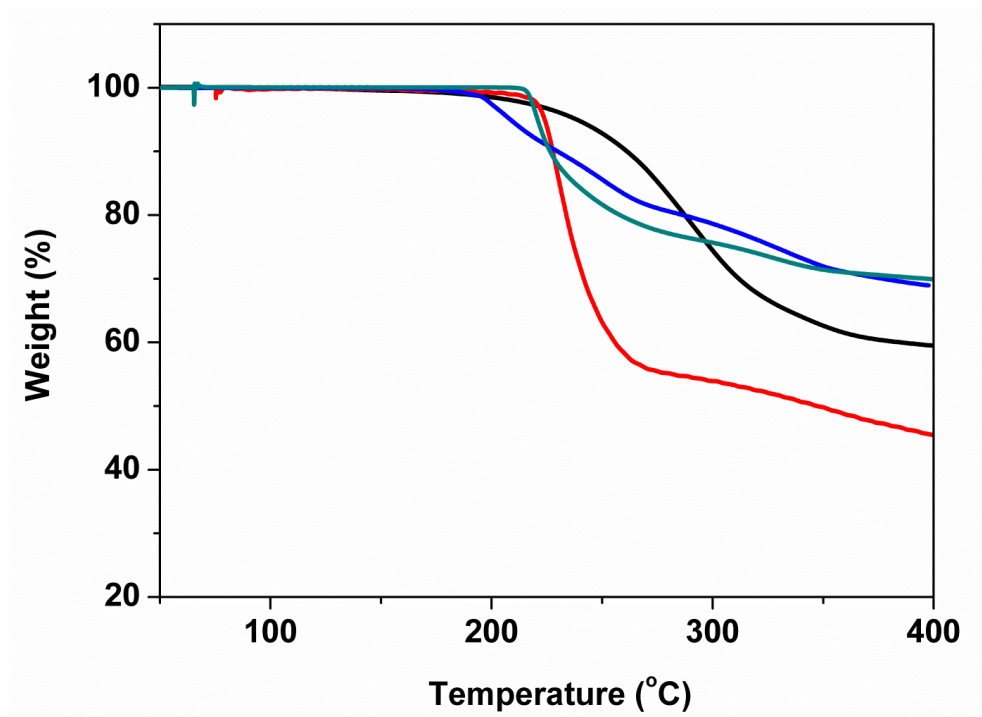


Figure 59. TG plots of structures in sub group (II). $\text{Cu}_2\text{I}_4(\text{mtp})_2$ (black), $\text{Cu}_4\text{I}_6(\text{tpp})_2(\text{btmdme})_2$ (red), $\text{Cu}_4\text{I}_6(\text{tpp})_2(\text{btmdme})_2$ (blue), and $\text{Cu}_6\text{I}_8(\text{btmdb})_2$ (green).

To further evaluate their suitability as lighting phosphors, $\text{Cu}_4\text{I}_6(\text{pr-td})_2$ and $\text{Cu}_4\text{I}_6(\text{tpp})_2(\text{btmdme})_2$ were selected from each sub-group for long-term photo- and thermal-stability tests. After heating the selected samples at 100 °C for 20 days without protection, their IQY values were maintained at > 90% compared to the initial values (Fig. 60). Similarly, nominal decreases in their IQYs were detected after continuous UV irradiation on these samples for 20 days (Inset of Fig. 60). The two reference materials, namely charge-neutral 0D- $\text{Cu}_2\text{I}_2(\text{py})_4$ dimer and 0D- $\text{Cu}_4\text{I}_4(\text{py})_4$ tetramer, however, suffered nearly 100% drop in their IQYs upon heating for merely one day, and these values were reduced by ~50% and ~80% at the end of the photostability experiment.

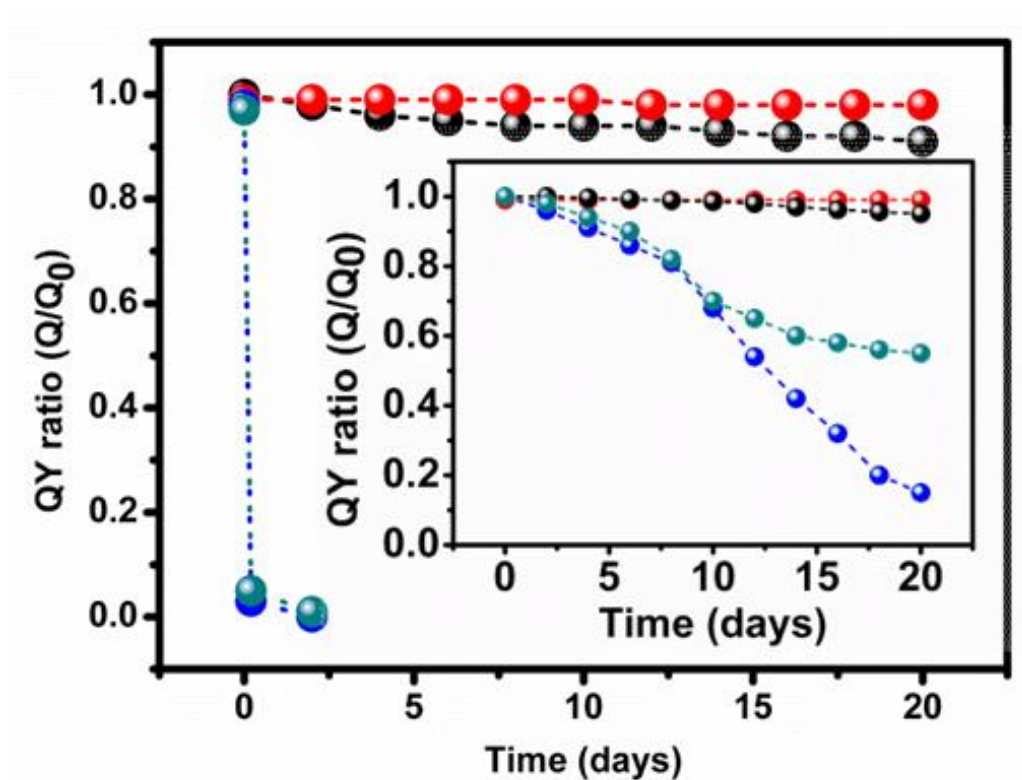


Figure 60. Plots of IQY ratios (Q_0 and Q are IQY values measured before and after heating the sample at 100 °C in air as a function of time). Inset is the plot of ratios of the IQY values after and before exposing to UV light as a function of time. Blue: 0D-Cu₂I₂(py)₄, green: 0D-Cu₄I₆(py)₄, red: Cu₄I₆(pr-td)₂, black: Cu₄I₆(tp)₂(bttmm)₂.

6.6 Solution dispersability and lighting device design

Another advantage of these molecular clusters is their excellent solubility and dispersibility in common organic solvents, including chloroform, dimethylformamide (DMF), dimethyl sulfoxide (DMSO) (Fig. 61a). This makes it possible to fabricate films of these materials by solution-based process. High quality, continuous films of Cu₄I₆(pr-td)₂ were made by spin coating followed by thermal annealing (Fig. 61b). The film samples were

characterized by optical microscope (Fig. 61c), powder X-ray diffraction analysis (PXRD) and atomic force microscopy (AFM) (Fig. 61d). Prototype LED bulbs using these materials as phosphors were assembled by remote model (Fig. 61e). The white-emitting bulb was generated by coating compound $\text{Cu}_4\text{I}_6(\text{tpp})_2(\text{btmm})_2$ on a commercial blue LED chip. High solution processability allows easy coating of the phosphors onto various substrates, including flexible papers or fabric.

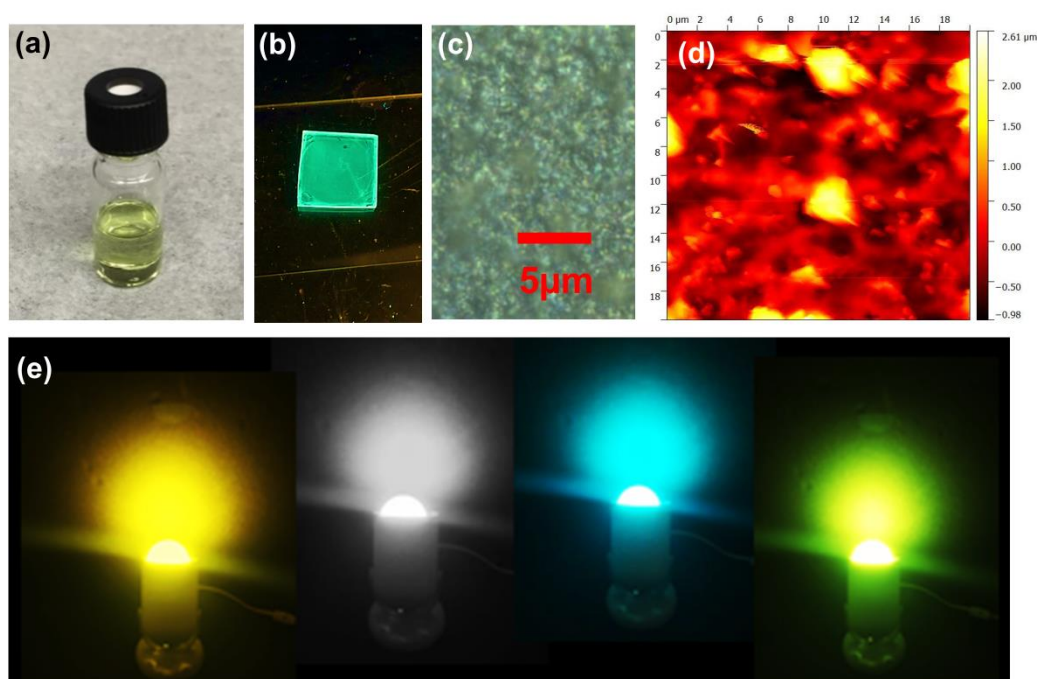


Figure 61. (a) Image of compound $\text{Cu}_4\text{I}_6(\text{pr-td})_2$ completely dissolved in DMF solution. (b) Thin film prepared using compound $\text{Cu}_4\text{I}_6(\text{pr-td})_2$ emitting green color under UV illumination. (c) Bright-field micrograph image of the spin-coated film of $\text{Cu}_4\text{I}_6(\text{pr-td})_2$. (d) AFM image of the thin film collected in tapping mode. (e) Illuminating LED light bulbs (110 V, 2 W) coated by selective AIO phosphors.

The AIO structures represent an entirely new sub-class of the CuI(L) hybrid material family. Compared to other three sub-classes that we have developed so far, namely the 1D-CuI(L) staircase chain compounds, the nD-Cu₂I₂ (n = 0, 1, 2) rhomboid dimer-based and nD-Cu₄I₄ (n = 0, 1, 2, 3) cubane tetramer-based structures,^{18,45,46} the new sub-family is the only one that meets all four standards that are essential for lighting phosphors: optical tunability, high quantum efficiency, excellent thermal and photo stability and solution dispersibility/processability (Table 12).

Table 10. Summary of crystal data of AIO type of compounds.

Structures	Cu ₃ I ₅ (<i>bz</i> - <i>ted</i>) ₂	Cu ₄ I ₆ (<i>β-Cl</i> - <i>pr-ted</i>) ₂	Cu ₄ I ₆ (<i>pr-ted</i>) ₂	Cu ₄ I ₆ (<i>2-Br-et-ted</i>) ₂	Cu ₅ I ₇ (<i>i-pr-ted</i>) ₂	Cu ₆ I ₈ (<i>bu-ted</i>) ₂	Cu ₂ I ₄ (<i>mtp</i>) ₂	Cu ₄ I ₆ (<i>tpp</i>) ₂	Cu ₄ I ₆ (<i>tpp</i>) ₂ (<i>b</i> - <i>btmm</i>) ₂	Cu ₆ I ₈ (<i>btm</i> - <i>db</i>) ₂
Empirical Formula	C ₂₆ H ₃₈ Cu ₃ I ₅ N ₄	C ₁₈ H ₃₆ Cl ₂ Cu ₄ I ₆ N ₄	C ₁₈ H ₃₈ Cu ₄ I ₆ N ₄	C ₁₆ H ₃₂ Br ₂ Cu ₄ I ₆ N ₄	C ₂₂ H ₄₄ Cu ₅ I ₇ N ₆	C ₂₀ H ₄₂ Cu ₆ I ₈ N ₄	C ₁₄ H ₂₀ Cu ₂ I ₄ N ₂ S ₂	C ₅₆ H ₆₀ Cu ₄ I ₆ N ₈ P ₂	C ₃₈ H ₆₄ Cu ₄ I ₆ N ₈ P ₂	C ₃₈ H ₆₆ Cu ₆ I ₈ N ₈
FW	1231.72	1394.97	1326.08	1455.83	1598.63	1735.01	915.12	1922.62	1950.67	2031.42
Space Group	Pna2 ₁	Pbca	Pbca	P2 ₁ /c	Cc	P2 ₁ /n	Pbca	P-1	P-1	P2 ₁ /n
<i>a</i> (Å)	24.0270 (11)	13.6462 (7)	14.6937 (12)	7.3080 (3)	8.7546 (4)	4.0654 (8)	14.1350 (5)	9.4270 (5)	9.4759 (4)	20.0887 (7)
<i>b</i> (Å)	9.7647 (5)	14.8791 (7)	14.4893 (12)	16.7452 (7)	32.8070 (13)	9.6542 (6)	11.2250 (4)	9.7963 (6)	9.8097 (4)	14.0472 (5)
<i>c</i> (Å)	14.1939 (7)	15.8035 (8)	14.7546 (12)	13.0857 (6)	13.9970 (6)	15.3742 (9)	14.4830 (5)	19.2714 (11)	19.4737 (8)	21.1752 (8)
α (°)	90	90	90	90	90	90	90	95.637 (2)	97.104 (2)	90
β (°)	90	90	90	91.875 (2)	104.049 (2)	109.777 (2)	90	94.470 (2)	93.506 (2)	109.720 (2)
γ (°)	90	90	90	90	90	90	90	118.055 (2)	117.500 (2)	90
<i>V</i> (Å ³)	3330.1 (3)	3208.8 (3)	3141.3 (4)	1600.49 (12)	1598.63 (2)	1949.3 (2)	2297.95 (14)	1547.30 (16)	1578.89 (12)	5625.0 (4)
<i>Z</i>	4	4	4	2	4	2	4	1	1	4
<i>T</i> (K)	100 (2)	100 (2)	100 (2)	298 (2)	100 (2)	100 (2)	150 (2)	100 (2)	100 (2)	100 (2)
λ (Å)	0.7749	0.7749	0.7749	0.7749	0.7749	0.7749	0.6888	0.7749	0.7293	0.7293
<i>R</i> ₁	0.0241	0.0170	0.0224	0.0349	0.0217	0.0213	0.0162	0.0295	0.0259	0.0327
<i>wR</i> ₂	0.0573	0.0409	0.0553	0.0918	0.0487	0.0477	0.0345	0.0746	0.0633	0.0600

^a Acetonitrile molecule was removed for the formulation consistency.

Table 11. Estimated optical band gaps, emission energies and colors, IQY values and decomposition temperatures of compounds.

#	Structure	Optical Bandgap (eV)	λ_{em} (nm)	Emission Color	IQY (EQY) (λ_{ex} : 360 nm)	IQY (EQY) (λ_{ex} : 450 nm)	T _D (°C)
Sub-Group 1							
1	Cu ₃ I ₅ (<i>bz-ted</i>) ₂	3.0	560	Yellow	75 (67)	--	270
2	Cu ₄ I ₆ (<i>3-Cl-pr-ted</i>) ₂	3.1	540	Green- yellow	92 (71)	--	270
3	Cu ₄ I ₆ (<i>pr-ted</i>) ₂	3.1	535	Green	92 (65)	--	280
4	Cu ₄ I ₆ (<i>2-Br-et-ted</i>) ₂	2.9	535	Green	75 (47)	--	280
5	Cu ₅ I ₇ (<i>i-pr-ted</i>) ₂	3.1	575	Orange	70 (54)	--	310
6	Cu ₆ I ₈ (<i>bu-ted</i>) ₂	3.0	530	Green	90 (69)	--	300
Sub-Group 2							
7	Cu ₂ I ₄ (<i>mtp</i>) ₂	2.3	555	Yellow	61 (49)	52 (41)	210
8	Cu ₄ I ₆ (<i>tp</i>) ₂ (<i>bttmm</i>) ₂	2.5	540	Green- yellow	90 (54)	71 (56)	200
9	Cu ₄ I ₆ (<i>tp</i>) ₂ (<i>btmdme</i>) ₂	2.4	545	Green- yellow	64 (45)	42 (30)	180
10	Cu ₆ I ₈ (<i>btmdb</i>) ₂	2.4	540	Green- yellow	70 (61)	51 (40)	200

Table 12. Comparison of the four types of copper iodide based hybrid phosphors.

Sub-family	Formula	Optical Tunability	High IQYs	High Stability	High Dispersibility
I	$\text{CuI}(L)$	√	X	X	X
II	$\text{Cu}_2\text{I}_2(L)_n$	√	√	X	X
III	$\text{Cu}_4\text{I}_4(L)_n$	X	√	√	X
IV	$\text{Cu}_m\text{I}_{m+n}(L)_n$	√	√	√	√

6.7 Summary

In summary, a new AIO type of inorganic-organic hybrid structures have been designed and synthesized, displaying the features of structural diversity, high luminescence and stability, and excellent dispersibility, making them suitable candidates as lighting phosphors. More importantly, their unique structural characteristics provide insights in understanding the structure-property correlations and open up new opportunities for designing new structures with more potential applications.

7. References

- (1) *Worldwide Trends in Energy Use and Efficiency*, 2008.
- (2) Mahmoudi, A.; Dehghanpour, S.; Babakhodaverdi, M. *Acta Crystallographica Section E* **2012**, *68*, m1277.
- (3) Dyason, J. C.; Healy, P. C.; Pakawatchai, C.; Patrick, V. A.; White, A. H. *Inorganic Chemistry* **1985**, *24*, 1957.
- (4) Bergh, A.; Craford, G.; Duggal, A.; Haitz, R. *Phys Today* **2001**, *54*, 42.
- (5) Kuo, C. P.; Fletcher, R. M.; Osentowski, T. D.; Lardizabal, M. C.; Craford, M. G.; Robbins, V. M. *Appl Phys Lett* **1990**, *57*, 2937.
- (6) Guo, N.; Huang, Y. J.; You, H. P.; Yang, M.; Song, Y. H.; Liu, K.; Zheng, Y. H. *Inorg Chem* **2010**, *49*, 10907.
- (7) Piao, X. Q.; Horikawa, T.; Hanzawa, H.; Machida, K. *Appl Phys Lett* **2006**, *88*.
- (8) Setlur, A. A.; Heward, W. J.; Gao, Y.; Srivastava, A. M.; Chandran, R. G.; Shankar, M. V. *Chem Mater* **2006**, *18*, 3314.
- (9) Su, L. T.; Tok, A. I. Y.; Boey, F. Y. C.; Zhang, X. H.; Woodhead, J. L.; Summers, C. J. *J Appl Phys* **2007**, *102*.
- (10) Uoyama, H.; Goushi, K.; Shizu, K.; Nomura, H.; Adachi, C. *Nature* **2012**, *492*, 234.
- (11) Park, S.-I.; Xiong, Y.; Kim, R.-H.; Elvikis, P.; Meitl, M.; Kim, D.-H.; Wu, J.; Yoon, J.; Yu, C.-J.; Liu, Z.; Huang, Y.; Hwang, K.-c.; Ferreira, P.; Li, X.; Choquette, K.; Rogers, J. A. *Science* **2009**, *325*, 977.
- (12) Reineke, S.; Lindner, F.; Schwartz, G.; Seidler, N.; Walzer, K.; Luessem, B.; Leo, K. *Nature* **2009**, *459*, 234.
- (13) Sun, Y. R.; Giebink, N. C.; Kanno, H.; Ma, B. W.; Thompson, M. E.; Forrest, S. R. *Nature* **2006**, *440*, 908.
- (14) Taniyasu, Y.; Kasu, M.; Makimoto, T. *Nature* **2006**, *441*, 325.
- (15) Anikeeva, P. O.; Halpert, J. E.; Bawendi, M. G.; Bulovic, V. *Nano Lett* **2007**, *7*, 2196.
- (16) Li, Y. Q.; Rizzo, A.; Cingolani, R.; Gigli, G. *Adv Mater* **2006**, *18*, 2545.
- (17) Nizamoglu, S.; Zengin, G.; Demir, H. V. *Appl Phys Lett* **2008**, *92*.
- (18) Fang, Y.; Liu, W.; Teat, S. J.; Dey, G.; Shen, Z.; An, L.; Yu, D.; Wang, L.; O'Carroll, D. M.; Li, J. *Advanced Functional Materials* **2017**, *27*, 1603444.
- (19) Mitzi, D. B. In *Progress in Inorganic Chemistry*; John Wiley & Sons, Inc.: 2007, p 1.
- (20) Mitzi, D. B.; Wang, S.; Feild, C. A.; Chess, C. A.; Guloy, A. M. *Science* **1995**, *267*, 1473.
- (21) Kagan, C. R.; Mitzi, D. B.; Dimitrakopoulos, C. D. *Science* **1999**, *286*, 945.
- (22) Mitzi, D. B. *Advanced Materials* **2009**, *21*, 3141.
- (23) Saparov, B.; Mitzi, D. B. *Chemical Reviews* **2016**, *116*, 4558.

- (24) Nie, W.; Tsai, H.; Asadpour, R.; Blancon, J.-C.; Neukirch, A. J.; Gupta, G.; Crochet, J. J.; Chhowalla, M.; Tretiak, S.; Alam, M. A.; Wang, H.-L.; Mohite, A. D. *Science* **2015**, *347*, 522.
- (25) Huang, X.; Li, J. *Journal of the American Chemical Society* **2007**, *129*, 3157.
- (26) Huang, X.; Li, J.; Fu, H. *Journal of the American Chemical Society* **2000**, *122*, 8789.
- (27) Huang, X.; Li, J.; Zhang, Y.; Mascarenhas, A. *Journal of the American Chemical Society* **2003**, *125*, 7049.
- (28) Ki, W.; Li, J. *Journal of the American Chemical Society* **2008**, *130*, 8114.
- (29) Roushan, M.; Zhang, X.; Li, J. *Angewandte Chemie International Edition* **2012**, *51*, 436.
- (30) Dohner, E. R.; Jaffe, A.; Bradshaw, L. R.; Karunadasa, H. I. *Journal of the American Chemical Society* **2014**, *136*, 13154.
- (31) Yuan, Z.; Zhou, C.; Tian, Y.; Shu, Y.; Messier, J.; Wang, J. C.; van de Burgt, L. J.; Kountouriotis, K.; Xin, Y.; Holt, E.; Schanze, K.; Clark, R.; Siegrist, T.; Ma, B. **2017**, *8*, 14051.
- (32) Yam, V. W.-W.; Au, V. K.-M.; Leung, S. Y.-L. *Chemical Reviews* **2015**, *115*, 7589.
- (33) Tsuge, K.; Chishina, Y.; Hashiguchi, H.; Sasaki, Y.; Kato, M.; Ishizaka, S.; Kitamura, N. *Coordination Chemistry Reviews* **2016**, *306*, Part 2, 636.
- (34) Ford, P. C.; Cariati, E.; Bourassa, J. *Chemical Reviews* **1999**, *99*, 3625.
- (35) Liao, Y.-C.; Lin, C.-H.; Wang, S.-L. *Journal of the American Chemical Society* **2005**, *127*, 9986.
- (36) Ogi, T.; Iwasaki, H.; Nandiyanto, A. B. D.; Iskandar, F.; Wang, W. N.; Okuyama, K. *Journal of Materials Chemistry C* **2014**, *2*, 4297.
- (37) Nakajima, T.; Isobe, M.; Uzawa, Y.; Tsuchiya, T. *Journal of Materials Chemistry C* **2015**, *3*, 10748.
- (38) Mao, Z.-Y.; Wang, F.; Chen, J.-J.; Wang, D.-J. *Journal of the American Ceramic Society* **2015**, *98*, 3856.
- (39) Rosson, T. E.; Claiborne, S. M.; McBride, J. R.; Stratton, B. S.; Rosenthal, S. J. *Journal of the American Chemical Society* **2012**, *134*, 8006.
- (40) Bowers II, M. J.; McBride, J. R.; Garrett, M. D.; Sammons, J. A.; Dukes III, A. D.; Schreuder, M. A.; Watt, T. L.; Lupini, A. R.; Pennycook, S. J.; Rosenthal, S. J. *Journal of the American Chemical Society* **2009**, *131*, 5730.
- (41) Dukes, A. D.; Samson, P. C.; Keene, J. D.; Davis, L. M.; Wikswo, J. P.; Rosenthal, S. J. *The Journal of Physical Chemistry A* **2011**, *115*, 4076.
- (42) Zhang, X.; Hejazi, M.; Thiagarajan, S. J.; Woerner, W. R.; Banerjee, D.; Emge, T. J.; Xu, W.; Teat, S. J.; Gong, Q.; Safari, A.; Yang, R.; Parise, J. B.; Li, J. *Journal of the American Chemical Society* **2013**, *135*, 17401.
- (43) Huang, X.; Roushan, M.; Emge, T. J.; Bi, W.; Thiagarajan, S.; Cheng, J.-H.; Yang, R.; Li, J. *Angewandte Chemie International Edition* **2009**, *48*, 7871.
- (44) Dohner, E. R.; Hoke, E. T.; Karunadasa, H. I. *Journal of the American Chemical Society* **2014**, *136*, 1718.

- (45) Zhang, X.; Liu, W.; Wei, G. Z.; Banerjee, D.; Hu, Z.; Li, J. *Journal of the American Chemical Society* **2014**, *136*, 14230.
- (46) Liu, W.; Fang, Y.; Wei, G. Z.; Teat, S. J.; Xiong, K.; Hu, Z.; Lustig, W. P.; Li, J. *Journal of the American Chemical Society* **2015**, *137*, 9400.
- (47) Liu, Z.; Qayyum, M. F.; Wu, C.; Whited, M. T.; Djurovich, P. I.; Hodgson, K. O.; Hedman, B.; Solomon, E. I.; Thompson, M. E. *Journal of the American Chemical Society* **2011**, *133*, 3700.
- (48) Liu, Z.; Qiu, J.; Wei, F.; Wang, J.; Liu, X.; Helander, M. G.; Rodney, S.; Wang, Z.; Bian, Z.; Lu, Z.; Thompson, M. E.; Huang, C. *Chemistry of Materials* **2014**, *26*, 2368.
- (49) Tsuge, K.; Chishina, Y.; Hashiguchi, H.; Sasaki, Y.; Kato, M.; Ishizaka, S.; Kitamura, N. *Coordination Chemistry Reviews*.
- (50) Pospisil, J.; Jess, I.; Nather, C.; Necas, M.; Taborsky, P. *New Journal of Chemistry* **2011**, *35*, 861.
- (51) Godbout, N.; Salahub, D. R.; Andzelm, J.; Wimmer, E. *Canadian Journal of Chemistry* **1992**, *70*, 560.
- (52) Sosa, C.; Andzelm, J.; Elkin, B. C.; Wimmer, E.; Dobbs, K. D.; Dixon, D. A. *The Journal of Physical Chemistry* **1992**, *96*, 6630.
- (53) Gordon, M. S. *Chemical Physics Letters* **1980**, *76*, 163.
- (54) Francl, M. M.; Pietro, W. J.; Hehre, W. J.; Binkley, J. S.; Gordon, M. S.; DeFrees, D. J.; Pople, J. A. *The Journal of Chemical Physics* **1982**, *77*, 3654.
- (55) Clark, T.; Chandrasekhar, J.; Spitznagel, G. W.; Schleyer, P. V. R. *Journal of Computational Chemistry* **1983**, *4*, 294.
- (56) Frisch, M. J.; Pople, J. A.; Binkley, J. S. *The Journal of Chemical Physics* **1984**, *80*, 3265.
- (57) Binning, R. C.; Curtiss, L. A. *Journal of Computational Chemistry* **1990**, *11*, 1206.
- (58) Blaudeau, J.-P.; McGrath, M. P.; Curtiss, L. A.; Radom, L. *The Journal of Chemical Physics* **1997**, *107*, 5016.
- (59) Rassolov, V. A.; Pople, J. A.; Ratner, M. A.; Windus, T. L. *The Journal of Chemical Physics* **1998**, *109*, 1223.
- (60) Ditchfield, R.; Hehre, W. J.; Pople, J. A. *The Journal of Chemical Physics* **1971**, *54*, 724.
- (61) Perruchas, S.; Tard, C.; Le Goff, X. F.; Fargues, A.; Garcia, A.; Kahlal, S.; Saillard, J.-Y.; Gacoin, T.; Boilot, J.-P. *Inorganic Chemistry* **2011**, *50*, 10682.
- (62) Perruchas, S.; Le Goff, X. F.; Maron, S.; Maurin, I.; Guillen, F.; Garcia, A.; Gacoin, T.; Boilot, J.-P. *Journal of the American Chemical Society* **2010**, *132*, 10967.
- (63) Benito, Q.; Le Goff, X. F.; Maron, S.; Fargues, A.; Garcia, A.; Martineau, C.; Taulelle, F.; Kahlal, S.; Gacoin, T.; Boilot, J.-P.; Perruchas, S. *Journal of the American Chemical Society* **2014**, *136*, 11311.
- (64) Blake, A. J.; Brooks, N. R.; Champness, N. R.; Cooke, P. A.; Crew, M.; Deveson, A. M.; Hanton, L. R.; Hubberstey, P.; Fenske, D.; Schröder, M. *Crystal Engineering* **1999**, *2*, 181.
- (65) Je; Taborsky, P.; Pospisil, J.; Nather, C. *Dalton Transactions* **2007**, 2263.
- (66) Huang, X. *Nat Photon* **2014**, *8*, 748.

30. (67) Choucair, M.; Thordarson, P.; Stride, J. A. *Nat Nano* **2009**, *4*,
- (68) and, C. B. M.; Kagan, C. R.; Bawendi, M. G. *Annual Review of Materials Science* **2000**, *30*, 545.
- (69) Zhou, H.-C.; Long, J. R.; Yaghi, O. M. *Chemical Reviews* **2012**, *112*, 673.
- (70) Ki, W.; Li, J.; Eda, G.; Chhowalla, M. *Journal of Materials Chemistry* **2010**, *20*, 10676.
- (71) Zhang, R.; Emge, T. J.; Zheng, C.; Li, J. *Journal of Materials Chemistry A* **2013**, *1*, 199.
- (72) Jessop, P. G. *Green Chemistry* **2016**, *18*, 2577.
- (73) Cui, Y.; Li, B.; He, H.; Zhou, W.; Chen, B.; Qian, G. *Accounts of Chemical Research* **2016**, *49*, 483.
- (74) Hu, M. Z.; Zhu, T. *Nanoscale Research Letters* **2015**, *10*, 1.
- (75) Harris, K. D. M. *Nat Chem* **2013**, *5*, 12.
- (76) Tanaka, K.; Toda, F. *Chemical Reviews* **2000**, *100*, 1025.
- (77) Yuan, W.; Friščić, T.; Apperley, D.; James, S. L. *Angewandte Chemie International Edition* **2010**, *49*, 3916.
- (78) Biswal, B. P.; Chandra, S.; Kandambeth, S.; Lukose, B.; Heine, T.; Banerjee, R. *Journal of the American Chemical Society* **2013**, *135*, 5328.
- (79) Jeon, I.-Y.; Choi, H.-J.; Jung, S.-M.; Seo, J.-M.; Kim, M.-J.; Dai, L.; Baek, J.-B. *Journal of the American Chemical Society* **2013**, *135*, 1386.
- (80) Ohara, H.; Kobayashi, A.; Kato, M. *Chemistry Letters* **2014**, *43*, 1324.
- (81) Stamboliadis, E.; Pantelaki, O.; Petrakis, E. *Minerals Engineering* **2009**, *22*, 587.
- (82) Klimakow, M.; Klobes, P.; Thünemann, A. F.; Rademann, K.; Emmerling, F. *Chemistry of Materials* **2010**, *22*, 5216.
- (83) Friščić, T.; Reid, D. G.; Halasz, I.; Stein, R. S.; Dinnebier, R. E.; Duer, M. J. *Angewandte Chemie International Edition* **2010**, *49*, 712.
- (84) Sakamoto, H.; Matsuda, R.; Kitagawa, S. *Dalton Transactions* **2012**, *41*, 3956.
- (85) Ford, P. C.; Cariati, E.; Bourassa, J. *Chemical Reviews* **1999**, *99*, 3625.
- (86) Fang, Y.; Liu, W.; Teat, S. J.; Dey, G.; Shen, Z.; An, L.; Yu, D.; Wang, L.; O'Carroll, D. M.; Li, J. *Advanced Functional Materials* **2016**, n/a.
- (87) Li, S.-L.; Zhang, F.-Q.; Zhang, X.-M. *Chem. Commun.* **2015**, *51*, 8062.
- (88) Hou, J.-J.; Li, S.-L.; Li, C.-R.; Zhang, X.-M. *Dalton Transactions* **2010**, *39*, 2701.
- (89) Li, S.-L.; Zhang, X.-M. *Inorganic Chemistry* **2014**, *53*, 8376.
- (90) Chan, H.; Chen, Y.; Dai, M.; Lu, C.-N.; Wang, H.-F.; Ren, Z.-G.; Huang, Z.-J.; Ni, C.-Y.; Lang, J.-P. *CrystEngComm* **2012**, *14*, 466.
- (91) Yu, L.; Li, M.; Zhou, X.-P.; Li, D. *Inorganic Chemistry* **2013**, *52*, 10232.
- (92) Xin, B.; Li, Y.; Zeng, G.; Peng, Y.; Li, G.; Shi, Z.; Feng, S. *Zeitschrift für anorganische und allgemeine Chemie* **2013**, *639*, 611.

- (93) Cho, S.-D.; Hwang, J.; Kim, H.-K.; Yim, H.-S.; Kim, J.-J.; Lee, S.-G.; Yoon, Y.-J. *Journal of Heterocyclic Chemistry* **2007**, *44*, 951.
- (94) Zhou, M.; Ni, C.; He, Z.; Hu, J. *Organic Letters* **2016**, *18*, 3754.
- (95) Katritzky, A. R.; Hughes, C. V.; Rachwal, S. *Journal of Heterocyclic Chemistry* **1989**, *26*, 1579.
- (96) Hou, Q.; Xu, J.-N.; Yu, J.-H.; Wang, T.-G.; Yang, Q.-F.; Xu, J.-Q. *Journal of Solid State Chemistry* **2010**, *183*, 1561.
- (97) Chen, Y.; Yang, Z.; Wu, X.-Y.; Ni, C.-Y.; Ren, Z.-G.; Lang, J.-P. *Physical Chemistry Chemical Physics* **2011**, *13*, 10781.
- (98) Jiao, X.; Niu, Y.; Zhang, H.; Zhu, L.; Zhao, F. *Journal of Chemical Crystallography* **2006**, *36*, 685.
- (99) Wang, Y. J.; Li, H. H.; Chen, Z. R.; Huang, C. C.; Liu, J. B. *Acta Crystallographica Section E* **2007**, *63*, m2736.
- (100) Pfrunder, M. C.; Micallef, A. S.; Rintoul, L.; Arnold, D. P.; Davy, K. J. P.; McMurtrie, J. *Crystal Growth & Design* **2012**, *12*, 714.
- (101) Leitl, M. J.; Krylova, V. A.; Djurovich, P. I.; Thompson, M. E.; Yersin, H. *Journal of the American Chemical Society* **2014**, *136*, 16032.
- (102) Czerwieniec, R.; Leitl, M. J.; Homeier, H. H. H.; Yersin, H. *Coordination Chemistry Reviews* **2016**, *325*, 2.
- (103) Hofbeck, T.; Monkowius, U.; Yersin, H. *Journal of the American Chemical Society* **2015**, *137*, 399.
- (104) Shishkin, M.; Kresse, G. *Physical Review B* **2007**, *75*, 235102.
- (105) Garza, A. J.; Scuseria, G. E. *The Journal of Physical Chemistry Letters* **2016**, *7*, 4165.
- (106) Zhan, S.-Z.; Li, M.; Ng, S. W.; Li, D. *Chemistry – A European Journal* **2013**, *19*, 10217.
- (107) Kyle, K. R.; Ryu, C. K.; Ford, P. C.; DiBenedetto, J. A. *Journal of the American Chemical Society* **1991**, *113*, 2954.

Acknowledgements of Previous Publications

Chapter 3, 4, 6 are adapted from the publication below:

1. Liu, W.; Fang, Y.; Wei, G. Z.; Teat, S. J.; Xiong, K.; Hu, Z.; Lustig, W. P.; Li, J., A Family of Highly Efficient CuI-Based Lighting Phosphors Prepared by a Systematic, Bottom-up Synthetic Approach, *Journal of the American Chemical Society* **2015**, 137, 9400. Copyright 2015 American Chemical Society.
2. Liu, W.; Zhu, K.; Teat, S.; Deibert, B.J.; Yuan, W.; Li, J.; Mechanochemical route toward rational, systematic, and cost-effective green synthesis of strongly luminescent copper iodide based hybrid phosphors, *Journal of Materials Chemistry C*, **2017**, 5, 5962. Copyright 2017 The Royal Society of Chemistry
3. Liu, W.; Zhu, K.; Teat, S.; Dey, G.; Shen, Z.; Wang; O'Carroll, D.M.; Li, J.; All-in-one: Achieving robust, strongly-luminescent and highly-dispersible hybrid materials by combining ionic and coordinate bonds in molecular crystals, *Journal of the American Chemical Society* **2017**, 139, 9281. Copyright 2017 American Chemical Society.

Chapter 2, 5 will be published in the near future.